



LIBRARY  
Michigan State  
University

This is to certify that the  
dissertation entitled

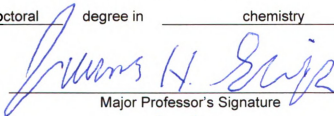
X-RAY CRYSTALLOGRAPHIC STUDIES OF CELLULAR  
RETINOIC ACID-BINDING PROTEIN II MUTANTS DESIGNED AS  
RHODOPSIN MIMICS

presented by

XIAOFEI JIA

has been accepted towards fulfillment  
of the requirements for the

\_\_\_\_\_  
doctoral degree in \_\_\_\_\_ chemistry

  
Major Professor's Signature

\_\_\_\_\_  
12/11/08

\_\_\_\_\_  
Date



**PLACE IN RETURN BOX** to remove this checkout from your record.

**TO AVOID FINES** return on or before date due.

**MAY BE RECALLED** with earlier due date if requested.

DATE DUE	DATE DUE	DATE DUE

**X-RAY CRYSTALLOGRAPHIC STUDIES OF CELLULAR RETINOIC ACID-  
BINDING PROTEIN II MUTANTS DESIGNED AS RHODOPSIN MIMICS**

**By**

**Xiaofei Jia**

**A DISSERTATION**

**Submitted to  
Michigan State University  
in partial fulfillment of the requirements  
for the degree of**

**DOCTOR OF PHILOSOPHY**

**Department of Chemistry**

**2008**

## ABSTRACT

### X-RAY CRYSTALLOGRAPHIC STUDIES OF CELLULAR RETINOIC ACID-BINDING PROTEIN II MUTANTS DESIGNED AS RHODOPSIN MIMICS

By

Xiaofei Jia

Color vision is one of the most fascinating mechanisms of the human anatomy. It is achieved by the collaboration of four visual pigments in the retina: the rod, red, green and blue rhodopsins. Upon binding of 11-*cis*-retinal, the four rhodopsins exhibit distinct absorption maxima, which altogether cover the entire visible spectrum and enable color vision. The underlying opsin-chromophore interactions within each rhodopsin are therefore of great interest and significance. Elucidation of these mechanisms, however, has been hampered by difficulties associated with the overexpression, purification, and routine crystallization of the membrane-bound rhodopsins. To overcome these difficulties and advance our understanding of the wavelength regulation mechanism in color vision, we have established a model system for rhodopsin, employing a mimic protein, cellular retinoic acid-binding protein II (CRABP II).

Upon binding of a shorter retinal analog, C<sub>15</sub>-aldehyde, several rationally designed CRABP II mutants exhibited altered absorption maxima of the bound chromophore. These mutants were characterized both biochemically and structurally. Chapter II of this dissertation focuses on the structural insights obtained for four such holo-CRABP II mutants based on the high-resolution crystal structures. The protonated Schiff base formation between Lys132 and the chromophore has been confirmed in all structures. Two distinctive binding orientations have been observed in different C<sub>15</sub>-aldehyde-

CRABP II complexes. A single mutation at 121 is shown to play a key role in determining the binding mode of the ligand. Based on the available high-resolution structures, further rational design of CRABP II has led to the discovery that placing negatively charged residues along the polyene chain of the chromophore leads to a clear trend in wavelength regulation.

High-resolution crystal structures of six apo-CRABP II mutants have also been determined. Chapter III details the discussion of how different mutations affect the structural integrity of the protein. A water-mediated hydrogen-bonding network has been observed in all apo-CRABP II structures, including both wild-type and mutants. Mutations usually lead to altered water-mediated networks and yet do not disrupt the overall structure of the protein. Mutations on the helical portal, however, tend to have detrimental structural effects.

Chapter IV presents an attempt toward elucidating the direct interaction between CRABP II and the retinoic acid receptor (RAR), which is responsible for the retinoic acid delivery.

Chapter V discusses the efforts toward obtaining the first crystal structure of the cellular retinaldehyde-binding protein (CRALBP), another important protein in vision. CRALBP functions in the regeneration process of 11-*cis*-retinal from all-*trans*-retinol in the retina pigment epithelium. Initial efforts toward crystallizing the full length CRALBP were unsuccessful. Subsequent mutagenesis combined with biochemical studies have helped identify suitable truncations at the N-terminal of this protein. Recent crystallization trials with a truncated CRALBP complexed with a synthetic ligand have shown encouraging results.

Copyright by  
XIAOFEI JIA  
2008



To my father

## ACKNOWLEDGMENTS

First and foremost, I would like to thank my two advisors, professor James H. Geiger and professor Babak Borhan. My journey of pursuing a doctoral degree in chemistry would have been interrupted if not for Jim and Babak, who provided me the opportunity to continue my study and advance myself in science. Jim and Babak share some of the finest qualities as scientists and mentors. They both have great passion for science and possess tremendous knowledge. Besides, what made them very special is their joyful attitude toward science. They both put their interests and passion to science in such a positive and contagious way that people around them are easily inspired. I consider myself very lucky to work in the labs of these two great scientists/mentors and learn a great deal from each of them.

I also feel very grateful to my colleagues working in the same project. Dr. Chrysoula Vasileiou has been with this project since the very beginning and has been the biggest factor for its success. Chrysoula not only contributes excellent scientific insights into the research, but also coordinates this group of people in a very enjoyable, cordial way. I especially thank her for all the suggestions she gave to me. Dr. Soheila Vaezslami worked on the structure determination of CRABPII mutants before me. Her success certainly paved the way for me. I owe a very special thanks to Kin-Sing Lee. Sing and I had the closest collaboration. We exchanged results and ideas on a regular basis. His intellectual inputs as well as his hard work have greatly aided the growth of the project and also helped me in doing my part of the research. Many of his data have been incorporated and discussed in this dissertation. I would also like to thank Calvin

Grant, Wenjing Wang, Camille Watson and Rafida Nossori who are working on other aspects of this project. I appreciate all your collaboration and support over the years.

I would like to thank my labmates in the Geiger group. Dr. Stacy Hovde was the one who helped me in everything when I first started in the lab. Her intelligence, diligence, friendliness and her super love for Spartan hockey all impressed me very much. It was very a pleasant experience working with her. Dr. Sara Cnude and Dr. Fang Sheng helped me a great deal on getting started with crystallography. Their kindness and patience had made my learning process very enjoyable. I also want to thank Lei Feng for the discussions and friendship over the years. I owe a special thanks to Susan Wortas for her taking so much time in proofreading my various writings. Her kindness and patience are deeply appreciated. I also want to thank Remie Touma for bringing her energy and positive attitude into the lab.

I would also like to thank the Borhan group members, especially Dr. Tao Zheng, Dr. Jun Yan and Xiaoyong Li. I could not list all the names, but I certainly appreciate the their friendship and support over the years.

I am deeply grateful to my friends, Dr. Jian Yi, Dr. Ningqing Ran, Dr. Yana Cen, Dr. Jinsong Yang, Dr. Gang Hu, Dr. Justas Jancauskas and Xianying Jiang. I am truly blessed by your friendship and support through all these years.

Last but not least, I thank my family for their unconditional love and support throughout my life. My father, mother, grandma and my sister have always been there for me whenever I needed them. My life would not be the same without everything they have done for me. This dissertation is dedicated to my father, Ping Jia, who passed away on December 6<sup>th</sup>, 2008, two days before my defense.

## TABLE OF CONTENTS

LIST OF TABLES

LIST OF FIGURES

ABBREVIATIONS

<b>CHAPTER I. Introduction .....</b>	<b>1</b>
1.1. <i>The Mystery of Vision</i> .....	1
1.2. <i>Rhodopsins as mammalian visual pigments: structure and function in photoactivation.</i> .....	9
1.3. <i>Other rhodopsins</i> .....	12
1.4. <i>Color vision</i> .....	15
1.5. <i>Designing CRABPII mutants as rhodopsin mimics</i> .....	30
1.5.1. <i>CRABPII general background.</i> .....	31
1.5.2. <i>Designing CRABPII mutants as rhodopsin mimics.</i> .....	35
1.6. <i>Cellular retinaldehyde-binding protein and the 11-cis-retinal regeneration.</i> .....	38
<i>Reference</i> .....	44
<b>CHAPTER II. Crystal Structures of Ligand-bound Cellular Retinoic Acid Binding Protein II Mutants .....</b>	<b>62</b>
2.1. <i>Introduction.</i> .....	62
2.1.1. <i>Need for a ligand that can be totally buried inside the CRABPII mutants.</i> .....	62
2.1.2. <i>Engineered CRABPII mutants as switchable colorimetric fusion proteins.</i> .....	65
2.2. <i>C<sub>15</sub>-aldehyde-bound CRABPII mutant structures.</i> .....	67
2.2.3. <i>Protonated Schiff base stabilization.</i> .....	74
2.2.4. <i>Cis versus trans protonated Schiff base.</i> .....	77
2.2.5. <i>Flexibility of the helix-turn-helix lid.</i> .....	79
2.2.6. <i>An evolutionary correlation between CRABPII and plasma retinol-binding protein?</i> .....	82
2.2.7. <i>Testing the point charge theory based on the C<sub>15</sub>-aldehyde-bound KLE-R59W-CRABPII structure.</i> .....	86
2.2.8. <i>Conclusion</i> .....	87
2.3. <i>Merocyanin-bound CRABPII mutant structure.</i> .....	89
<i>References</i> .....	93
<b>CHAPTER III. Crystal Structures of the Apo-CRABPII Mutants .....</b>	<b>98</b>
3.1. <i>Introduction</i> .....	98

3.2. Results.....	100
3.2.1. Mutations of conserved and non-conserved residues .....	100
3.2.2. The structure of apo-R132K:R111L:L121E:R59E-CRABPII (apo-KLE-R59E) .....	102
3.2.3. The structure of apo-R132K:Y134F:R111L:L121E-CRABPII (apo-KFLE).....	105
3.2.4. The structure of apo-R132K:Y134F:R111L:L121D-CRABPII (apo-KFLD) .....	107
3.2.5. The structure of apo-R132K:Y134F:R111L:L121D:T54V-CRABPII (apo-KFLD-T54V).....	108
3.2.6. The structure of apo-R132K:R111L:T54E-CRABPII (apo-KL-T54E) .....	109
3.2.7. The structure of apo-R132K:R111L:A32E-CRABPII (apo-KL-A32E).....	111
3.3. Discussion.....	112
3.3.1. Rigid overall fold of the apo-CRABPII mutant structures .....	112
3.3.2. A32E mutation is detrimental to the $\alpha$ 2 helix in apo-KL-A32E .....	114
3.3.3. Water-mediated network acts as a pillar inside the cavity .....	116
3.3.4. The hydrophobic cavity allows binding of BTP.....	117
3.5. Conclusion.....	118
Reference .....	119
<b>CHAPTER IV. Investigation of the Interaction between Cellular Retinoic Acid Binding Protein II and Retinoic Acid Receptor Gamma Ligand Binding Domain.</b>	<b>122</b>
4.1. Background.....	122
4.2 Results and discussion.....	128
4.2.6. Circular dichroism of RAR $\gamma$ -LBD and fluorescence titration of RAR $\gamma$ -LBD with retinoic acid. ....	133
4.2.7. Titration of KLE-CRABP II with retinal followed by UV.....	135
4.2.8. <i>In vitro</i> binding assay using RAR $\gamma$ -LBD directly from Ni-NTA resin. ....	135
4.3. Conclusions .....	137
References.....	138
<b>CHAPTER V. Preliminary X-Ray Crystallographic Studies of Cellular Retinaldehyde Binding Protein .....</b>	<b>140</b>
5.1. Background.....	140
5.2. Crystallization of the full-length CRALBP .....	140
5.2.1. His-tagged full-length CRALBP crystallization.....	140
5.2.2. Non-fusion full-length CRALBP crystallization. ....	142
5.2.3. Full-length CRALBP with a cleavable His-tag. ....	144
5.3. Crystallization of the N-terminal-truncated CRALBP.....	145
5.3.1. Truncation at 43/44 on the N-terminal of CRALBP. ....	145
5.3.2. Discovery of the ideal N-terminal truncation site.....	147
5.3.3. Enhancing the expression and purification of functional CRALBP.....	158
5.3.4. Crystallization trials.....	159



<i>5.4. Conclusion</i> .....	160
<i>Reference</i> .....	161
<b>CHAPTER VI. Experimental</b> .....	<b>162</b>
<i>6.1. Cloning, mutagenesis, expression and purification</i> .....	162
6.1.1. Cloning, mutagenesis, expression and purification of CRABPII mutants. ...	162
6.1.2. Cloning, expression and purification of RAR $\gamma$ -LBD. ....	164
6.1.3. Cloning, mutagenesis, expression and purification of CRALBP. ....	165
<i>6.2. Protein crystallization</i> .....	170
6.2.1. Co-crystallization of CRABPII mutants bound with ligands. ....	170
6.2.2. Crystallization of apo-CRABPII mutants.....	173
<i>6.3. Data processing and structure determination</i> .....	175
6.3.1. Structures of the C <sub>15</sub> -aldehyde-bound CRABPII mutants. ....	175
6.3.2. Structure of the merocyanin-bound KLE-R59W-CRABPII mutant. ....	176
6.3.3. Structures of the apo-CRABPII mutants. ....	177
<i>6.4. Protein characterization</i> .....	193
6.4.1. General procedure for UV-vis titrations of CRABPII/CRALBP with retinoids. .....	193
6.4.2. Determination of the extinction coefficients of proteins. ....	193
6.4.3. Reductive amination procedure. ....	195
6.4.4. Circular Dichroism of protein samples.....	195
6.4.5. Fluorescence. ....	196
6.4.6. General protocol followed for Fluorescence Quenching and K <sub>d</sub> determination experiments.....	198
<i>References</i> .....	203

## LIST OF TABLES

Table I-1. Rhodopsins of various species. ....	17
Table II-1. CRABP II mutants bound with C <sub>15</sub> -aldehyde. ....	64
Table II-2. Residues around the ionone rings. ....	86
Table II-3. Absorption maxima observed for the KLE-X-CRABP II series of mutants ....	87
Table II-4. UV maximum absorption of the merocyanin-bound CRABP II mutants. ....	89
Table VI-1. X-ray data collection statistics of the ligand-bound CRABP II mutant crystals. .....	178
Table VI-2. Structure refinement statistics of the ligand-bound CRABP II mutant crystals. .....	179
Table VI-3. X-ray data collection statistics of the apo-CRABP II mutant crystals. ....	180
Table VI-4. Structure refinement statistics of the apo-CRABP II mutant crystals. ....	181

## LIST OF FIGURES

Figure I-1. The human eye.....	2
Figure I-2. A. rod and cone cells in retina; B. rhodopsins embedded in the disks in photoreceptor cells.....	3
Figure I-3. Schematic representation of the intermediates observed in the isomerization of 11- <i>cis</i> -retinal to all- <i>trans</i> -retinal in rhodopsin.....	5
Figure I-4. Photoactivation cascade.....	7
Figure I-5. Crystal structure of bovine rod rhodopsin. ....	10
Figure I-6. Absorption profiles of different human rhodopsins. ....	16
Figure I-7. Model compounds used to study wavelength shifts controlled by distance between the PSB and the counter anion. ....	20
Figure I-8. The point charge model.. ....	21
Figure I-9. Hypothesis of steric interactions leading to wavelength regulation.. ....	23
Figure I-10. Vicinity of retinal in cone pigments as shown in the homology models.....	24
Figure I-11. Illustration of the sites of mutations for converting the red rhodopsin to a green-rhodopsin-like pigment.....	27
Figure I-12. Illustration of the sites of mutations for converting the green rhodopsin to a red-rhodopsin-like pigment. ....	27
Figure I-13. Illustration of the sites of mutations for converting the rod rhodopsin to a red-shifted pigment.....	28
Figure I-14. Crystal structure of retinoic acid bound in WT-CRABPII .....	32
Figure I-15. Water-mediated hydrogen bonding interactions observed in the molecule A of the apo-WT-CRABPII crystal structure .....	34
Figure I-16. Crystal packing observed in the structure of apo-WT-CRABPII.....	35
Figure I-17. All- <i>trans</i> -retinal bound in KLE-CRABPII.....	37
Figure I-18. The visual cycle.....	39
Figure I-19. Stereoview of the structure models built for CRALBP.....	42

Figure II-1. Retinoic acid bound in wild-type-CRABPII. ....	63
Figure II-2. Structures of the related compounds. ....	63
Figure II-3. Overlay of the ligands bound in different binding orientations.....	69
Figure II-4. 2Fo-Fc electron density map calculated at 1.0 $\sigma$ for bound ligands. A. C <sub>15</sub> -aldehyde bound to Lys132 (upper) and bis-tris-propane (lower) in KLE-R59W; B. C <sub>15</sub> -aldehyde bound to Lys132 in KL-A32E.....	69
Figure II-5. Interactions between the PSB and the residues nearby in different C <sub>15</sub> -aldehyde-bound CRABPII mutants. ....	70
Figure II-6. A. The structures of KLE-Rt and C <sub>15</sub> -aldehyde-KL-A32E are overlaid. Glu121 from KLE-Rt (magenta) and C <sub>15</sub> -aldehyde from <i>holo</i> -KL-A32E (green) are shown; B. Overlay of the C <sub>15</sub> -aldehyde bound in three CRABPII mutants: KL-A32E (magenta), KL-T54E (green), and KFLDV (yellow).....	72
Figure II-7. A. Proposed nucleophilic attack of lysine amino group to the aldehyde following the Bürgi-Dunitz model; B. Surface representation of C <sub>15</sub> -aldehyde (yellow) bound in KL-A32E (gray).....	78
Figure II-8. Stereoview of the overlay between <i>holo</i> -KL-A32E (green) and <i>holo</i> -KLE-R59W (magenta).....	80
Figure II-9. Overlay between C <sub>15</sub> -aldehyde-bound KLE-R59W (blue) and <i>apo</i> -KLE-R59E (green). A. Model of C <sub>15</sub> -aldehyde in <i>apo</i> -KLE-R59E; B. Crystal structure of C <sub>15</sub> -aldehyde bound in KLE-R59W. ....	81
Figure II-10. Stereoview of the overlay of C <sub>15</sub> -aldehyde-bound KL-A32E (green) and retinol-bound RBP (pink).. ....	84
Figure II-11. C <sub>15</sub> -aldehyde bound in the KLE-R59W-CRABPII mutant. ....	87
Figure II-12. Structures of merocyanin and MES. ....	89
Figure II-13. Merocyanin bound in KLE-R59W-CRABPII mutant.....	91
Figure III-1. Stereoview of the mutation sites involved in these CRABPII mutants.. ....	101
Figure III-2. Structure of the <i>apo</i> -KLE-R59E-CRABPII.. ....	104
Figure III-3. Structure of the <i>apo</i> -KFLE-CRABPII.. ....	106
Figure III-4. Structure of the <i>apo</i> -KFLD-CRABPII. ....	107
Figure III-5. Structure of the <i>apo</i> -KFLD-T54V-CRABPII.. ....	109
Figure III-6. Structure of the <i>apo</i> -KL-T54E-CRABPII.....	110

Figure III-7. Structure of the apo-KL-A32E-CRABPII..	111
Figure III-8. Stereoview of the overlay of all apo structures together.....	113
Figure IV-1. <i>all-trans</i> retinoic acid and <i>9-cis</i> retinoic acid. ....	122
Figure IV-2. Structural organization of nuclear receptors.....	123
Figure IV-3. Comparison of the crystal structures of the apo-RXR $\alpha$ (A, PDB: 1LBD) and holo-RAR $\gamma$ (B, PDB: 2LBD) ligand-binding domains reveals the ligand-induced conformational change.....	124
Figure IV-4. The synthetic retinoid analog CD270. ....	127
Figure IV-5. <i>In vitro</i> binding assay.....	129
Figure IV-6. Detergent titration of the protonated Schiff base formed between KLE-CRABPII and retinal.....	131
Figure IV-7. Fluorescence titration of RAR $\gamma$ -LBD with <i>all-trans</i> -retinoic acid. ....	133
Figure IV-8. Titration of KLE-CRABPII with retinal.....	134
Figure IV-9. <i>In vitro</i> binding assay using RAR $\gamma$ -LBD directly from Ni-NTA resin. ....	136
Figure V-1. Pure fractions of His-rCRALBP eluted after Ni-NTA purification.....	141
Figure V-2. Non-fusion CRALBP purified. ....	142
Figure V-3. UV titration of non-fusion CRALBP with 11- <i>cis</i> -retinal. ....	143
Figure V-4. Full length CRALBP expressed in pET28a and purified with his-tag cleaved.. ....	144
Figure V-5. N-43/44-truncated CRALBP expressed from pET28a and purified by Ni-column.. ....	147
Figure V-6. Expression of the truncated CRALBPs.....	148
Figure V-7. UV titration of full-length and truncated CRALBPs with 11- <i>cis</i> -retinal.....	149
Figure V-8. Gel filtration separation of full-length-CRALBP. ....	152
Figure V-9. UV titration of different fractions from gel filtration separation of $\Delta$ 20-CRALBP.....	153
Figure V-10. CD spectra of different fractions from gel filtration separation of $\Delta$ 20-CRALBP.....	155



Figure V-11. Gel filtration purification of the $\Delta 20$ -CRALBP grown at different temperatures.....	157
Figure V-12. Trypsin digestion performed for both full length and $\Delta 20$ -CRALBP under 4°C. ....	158
Figure V-13. Crystals of merocyanin-bound proteins. A. merocyanin-bound $\Delta 20$ -CRALBP; B. merocyanin-bound KLE-R59W-CRABPII. ....	159
Figure VI-1. R132K:Y134F:R111L:L121E-CRABPII (KFLE) purified after source-15Q anion exchange column. ....	162
Figure VI-2. Elution fractions of RAR $\gamma$ -LBD from Ni-NTA purification. ....	164
Figure VI-3. Pure fractions of the his-tagged rCRALBP eluted off the Ni column. ....	166
Figure VI-4. Non-fusion CRALBP after purification. ....	166
Figure VI-5. Primers used for constructing different N-terminal deletion CRALBP.. ...	167
Figure VI-6. Typical size-exclusion purification profile of CRALBP represented by $\Delta 20$ -CRALBP grown at 16°C. ....	169
Figure VI-7. CRALBP after purification.....	169
Figure VI-8. Pictures of crystals of the ligand-bound CRABPII mutants.....	171
Figure VI-9. Pictures of crystals of the apo-CRABPII mutants.. ....	174
Figure VI-10. Ramachandran plot of the C <sub>15</sub> -aldehyde-bound-KLE-R59W-CRABPII. ....	182
Figure VI-11. Ramachandran plot of the C <sub>15</sub> -aldehyde-bound-KL-A32E-CRABPII. ....	183
Figure VI-12. Ramachandran plot of the C <sub>15</sub> -aldehyde-bound-KL-T54E-CRABPII. ....	184
Figure VI-13. Ramachandran plot of the C <sub>15</sub> -aldehyde-bound-KFLDV-CRABPII.....	185
Figure VI-14. Ramachandran plot of the merocyanin-bound-KLE-R59W-CRABPII....	186
Figure VI-15. Ramachandran plot of the apo-KLE-R59E-CRABPII. ....	187
Figure VI-16. Ramachandran plot of the apo-KFLE-CRABPII.....	188
Figure VI-17. Ramachandran plot of the apo-KFLD-CRABPII. ....	189
Figure VI-18. Ramachandran plot of the apo-KFLDV-CRABPII. ....	190
Figure VI-19. Ramachandran plot of the apo-KL-T54E-CRABPII. ....	191

Figure VI-20. Ramachandran plot of the apo-KL-A32E-CRABPII.....	192
Images in this dissertation are presented in color.	

## ABBREVIATIONS

### Amino Acids

Ala, A	Alanine
Arg, R	Arginine
Asn, N	Asparagine
Asp, D	Aspartic acid
Cys, C	Cysteine
Gln, Q	Glutamine
Glu, E	Glutamic acid
Gly, G	Glycine
His, H	Histidine
Ile, I	Isoleucine
Leu, L	Leucine
Lys, K	Lysine
Met, M	Methionine
Phe, F	Phenylalanine
Pro, P	Proline
Ser, S	Serine
Thr, T	Threonine
Trp, W	Tryptophan
Tyr, Y	Tyrosine
Val, V	Valine

### CRABPII Mutants Abbreviations

KFLD	R132K:Y134F:R111L:L121D
KFLDV	R132K:Y134F:R111L:L121D:T54V
KFLE	R132K:Y134F:R111L:L121E
KFLEV	R132K:Y134F:R111L:L121E:T54V
KL	R132K:R111L
KL-A32E	R132K:R111L:A32E
KL-T54E	R132K:R111L:T54E
KLE	R132K:R111L:L121E
KLE-R59E	R132K:R111L:L121E:R59E
KLE-R59W	R132K:R111L:L121E:R59W

### Other Symbols and Abbreviations

Å	Ångström
Abs	Absorption

Amp	Ampicillin
APS	Advanced Photon Source
bp	Base pair
BTP	Bis-tris-propane
C $\alpha$	The alpha carbon in the peptide bond
CCP4	Collaborative computational project, number 4
CD	Circular dichroism
cGMP	Guanisine 3', 5'-cyclic monophosphate
Chlor.	Chloramphenicol
CRABP II	Cellular retinoic acid-binding protein II
CRALBP	Cellular retinaldehyde-binding protein
CRBP	Cellular retinol binding protein
C-terminal	Carboxy terminal
Da	Dalton
DEAE	Diethylaminoethyl cellulose
DNA	Deoxyribonucleic acid
dNTP	Deoxynucleotide triphosphate
DTT	Dithiothreitol
$\epsilon$	Extinction coefficient
<i>E. coli</i>	<i>Escherichia coli</i>
FABP	Fatty acid binding protein
FPLC	Fast protein liquid chromatography
FTIR	Fourier transform infra red
G*	Transducin, activated
GDP	Guanisine diphosphate
GMP	Guanisine monophosphate
GPCR	G-protein coupled receptor
GTP	Guanisine triphosphate
h	Hour
HTP	Hydroxyapatite
iLBP	Intracellular lipid binding protein
IPTG	Isopropyl-1-thio- $\beta$ -D-galactopyranoside
K <sub>D</sub>	Dissociation constant
L	Liter
LB	Luria broth
$\lambda_{\max}$	Wavelength of the maximum absorption

M	Molar
MES	2-Morpholinoethanesulfonic acid, monohydrate
μl	microliter
ml	milliliter
mm	millimeter
MOPS	3-( <i>N</i> -Morpholino)-propanesulfonic acid
MPD	2-Methyl-2,4-pentanediol
MW	Molecular weight
nm	Nanometer
nM	Nanomolar
NMR	Nuclear Magnetic Resonance
N-terminal	Amino terminal
PCR	Polymerase chain reaction
PDB	Protein Data Bank
PDE	Phosphodiesterase
PEG	Polyethylene glycol
PSB	Protonated Schiff base
R*	Rhodopsin, activated
RA	Retinoic acid
RAR	Retinoic acid receptor
RARE	RAR-response element
RBP	Retinol-binding protein
R-factor	Reliability factor
Rmsd	root mean square deviation
RNA	Ribonucleic acid
RPE	Retinal pigment epithelium
RXR	Retinoid X receptor
SB	Schiff base
SDS-PAGE	Sodium dodecyl sulfate – polyacrylamide gel electrophoresis
Tris	2-Amino-2-(hydroxymethyl)-1,3-propanediol
UV	Ultraviolet light
vdw	Van der Waals
vis	Visible light
WT	wild type



# CHAPTER I. Introduction

## 1.1. *The Mystery of Vision*

Vision is a precious gift that deeply enriches our lives. Through vision, one is able to perceive the order and beauty of the world. The visual process is one of the most delicate and efficient mechanisms of the human anatomy.

Given the fascinating nature of vision, it is not surprising that people have been intrigued by the question of how one is enabled to see since the early days of human history. Ancient Greek philosophers, Plato (ca. 450 BC), Democritus (ca. 350 BC), Aristotle (ca. 330 BC) and Euclid (ca. 300 BC), were the first known to seek the explanations of vision (1). However, only Aristotle's theory, which was later extended by his student Theophrastus (ca. 300 BC), was close to capturing the true nature of this process: light is reflected by the objects, travels through the medium (air), and is then received by the eye (2). Although not popular at its time, this theory was improved throughout the centuries and eventually revisited by Johannes Kepler (1571-1630) in 1604 (3). He postulated the first complete description of the optics of the eye, refuting the once-popular theory that vision is enabled when the objects are being touched by the emissions sent out from the eyes. In 1704, Isaac Newton (1642-1727) published the book *Opticks*, which revolutionized the understanding of the laws that govern light (4). Most of his insights on the physical and physiological nature of color remain valid today. In the 1830s it was discovered that the perception of light happens in the rod and cone cells of the retina, the inner part of the eye. In 1878 the photosensitive protein in the rod cells,

now known as rhodopsin, was isolated by F. W. Kuhne (1837-1900) (5). The active research of the subject over many years finally led to the revolutionary discovery by Wald (1906-1997) and coworkers that greatly advanced our understanding of the first steps in the vision process (6-8).

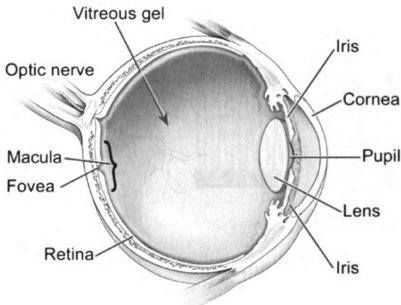


**Figure I-1. The human eye (9).**

In a simplified picture, the current model of the vision process can be depicted as follows. When light enters the eye through the pupil, it is immediately focused by the lens before being sensed by the photoreceptor cells in the retina (Figure I-1) (10). Through a cascade of complicated events, the absorption of photons is converted into specific electrical signals in the photoreceptor cells. These signals are then transmitted in specific patterns out of the photoreceptor cells, through the optic nerves, and onto certain parts of the brain.

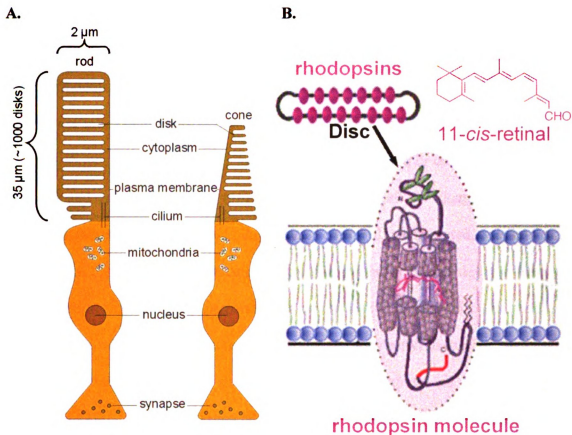


**Figure I-2. A. rod and cone cells in retina (11); B. rhodopsins embedded in the disks in photoreceptor cells (12).**

Through decades of hard work by many scientists, a more thorough and complete picture of this process has been achieved. For vertebrates, in the retina where vision initiates, two types of photoreceptor cells, rod and cone, exist (Figure I-2A) (13). The human eye contains approximately 100 million rod cells and about 6 million cone cells (14). Both types of the photoreceptor cells contain the visual pigments, known as rhodopsins. Rhodopsins refer to the specific proteins, called opsins, when they are bound to retinal via a Schiff base linkage with the active site lysine. In human eyes, each rod cell uses rod rhodopsins as its sole visual pigments, which are responsible for dim vision,

while each cone cell contains its own specific rhodopsins: blue, green or red opsins, respectively. The blue, green and red cones are responsible for color vision. In the dark state, all four opsin proteins bind to the same natural substrate, 11-*cis*-retinal. Although the four rhodopsins differ in their absorption spectrum, they share the same mechanism in the process called phototransduction (15-17).

As shown in Figure I-2A, a photoreceptor cell, either rod or cone, contains an outer segment and an inner segment (18). Taking the rod cell for example, in the outer segment hundreds of phospholipid bilayer disks are stored in an ordered, parallel fashion. Rhodopsins, the 7-helical trans-membrane protein, are embedded inside these disks with an orientation that is mostly perpendicular to the disk (Figure I-2B). The rhodopsins occupy ~50% of the disk surface area. Although it varies between species, each rod cell typically contains 1700 disks and each disk contains up to 1.5 million rhodopsin molecules (19). The inner segment contains the mitochondria, the nucleus and the synaptic end.

The human vision process starts with the photolysis of rhodopsin, which involves a *cis-trans* isomerization of the bound 11-*cis*-retinal. This activation-deactivation process of rhodopsin involves several thermal/dark steps characterized by intermediates identified at very low temperatures (Figure I-3) (20-25). In the dark state, 11-*cis*-retinal binds within rhodopsin through a protonated Schiff base (PSB) with Lys296 (26-29). Within femtoseconds after radiation, photorhodopsin is formed as a highly distorted "all-*trans*" PSB moiety (30), which then relaxes to the first isolatable intermediate, bathorhodopsin (31, 32). The formation of lumirhodopsin immediately follows within nanoseconds, followed by metarhodopsin I and then metarhodopsin II. The formation of

metarhodopsin II happens millisecond after light absorption. Metarhodopsin II turns out to be the activated form of rhodopsin, which triggers the subsequent phototransduction cascade. The Schiff base is found to be unprotonated at metarhodopsin II. Following the metarhodopsin II activation, the imine bond is protonated to afford metarhodopsin III. Finally, dissociation of all-*trans*-retinal from rhodopsin is achieved through hydrolysis.

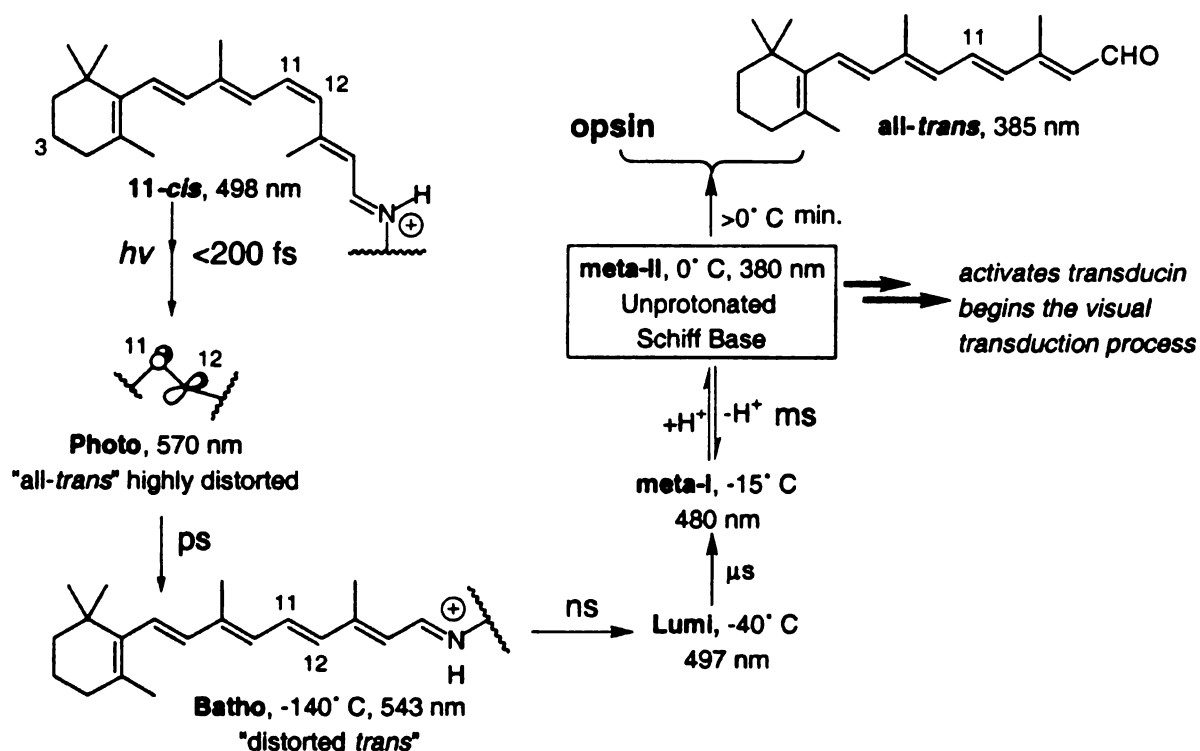


**Figure I-3. Schematic representation of the intermediates observed in the isomerization of 11-*cis*-retinal to all-*trans*-retinal in rhodopsin (21).**

The electric signal is generated as follows (Figure I-4). In vertebrate, a dark current carried by  $Na^+$  and  $Ca^{2+}$  enters the outer segment of the rod cell through cGMP-gated channels keeping the cytoplasmic membrane relatively depolarized (33-35). The

activation of rhodopsin through photon absorption generates metarhodopsin II (36, 37), which is able to bind to transducin, a G-protein consisting of three subunits:  $T\alpha$ ,  $T\beta$  and  $T\gamma$ . It is believed that this interaction is achieved when the  $\alpha$ -subunit of transducin binds to amino acids located in the second and third cytoplasmic loops of metarhodopsin (38-41). This interaction triggers a conformational change in  $T\alpha$ , which involves the opening of the nucleotide-binding pocket and release of the guanosine-5'-diphosphate (GDP) bound (42). Transducin is then activated through binding to guanosine-5'-triphosphate (GTP) and subsequently the dissociation of  $T\alpha$  from  $T\beta$  and  $T\gamma$ , which eventually enables the signal transduction going from transducin to the next entity, the cyclic guanosine-5'-monophosphate (cGMP)-specific phosphodiesterase (PDE).

PDE is a membrane-bound protein consisting of four subunits:  $P\alpha$ ,  $P\beta$  and  $2P\gamma$ . The catalytic activity of PDE is enabled by the two subunits,  $P\alpha$  and  $P\beta$ . In the inactive state, the two inhibitory  $P\gamma$  subunits block the activity of PDE. Activation of PDE is achieved through binding with  $T\alpha$ -GTP and subsequent removal of the two inhibitory  $P\gamma$  subunits (43, 44). The activated PDE then hydrolyzes the cGMP into 5'-GMP, reducing the cellular concentration of cGMP. The lowered concentration of cGMP signals the closing of the cGMP-gated ion channels, which then results in interruption of the dark current. In this way, the absorption of light is transformed by the rod cells to a hyperpolarized electrical signal which is subsequently transmitted to the synaptic end and sent out to the brain through the optic nerves.

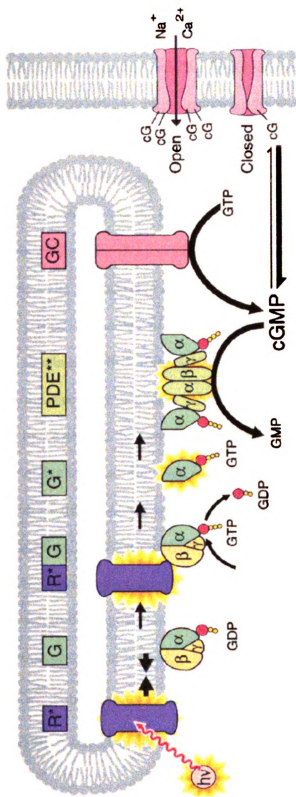


**Figure 1-4. Photoactivation cascade (45).** Absorption of photon leads to an activated rhodopsin ( $R^*$ ). Each  $R^*$  then contacts numerous transducins, upon which the transducins become activated ( $G^*$ ) by exchanging a bound-GDP for a GTP.  $G^*$  subsequently activates PDE by interacting with its  $\gamma$  subunits, followed by dissociation of the  $\gamma$  subunits. The activated PDE ( $PDE^{**}$ ) catalyzes the hydrolysis of cGMP, reducing its cytoplasmic concentration. Lower level of cGMP concentrations eventually results in the closure of cGMP-gated ion channels in the plasma membrane.

Phototransduction in vertebrate involves a light-activated isomerization of a double bond, which triggers a cascade of events and eventually leads to vision. This process is one of the most efficient and sensitive biological processes known, with a quantum yield of  $\sim 0.67$  (46). The energy amplification of the visual process is calculated to be in the order of 100,000 based on quantitative analysis of the electrical response to a single photon (47, 48). On the molecular level, the amplification is achieved in primarily two steps. The first step lies in the interaction between metarhodopsin II ( $R^*$ ) with transducin (T). Within a fraction of a second, one molecule of  $R^*$  is able to contact hundreds of transducins. The second stage of amplification is provided by the activity of PDE which catalyzes  $\sim 1000$  molecules of cGMP per second (49, 50). The total amplification therefore equals to  $\sim 100 \times 1000 = 100,000$ , which is in agreement with the calculations based on the electrical response. This explains the excellent sensitivity of vision that allows us to see even in the darkest environments.

The above steps are involved in the rising phase of the light-signal response. The inactivation of this response is also important and involves mainly three mechanisms. The first mechanism is the guanylate cyclase-catalyzed generation of cGMP from GTP. This process compensates the loss of cGMP caused by light-activation. The decreased cGMP concentration signals closing of the ion channels, which leads to a decrease in the concentration of calcium (35, 51). The activity of guanylate cyclase is stimulated by the lowered  $Ca^{2+}$  concentration in the rod cell. The cGMP concentration then increases so that the cGMP-gated channels are open and the dark current is restored.



The second mechanism of inactivation is through phosphorylation of rhodopsin. The major role of rhodopsin phosphorylation, mediated by rhodopsin kinase and protein kinase C, is to promote arrestin binding and decrease transducin binding (52, 53).

The third mechanism involves the transducin-catalyzed hydrolysis of GTP to GDP (54, 55). The GTPase activity is greatly accelerated during the rising phase of the light activation, which later on leads to reduced concentration of activated transducin,  $T\alpha$ -GTP.

Phototransduction in invertebrates shares a great deal of similarity with that of vertebrates in the overall strategy. Light activation of rhodopsin triggers a series of intermediates leading to metarhodopsin. Similarly, this metarhodopsin also triggers a cascade of events leading to an electrical response. One difference is that the metarhodopsin in invertebrates is stable and inter-convertible with rhodopsin. Another interesting difference of the phototransduction in invertebrates is that the electrical signal is generated by depolarization of the plasma membrane, which is caused by the light-activated closing of the ion channels (56). Overall, the vision process in invertebrates shares several important features and similar sensitivity with that in vertebrates (57, 58).

## ***1.2. Rhodopsins as mammalian visual pigments: structure and function in photoactivation.***

Rhodopsin is a 39KD protein, consisting of 348 amino acids and two oligosacchride chains (59, 60). It belongs to the family of G protein-coupled receptors (GPCR), which is by far the largest class of cell surface signal transducing receptors. Similar to the other membrane-bound GPCR family proteins, rhodopsin features a typical 7-helical structure.

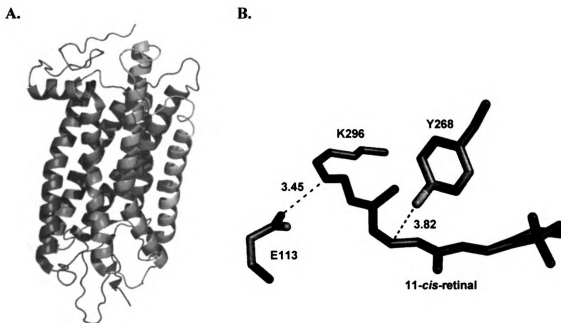


**Figure I-5. Crystal structure of bovine rod rhodopsin.** A. Overall fold; B. Binding of 11-*cis*-retinal in rhodopsin.

Our understanding of rhodopsin was greatly advanced with the determination of the crystal structure of bovine rod rhodopsin at 2.8 Å in the year 2000 by Palczewski and coworkers (28). This first-ever crystal structure of rhodopsin was able to define 95% of the amino acids as well as the posttranslational modifications (Figure I-5A). Continued efforts from different research groups has since yielded rhodopsin crystal structures in different crystal forms and improved resolutions to 2.2 Å (61, 62). As revealed by the crystal structure, 11-*cis*-retinal is bound to the transmembrane portion of rhodopsin through a covalent *trans*-imine bond with Lys296 (Figure I-5B). This confirms the protonated Schiff base (PSB) formation between the chromophore and Lys296 that was suggested previously based on other biochemical evidence (26, 27). Glu113 is identified as the counter anion that stabilizes the PSB 3.45 Å away. This electrostatic interaction

between the PSB and the carboxylate counter anion is found to be conserved only among visual pigments and is considered to be important for wavelength shift of the bound chromophore as well as for maintaining the inactive, dark state conformation of rhodopsin (63-66). Prior to the determination of the crystal structure of rhodopsin, the role of Glu113 acting as a counter anion had been identified through mutagenesis studies (65). Mutation of Glu113 to Gln113 leads to a dramatic change in the absorption maximum from 500 nm to 380 nm, which is accompanied by a decrease in  $pK_a$  from over 16 to around 6.

Rhodopsin also features a compact extracellular (intradiscal) portion, part of which folds inward to enclose the bound chromophore (67). The two oligosacchrides are also present in the extracellular part of the protein, linked through two Asn residues, Asn2 and Asn15, at the N-terminus. The cytoplasmic portion of rhodopsin is not as rigid as the extracellular portion. In fact, the B-factors for this region vary considerably among different ground-state crystal structures, indicating the flexible nature of this part of rhodopsin (68). The transmembrane (TM) portion of rhodopsin constitutes as much as 60% of its secondary structure (69, 70). This region also contains the majority of the conserved residues in rhodopsin and other GPCRs, many of which are suggested to play important roles in maintaining the stability of rhodopsin.

As mentioned earlier, the initial light activation of rhodopsin leads to several photoproducts. The crystal structures of some of these photoproducts have been successfully obtained after trapping these photolyzed states at low temperatures (71-73). Three-dimensional structures have been obtained for bathorhodopsin and lumirhodopsin. A structural model for metarhodopsin I has also been obtained based on electron

crystallography of two-dimensional crystals. Even though these structures are only at moderate to low resolutions (2.7 - 5.5 Å), comparison of them with the dark-state structure of rhodopsin reveals that the double bond between C11 and C12 in retinal adopts the *trans* conformation upon light-activation (74). From bathorhodopsin to lumirhodopsin, a positional/conformational change of the  $\beta$ -ionone ring of retinal has been suggested, but only by low-resolution structures. A structural model of an intermediate containing a deprotonated Schiff base has been obtained from lumirhodopsin crystals (75). This metarhodopsin II-like photoproduct seems to be similar to the dark state rhodopsin in overall structure. However, parts of the second and third loops in the cytoplasmic portion are found to be disordered in this photoactivated rhodopsin. In addition, residues Phe212, Trp265, Leu266 and Tyr268, were found to make direct contact with the  $\beta$ -ionone ring of the chromophore, which is consistent with observations from solid state NMR studies.

### **1.3. Other rhodopsins**

Rhodopsins exist in all three domains of life, Archaea, Bacteria and Eukarya (76). However, not all rhodopsins function as visual pigments as they do in higher animals. In fact, microbial rhodopsins represent a diverse group of photochemically reactive proteins, whose functions involve converting light energy for either ion transport or photosensory movement of cells (77). A generally accepted hypothesis that unifies microbial rhodopsin transport and signaling is that the accessibility of the Schiff base is switched

from the periplasmic side to the cytoplasmic side through structural changes, which opens the cytoplasmic channel for ion pumping and contributes to signal relay in the sensors (78).

Bacteriorhodopsin, isolated from the haloarchaea *Halobacterium halobium*, was the first microbial rhodopsin discovered (79). It functions as a proton pump through converting light energy into a proton gradient across the bacterial cell wall (80). Bacteriorhodopsin binds all-*trans*-retinal through a protonated Schiff base with Lys216 (81). The PSB is stabilized by two Asp residues through water-mediated hydrogen bonding interactions. The  $pK_a$  of this PSB was measured to be over 12 (82, 83). With the chromophore bound, bacteriorhodopsin is able to absorb at 570 nm (84). Similar rhodopsin proton pumps have been observed in systems other than Haloarchaea, including marine Archaea (euryarchaeotic rhodopsins) (85) and Bacteria (proteorhodopsin and xanthorhodopsin) (86, 87).

A similar case is halorhodopsin which is found in haloarchaea (88). Halorhodopsin functions as a chloride pump, transporting chloride ions into the cytoplasm and hyperpolarizing the cell membrane (78). In halorhodopsin, the PSB is stabilized by a tightly bound chloride ion which is translocated upon photoactivation. This unique structural feature enables the specific function of halorhodopsin. Halorhodopsin has also been found in the halophilic bacterium *Salinibacter ruber* (89).

Another major class of microbial rhodopsins consists of the sensory rhodopsins (90). The first sensory rhodopsin, sensory rhodopsin I (SRI), was discovered in a search for receptors responsible for phototaxis in the haloarchaeal prokaryote *Halobacterium salinarum* (91, 92). SRI can signal the cells to be either attracted or repelled by the light,

depending on the light-activation mechanisms. Sensory rhodopsin II (SRII) is functional only as a repellent phototaxis receptor in haloarchaea. Both SRI and SRII have been well characterized both structurally and functionally. As revealed in the atomic structure of SRII, the PSB in SRII is stabilized by water-mediated hydrogen bonding interactions with two adjacent Asp residues, Asp85 and Asp212 (93). SRII absorbs at ~500 nm, similar to the rod rhodopsin in humans. The photoactivated intermediates of SRII have also been characterized using Fourier transformed infrared spectroscopy (FTIR) (94-97). Upon activation, both SRI and SRII form 2:2 complexes in haloarchaeal membranes with their cognate transducers, HtrI and HtrII, respectively. Formation of the complexes initiates the signal relay and is now under intense investigation.

A unique sensory rhodopsin, *Anabaena* sensory rhodopsin (ASR), has been identified from the freshwater cyanobacterium *Anabaena* sp. PCC7120 (98). The crystal structure of ASR has been solved at 2.0 Å resolution (99). The overall membrane-embedded seven helical structure of ASR resembles the other haloarchaeal rhodopsins. However, there are also striking differences separating ASR from other haloarchaeal rhodopsins. First, the interior of the cytoplasmic side of ASR is rather hydrophilic, compared to other haloarchaeal rhodopsins. These hydrophilic residues are stabilized through a water-mediated hydrogen bonding network, which extends toward the cytoplasmic surface where ASR interacts with its transducer. Second, ASR exists in a mixture of both *all-trans* and *13-cis* retinal isomeric forms, with absorption maxima at 550 nm and 537 nm, respectively. Each of the two forms exhibits efficient light-induced conversion to the other, which results in the ratio of the two being dependent on the wavelength of illumination. This mechanism resembles that of the phytochrome in

plants, which led to the suggestion that ASR might be responsible for modulating chromatic adaptation in photosynthesis by triggering differential biosynthesis of light-absorbing pigments based on the quality of light.

An interesting discovery reported recently shed light on the relationship between the transport rhodopsins and the sensory rhodopsins (100). Spudich and coworkers successfully converted the bacteriorhodopsin (BR) to a SRII-like sensor by replacing three residues in BR with the corresponding residues in SRII. The resulting protein is capable of relaying the retinal photoisomerization signal to the transducer HtrII, which then induces robust phototaxis responses. This finding not only identified the key residues in determining the functions of the two proteins, but also demonstrated the elegant and yet simple design by nature to achieve functional diversity from the same protein scaffold and similar ligand-protein complexation.

#### **1.4. Color vision**

Rod rhodopsin is the most studied and best understood rhodopsin among the over 1000 visual rhodopsins discovered so far due to its importance in animal vision and also its abundance in the retina. The cone rhodopsins, however, are less understood despite their equal or even greater importance in vision. As mentioned before, rod rhodopsins are responsible for dim vision and cone rhodopsins are responsible for color vision.

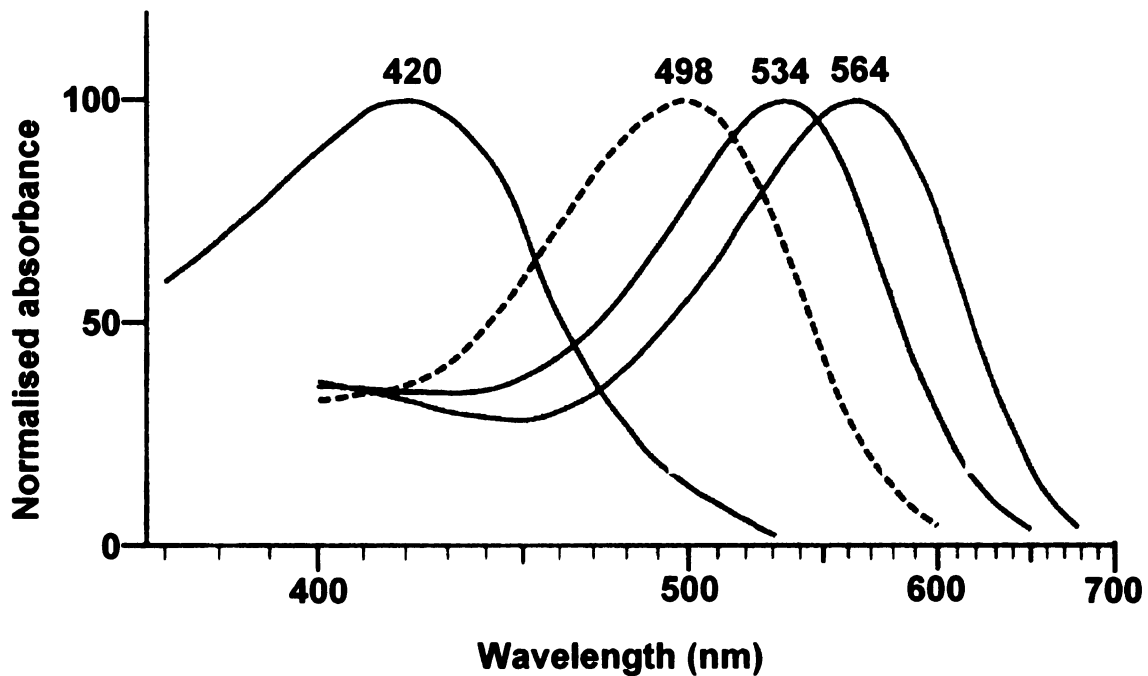


**Figure I-6. Absorption profiles of different human rhodopsins (101).**

In the human vision process, cone rhodopsins share similar photoactivation cascades as rod rhodopsins. However, the maximal sensitivities of each rhodopsin differ at different wavelengths. Human rod rhodopsin absorbs at 500 nm. The human cone rhodopsins: red, green and blue, absorb at 560 nm, 530 nm and 420 nm, respectively (102-105). All four rhodopsins exhibit red-shifted maximal absorption wavelengths after binding to the chromophore 11-*cis*-retinal, which by itself absorbs at 380 nm as a free aldehyde. The combination of the four pigments constitutes the whole 400-700 nm range, which is defined as the visible spectrum (Figure I-6).



**Table I-1. Rhodopsins of various species (106).**

Species	Cone		sensor	group (nm)	
	SWS1	SWS2	M	M/L	L
Human		420		530	560
Dog		430		555	
Horse		430		540	
Squid			470/485	500	
Black bream			475		560
Gold fish	360		450	540	625
Chicken		420	455	510	560
Peking robin	355		455	500	570
Pacific shearwater		405	450	505	565
Butterfly	360	400	450	520	610
Housefly	355		460/49	530	
Honey bee	350	445	550		

Within animals, the requirement for color vision has been met in different ways, suggesting that color vision has developed independently several times during evolution (107). Depending on the number of types of cone photoreceptors present, some degree of color vision becomes possible. Primates express three types of cone opsins, while many animals have two and some insects, birds and fish have four (108). These are described as being trichromats, dichromats and tetrachromats, respectively. As a general classification, the cone rhodopsins can be roughly grouped into the following categories: very short wavelength (i.e. UV)-sensitive (SWS1), short wavelength ("blue")-sensitive (SWS2), medium wavelength ("green")-sensitive (MWS), and long wavelength ("red")-sensitive (LWS) (106). Table I-1 shows how certain cone rhodopsins are classified based on their maximal absorption wavelengths. Apparently, most of the cone rhodopsins display red-shifted absorption maxima ( $\lambda_{\text{max}}$ ), while other cone rhodopsins are blue-shifted.

Though to different extents, the red shift of  $\lambda_{\text{max}}$  observed in most of the rhodopsins had been found to be partly due to the formation of the protonated Schiff base (PSB) between 11-*cis*-retinal and the active site lysine. The discovery of the PSB started with the isolation of retinal from rhodopsin in 1933 by Wald (109). In 1944, Morton and Goddwin showed that retinal is the aldehyde form of vitamin A (110), which was confirmed to be 11-*cis*-retinal in 1950 (111). As early as 1955, the formation of the PSB between retinal and a lysine residue in rhodopsin was proposed to account for the bathochromic shift in visual pigments. During the late 1960's, Bownds and Akhtar, through independent studies, provided evidences for the formation of a Schiff base between retinal and a lysine within rhodopsin (112, 113). It was not until 1974 that protonation of the Schiff base was unambiguously confirmed by Callender through resonance Raman studies (114).

As a free aldehyde, 11-*cis*-retinal absorbs at 380 nm. When the Schiff base is formed with *n*-butylamine, a slight blue shift in absorbance can be observed and the deprotonated Schiff base absorbs at 365 nm. However, when the Schiff base is protonated there is a significant red shift of the chromophore's absorbance to 440 nm (115, 116). With controlled concentration of the chromophore and careful choice of solvent this value may shift up to ~500 nm (117, 118). Protonation of the Schiff base alone, however, is probably not responsible for the spectral tuning in color vision as 440 nm is just the beginning of the region of the electromagnetic spectrum that we can actually see (~400 – 700 nm). The differences in the absorbance observed for different visual pigments as compared to the PSB of 11-*cis*-retinal in solution are defined as *opsin*

*shifts* and are believed to result from specific interactions of each individual opsin protein with the retinylidene chromophore (119, 120).

Several hypotheses have been proposed to explain the opsin shifts. Although progress has been made, a complete and satisfactory explanation for color vision is still missing. The following is a brief description of the hypotheses and accomplishments achieved in this field of research.

In 1958, Hubbard made the first attempt to explain the opsin shift (121). He not only suggested formation of a protonated Schiff base, but also proposed that specific electrostatic interactions between the chromophore and the protein could induce a delocalization of the PSB charge along the polyene backbone, leading to altered spectroscopic behavior of the bound chromophore. Later, in the 1970's, theoretical calculation studies suggested that a pigment protein should be able to regulate the wavelength shifts by placing polar or charged residues around the chromophore (122-126). In 1976, Honig proposed, through theoretical calculation, that the PSB is closely associated with a counterion and additional negatively charged or polar groups are positioned by the protein in the vicinity of the ring half of the chromophore (123). Later, Honig provided further support for this external point-charge model using theoretical calculations based on spectroscopic data of model compounds (123). Despite the lack of absolute validity, additional support from Nakanishi and others made this model generally accepted at the time (127-129).

The confirmation of the PSB counter anion was achieved in 1989 when three independent studies indicated that Glu113, a highly conserved residue within vertebrate visual pigments (130), functions as the counter anion in bovine rhodopsin (63-65).



red shifted pigment than the native rod rhodopsin (64). Furthermore, the effect of varying both distance and angle between the PSB and the counterion was also investigated. Sheves and coworkers synthesized a series of model compounds (Figure I-7), each adopting a unique arrangement of the PSB and a nearby carboxylate (131). The measured wavelength shifts as well as pKa values were shown to vary according to each molecule. However, the maximum difference in red shifted  $\lambda_{\text{max}}$  among these synthetic model molecules was only 10 nm, which is much smaller than the maximum difference observed between the visual pigments (133, 134). Therefore, although the position and orientation of the counterion could affect the  $\lambda_{\text{max}}$ , it could not be the cause for the whole spectrum shift in different rhodopsins.

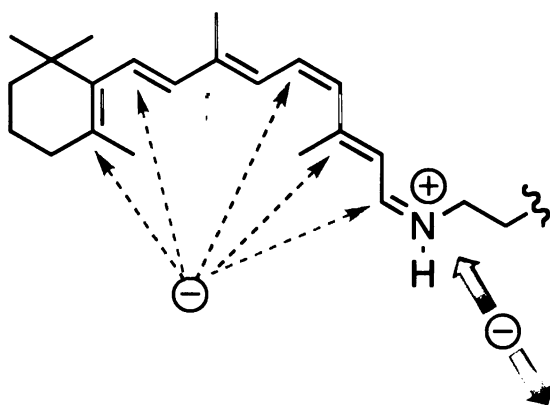


**Figure I-8. The point charge model.** Positioning negative charges at different places along the polyene chain of the chromophore may modulate the maximum absorption wavelength.

As discussed earlier Honig suggested in 1976 that additional charged or polar residues are placed close to the polyene chain (123). Following this hypothesis Nathans

suggested, by examining and comparing the gene sequences of all four human opsins, that the placement of different negatively charged amino acids along the polyene backbone in different proteins could result in extended or disrupted conjugation of the positive charge, which could be nature's way of tuning the wavelength (Figure I-8) (130).

In addition to the point charge theories that mostly focus on the electrostatic or polar interactions between the chromophore and the opsin protein is another series of hypotheses that emphasize the steric interactions between the two parties. An early proposal by Blatz suggested that twisting the planes about the single bonds of the chromophore would lead to different levels of conjugation and therefore wavelength regulation (Figure I-9) (135). Although the polyene system in retinal tends to adopt the planar conformation in order to achieve maximum conjugation, steric constraints in 11-*cis*-retinal in fact results in a non-planar molecule. NMR studies had shown that the C6-C7 single bond of 11-*cis*-retinal bound in rhodopsin adopts a *cis*-like conformation, namely 6-*S-cis* (128). Further investigation of the system revealed that, due to the steric interactions between the C5-Me and C8-H, the 6-*S-cis* conformation is indeed twisted to be non-planar. A similar situation is suggested for the non-planar 12-*S-trans* conformation, where the steric interaction between C13-Me and C10-H forces a twisting in the C12-C13 single bond (136, 137). According to this theory, red rhodopsin should adopt the retinal in a more planar conformation, optimizing the orbital overlap and leading to a more red-shifted  $\lambda_{\text{max}}$ . However, theoretical studies combined with NMR have also shown that the induced degree of conjugation does not appear to be solely responsible for the opsin shifts (138).

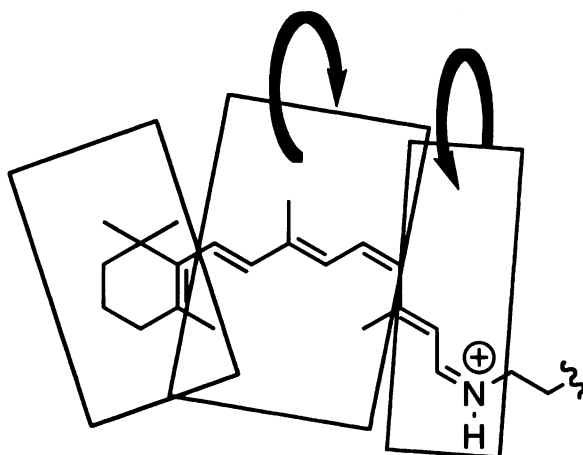


**Figure I-9. Hypothesis of steric interactions leading to wavelength regulation.** Twisting the single bonds will reduce the degree of conjugation and therefore lead to different absorption maxima.

Another hypothesis in explaining the opsin shift involves excitonic coupling between the chromophore's excited states and nearby aromatic residues. Based on mathematical analysis of the excited state energies of 11-*cis*-retinal, the bathochromic shift in visual pigments were proposed to be caused by excitonic coupling, which could lead to the formation of superconducting pairs in the pigments (9). Light-induced perturbation of aromatic residues in bovine rhodopsins and bacteriorhodopsins (139) as well as photoexcited energy transfer in frog rhodopsins (11) were observed in support of the existence of such coupling. Recent spectral studies demonstrated the presence of excitonic coupling between retinal and tryptophan residues in the visual pigments. The coupling induced by alignment of dipole moments of the chromophore and a nearby tryptophan has been suggested to be responsible for driving the torsional motion of the chromophore and leading to the *cis-trans* isomerization (12). However, no correlation between the excitonic coupling and spectral tuning in the visual pigments has been observed.

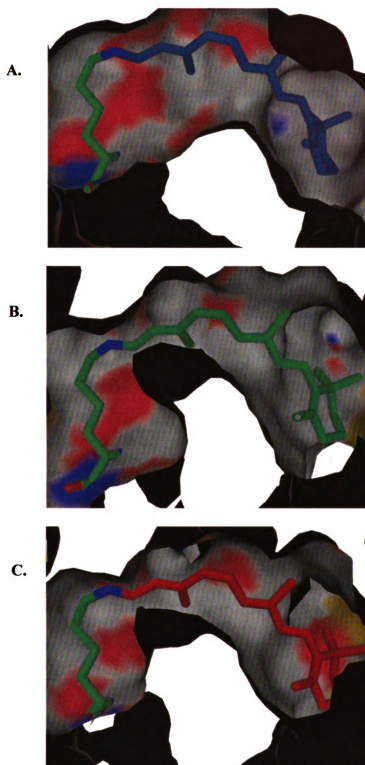


**Figure I-10. Vicinity of retinal in cone pigments as shown in the homology models (140). Charged amino acids are indicated in red. (A) Blue cone pigment; (B) Green; (C) Red.**



The determination of the first crystal structure of bovine rod rhodopsin in 2000 by Palczewski marked one of the most remarkable milestones in the field (28). This 2.8 Å structure not only provided absolute evidence for many previous results and suggestions, but also paved the way for future research on other visual pigments. Continued efforts on the crystallography of rhodopsin has since yielded improved resolutions as good as 2.2 Å (62).

As shown in Figure I-5B, the formation of the PSB between 11-*cis*-retinal and Lys296 is confirmed. Glu113 acts as the counter anion at 3.45 Å away from the PSB nitrogen. A negatively charged residue is observed to be over 5 Å away from the double bond between C11 and C12, which is further away than what is expected based on both the hypothesis of Honig and the results from related NMR studies. However, two polar residues, Thr118 and Tyr268, are found to be in the vicinity of the central part of the polyene. Twisting of the single bonds is also observed, suggesting the contribution from the steric-induced non-planarity of the chromophore on wavelength regulation. The double bond between C11 and C12 has also been shown to adopt a twisted conformation as revealed by the 2.2 Å-resolution structure, which is consistent with the predictions based on theoretical calculations. Furthermore, Trp265 is found in the structure to be near the ionone ring as well as the C13-Me of the chromophore, suggesting possible excitonic coupling effects.

The determination of the crystal structure also led to construction of homology models for the three human cone pigments using the rod rhodopsin structure as a template (140). The amino acid sequence identities for the blue, green and red cone pigments with rhodopsin are 41%, 38% and 37%, respectively. According to the homology models, the

secondary structures of all three cone opsins are nearly identical to that of the rod rhodopsin, exhibiting a seven helical transmembrane portion together with one cytoplasmic helix and two beta strands. The only difference, the same for all three cone opsins, is the one-amino-acid extension at the N-terminal  $\beta$  strand. Similar to rod rhodopsin, the retinal binding environment is highly hydrophobic in all three cone rhodopsins (Figure I-10). Red and green rhodopsins share almost identical binding probably due to their high homology (96% homologous, differ by only 15 amino acids) (130). Both contain a Trp182 in the vicinity of the central part of the polyene. The two opsins also share an additional glutamate at 102, besides the counter anion Glu129 that is analogous to Glu113 in rod rhodopsin. The blue opsin, however, displays a much different arrangement of amino acids around the retinal. As shown in the model, the central residue forming the cavity in the blue cone pigment is Tyr262. Because of its proximity to the retinal  $\beta$ -ionone ring, Tyr262 is believed to be the major factor in the blue shift of this pigment. The additional glutamate observed in red and green rhodopsin models is missing in the blue pigment model structure, which is suggested to be responsible for additional blue shift of the  $\lambda_{\max}$ .

In fact, prior to the rhodopsin crystal structure, mutational studies involving specific key residues in visual pigments also yielded very interesting results. Inspired by the high sequence homology between red and green rhodopsins, Oprian and coworkers showed that the red cone can be converted into a green-rhodopsin-like pigment by implanting seven specific mutations, S116Y:S180A:I230T:A233S:Y277F:T285A:Y309F (Figure I-11) (102). The artificial pigment is able to constitute a nearly 40 nm shift in the  $\lambda_{\max}$ . Within the seven sites, three were identified to play more significant roles in the spectrum

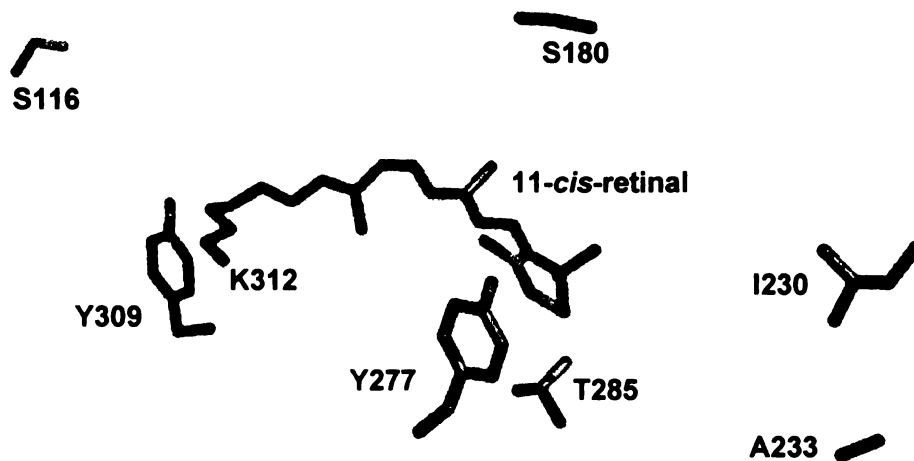


**Figure I-11. Illustration of the sites of mutations for converting the red rhodopsin to a green-rhodopsin-like pigment (102).**

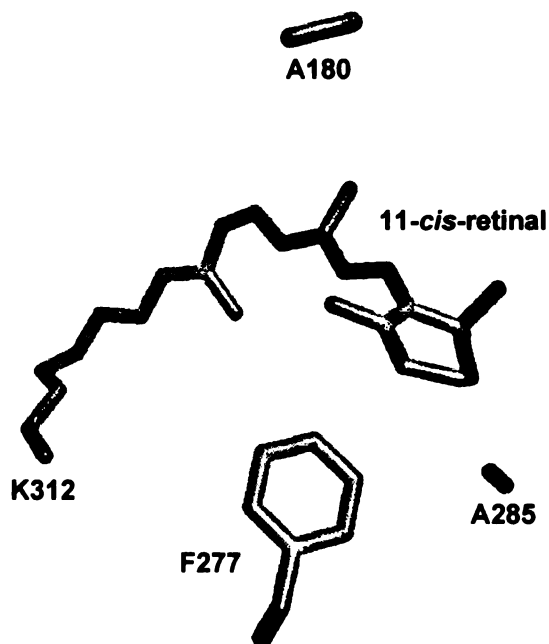


**Figure I-12. Illustration of the sites of mutations for converting the green rhodopsin to a red-rhodopsin-like pigment (141).**

tuning. A triple mutant of the green opsin, F277Y:A285T:A180S (Figure I-12), is able to account for a majority of the red shift, going from green rhodopsin to a red-rhodopsin-like pigment (*141*). Interestingly, all three mutations are in fact conversions from hydrophobic residues to polar residues around the beta-ionone ring of the chromophore. A similar trend was also observed in mutagenesis studies of the rod rhodopsin. A rod rhodopsin mutant, F261Y:A269T:A164S (Figure I-13), red shifts to 520 nm, achieving an amazing 200 nm red shift (*142*).

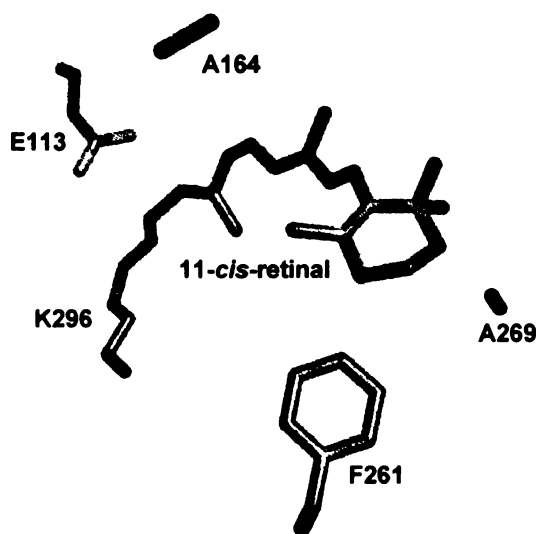


**Figure I-13. Illustration of the sites of mutations for converting the rod rhodopsin to a red-shifted pigment (*142*).**

In recent years, quantum mechanics (QM) combined with molecular mechanics (MM) (denoted as QM/MM) techniques have been used intensively in studying the spectral tuning in the visual pigments (*143*). Electrostatic interactions have been suggested to affect the wavelength shifts between different rhodopsins due to the fact that

the HOMO-LUMO transition is actually an intramolecular electron transfer from the ionone ring to the PSB (144-147). The charge distributions within the 11-*cis*-retinilidene were shown to be different for the ground states and excited states (148).

In a most recent study done by Nakatsuji and co-workers, QM/MM calculations were performed based on the homology models of the cone pigments. The results suggested that the color tuning is regulated by amino acids at specific positions (145). More specifically, a common Ser (186 in rod rhodopsin) was shown to discriminate human blue rhodopsins from other human rhodopsins presumably due to its unique orientation relative to the  $\pi$  system of the chromophore. In the human red rhodopsin, Tyr277 and Thr285 (replacing Phe and Ala, respectively, in other human rhodopsins), were shown to provide negative electrostatic potential around the ionone ring, which differentiates the red human rhodopsins from other rhodopsins.

Studies from Goddard and co-workers, however, indicated that conformational twisting is what causes major blue shift of the absorption maxima in blue pigments (149). They also suggested the red-shifting role of dipolar side chains in the binding pocket as a fine adjustment to the opsin shift. Besides, electronic polarization effects of the protein environment were also suggested to play a predominant role in causing bathochromic shifts in bacteriorhodopsins (150, 151).

In addition, a counterion switch mechanism was proposed by Mathies and co-workers (152). Glu113 was shown earlier to be the counterion that stabilizes the PSB in the ground state. Mutation E181Q resulted in nearly unchanged Raman vibrational spectra in the ground state. However, it was shown that the same E118Q mutation led to a dramatic shift of the  $pK_a$  of the PSB in the metarhodopsin II state. Mathies then

proposed that a counterion switch occurs within the photoactivation process through a proton transfer from Glu181 to Glu113. This is accompanied by a specific conformational change of the rhodopsin protein, leading to its activation. This model has been validated by several theoretical calculations (153, 154). Such mechanism is possibly responsible for the shifted absorption maxima observed for certain photo intermediates.

In conclusion, environmental differences around the ionone ring and the PSB of the bound chromophore among different visual pigments seem to play major roles in the wavelength regulation mechanism. Other factors, including distortion of the planar conformation of retinal as well as excitonic coupling, might also contribute to the wavelength changes. The real spectrum tuning mechanism very possibly is achieved by a combination of these factors. The wavelength regulation mechanism is indeed much more complicated than anticipated. Alternative approaches are therefore desired in trying to provide a clearer picture of the mechanism.

### ***1.5. Designing CRABPII mutants as rhodopsin mimics***

As concluded above, the hypotheses regarding the wavelength regulation in visual pigments need to be further tested. However, difficulties associated with working with the membrane-bound protein rhodopsins, such as complication in mutagenesis, low heterologous expression level, and difficulties in obtaining 3-D structures, still pose

problems. This is why our research team opted for a model system that can be used to elucidate the wavelength regulation mechanism.

Our goal is to develop a model protein that mimics rhodopsin in the binding of the chromophore, retinal. Through protein engineering techniques, we created different situations for the bound retinal, such as placing charged or polar residues at various positions along the chromophore backbone, introducing steric interactions to force the non-planarity of the molecule, or placement of aromatic residues in the vicinity of the chromophore. For this particular purpose, this protein mimic should first show good affinity for retinal and also be very tolerant towards mutagenesis. Additionally, this system should also be more friendly than rhodopsin in heterologous expression, purification and crystallization, which would facilitate the determination of the 3-D structures and therefore provide valuable information in terms of both binding details and directions for future rational redesign.

### **1.5.1. CRABP II general background.**

Retinoic acid (RA), the biologically active metabolite of vitamin A, functions as a morphogen during embryonic morphogenesis (155) and has been suggested to play an indispensable role in regulating cell differentiation and growth (156-158). RA and synthetic retinoids have been used successfully for treatment of acute promyelocytic leukemia (APL), skin disorders, and epithelial malignancies, such as skin cancer and cervical cancer (155, 158-163).

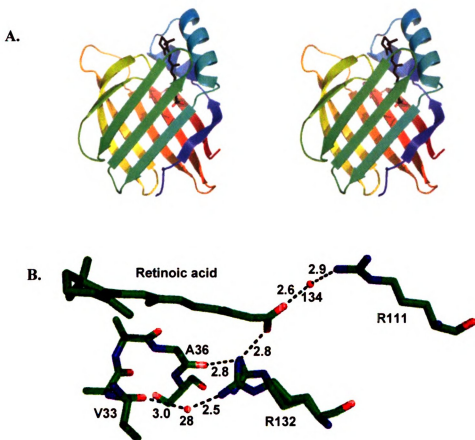


**Figure I-14. Crystal structure of retinoic acid bound in WT-CRABP II (164).** A. Stereoview of the overall fold of the protein; B. Binding of retinoic acid in the active site.

RA exerts its regulatory function in the nucleus by association with the transcriptional activator, retinoic acid receptor (RAR) (155, 165-170). Upon complexation with RA, the RAR/RXR (retinoid X receptor) heterodimer recognizes the RA-response elements (RARE) in the promotor region of certain genes and regulates their transcription.

The association of RA to RAR is facilitated by cellular retinoic acid binding proteins, CRABPI and CRABP II (171-174). CRABPs belong to the intracellular Lipid Binding Protein (iLBP) family and are present in virtually all vertebrates (175). The



overexpression of CRABPs has been reported in a wide variety of human cancers, suggesting important roles in cancer development (176-183). CRABPs specifically bind to RA and modulate its cellular concentration in the cytoplasm. The RA delivery mechanism has been suggested to be different between CRABPI and CRABPII. While CRABPI shows no evidence of interacting with RAR, CRABPII shuttles RA to RAR through direct protein-protein interaction (184, 185). Nuclear localization of CRABPII, but not CRABPI, upon ligand binding has also been observed, providing further evidence for its interaction with the nuclear receptor RAR (186).

Recently we reported the first crystal structure of apo-WT CRABPII (187). The crystal structure of WT-CRABPII•RA has been reported previously by other groups (188), however a higher resolution structure of this complex (Figure I-14), determined at 1.48 Å, is now available (187). In the latter work, using three different data sets collected on apo-WT CRABPII we showed that apo- and holo-CRABPII share very similar structures. Binding of RA appeared to increase the overall rigidity of the structure, although the induced structural changes were not as pronounced as previously thought (189). The enhanced structural rigidity may be an important determinant for the enhanced nuclear localization of the RA-bound protein. Interestingly, water-mediated interactions are observed in the cavity of apo-WT-CRABPII MolA, connecting the Arg111 deep inside the cavity through Arg132 to Ala36 and Val33 both located on the  $\alpha$ 2 helix (Figure I-15). The water-mediated network is not observed in MolB probably due to crystal packing. The difference in crystal packing environments between MolA and MolB at the  $\alpha$ 2 helix region is significant (Figure I-16), which is apparent from the number of intermolecular interactions that each  $\alpha$ 2 helix makes with the neighboring

molecules: MolA has 0 hydrogen bond and 8 vdw contacts and MolB has 7 hydrogen bonds and 43 vdw contacts.

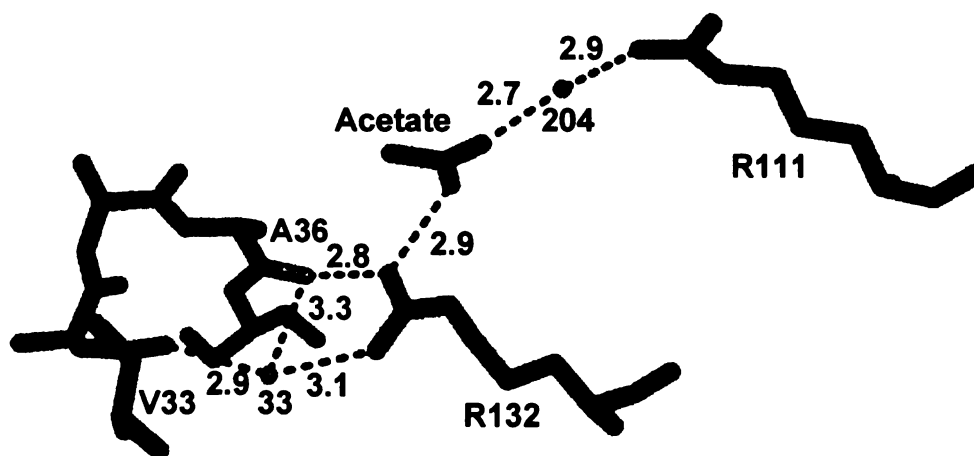


**Figure I-15. Water-mediated hydrogen bonding interactions observed in the molecule A of the apo-WT-CRABPII crystal structure (164).**

Similar water-mediated networks have been observed in other members of the iLBP family, such as CRABPI (190) and intestinal fatty acid-binding protein (191), and were suggested to play important roles in maintaining the stability of these proteins as well. In the rat intestinal fatty acid-binding protein (FABP) structure (1IFC, 1.2 Å), the water-mediated network connects the Arg106 (conserved residue of Arg111 in CRABPII) through Arg126 (conserved residue of Arg132 in CRABPII) to Asp34 and Ala32 on the  $\alpha$ 2 helix at the portal. In the CRABPI structure (1CBI), the network is observed in part, but the lower resolution of the structure (2.7 Å) probably leads to an incomplete observation of all the ordered water molecules in the cavity. In the high resolution structure of cellular retinol-binding protein II (CRBP II, 1.2 Å, PDB ID: 2RCQ), which is also an iLBP family member, the water-mediated network is again observed, which also

resembles the one in apo-WT-CRABP II. In the apo-CRBP II structure, the network starts at the Glu108 (conserved residue of Arg111 in CRABP II based on similarity) and extends to Ala36 and Val33 (both conserved in CRABP II based on identity). These observations further emphasize the structural importance of these water-mediated networks for the iLBP family proteins.

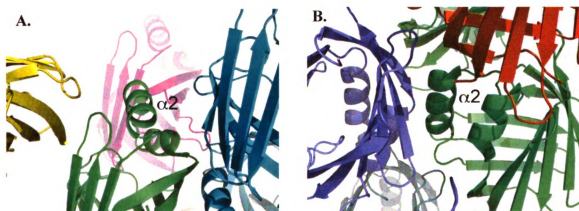


**Figure I-16. Crystal packing observed in the structure of apo-WT-CRABP II.** A. Molecule A; B. Molecule B.

### 1.5.2. Designing CRABP II mutants as rhodopsin mimics.

CRABP II was chosen as our model protein for mimicking rhodopsin. First, all-*trans* retinoic acid, the natural substrate of CRABP II, resembles retinal that is bound in rhodopsin. This similarity therefore eases our way in introducing retinal into our model systems, minimizing the risks in redesigning an entire binding site. Second, CRABP II is a small and soluble protein that is easily expressed and purified in large quantities using

recombinant expression systems, which represents a huge advantage over the membrane-bound rhodopsin. Third, CRABP II and other iLBP family proteins are well known for their excellent tolerance of multiple mutations (192). The stability of CRABP II in the presence of multiple mutations provides us additional freedom in introducing mutations for protein redesign. Fourth, CRABP II mutants can be readily crystallized routinely using established conditions, leading to three-dimensional structures usually at atomic resolution (189, 193, 194). This feature contrasts drastically with that of rhodopsin, which is more difficult to crystallize. The excellent tendency of CRABP II toward crystallization gives us routine access to detailed structural information, leading to more rapid data acquisition/analysis.

Previously, through rational design, CRABP II mutants were obtained that were capable of forming protonated Schiff bases (PSB) between *all-trans*-retinal (Rt) and an active site lysine introduced through site-directed mutagenesis (195, 196). A triple mutant, R132K:R111L:L121E (KLE), is of particular interest due to its excellent ability to shift the absorption maxima of the chromophore as well as its nanomolar dissociation constant toward Rt (Figure I-17) (196). Besides the active site Lys132, it has been proven that the Glu121 that provides the counterion stabilization for the PSB is also required for the bathochromic shift. The mutation of Arg to Leu at position 111 is also required in that an ordered water molecule is removed upon this mutation, which helps place the aldehyde group of Rt in a favorable position for nucleophilic attack and eventually leads to PSB formation.

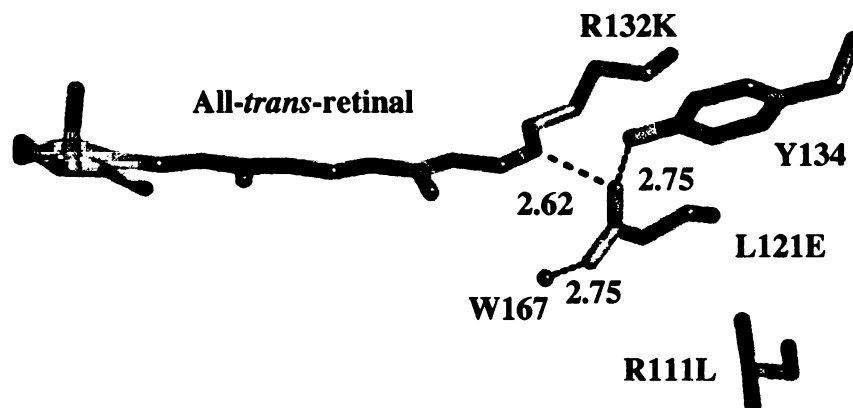


**Figure I-17. All-*trans*-retinal bound in KLE-CRABP II (196).**

The triple mutant KLE-CRABP II served as a great example, demonstrating the importance of formation of the PSB as well as a stabilizing counter anion nearby. However, although the red shift to 447 nm observed for the *all-trans*-retinal-bound KLE-CRABP II complex is impressive, the mechanism identified within it does not seem to fully explain the wavelength regulation. As shown earlier, the PSB formed between retinal and n-butylamine absorbs at 440 nm and the red cone rhodopsin absorbs at 564 nm. Apparently, other mechanisms besides the PSB formation and the counter anion interaction must be functioning in order to achieve the dramatic red shift in red rhodopsin. Our next mission then is to further engage our model system into testing the hypotheses proposed for the wavelength regulation mechanism in color vision. Most recent work in this project features manipulation of the absorption maxima of rationally designed CRABP II mutants when bound to a shorter retinal analog, C<sub>15</sub>-aldehyde.

Chapter II of this dissertation details about the X-ray crystallographic studies of such C<sub>15</sub>-aldehyde-CRABPII mutant complexes. Chapter II also includes brief descriptions of the results from the biochemical studies performed by other colleagues. Chapter III describes the structural insights derived from the crystal structures of the holo-CRABPII mutants in terms of structural integrity upon mutations and the structural role of the water-mediated network. Chapter IV describes an effort that we took toward understanding the direct channeling of retinoic acid from CRABPII to RAR through protein-protein interactions.

### ***1.6. Cellular retinaldehyde-binding protein and the 11-cis-retinal regeneration.***

Cellular retinaldehyde binding protein (CRALBP) is a water-soluble protein found in the retina and pineal gland (197). This 36 KD protein is remarkably stereoselective, carrying as endogenous ligands 11-*cis*-retinol and 11-*cis*-retinaldehyde (11-*cis*-retinal) that are only known to function in vision. Notably, 11-*cis*-retinal bound to CRALBP is less susceptible to photo-isomerization than when bound to rhodopsin (198). Mouse knockout studies have shown that CRALBP gene defects impair regeneration of visual pigments (199).

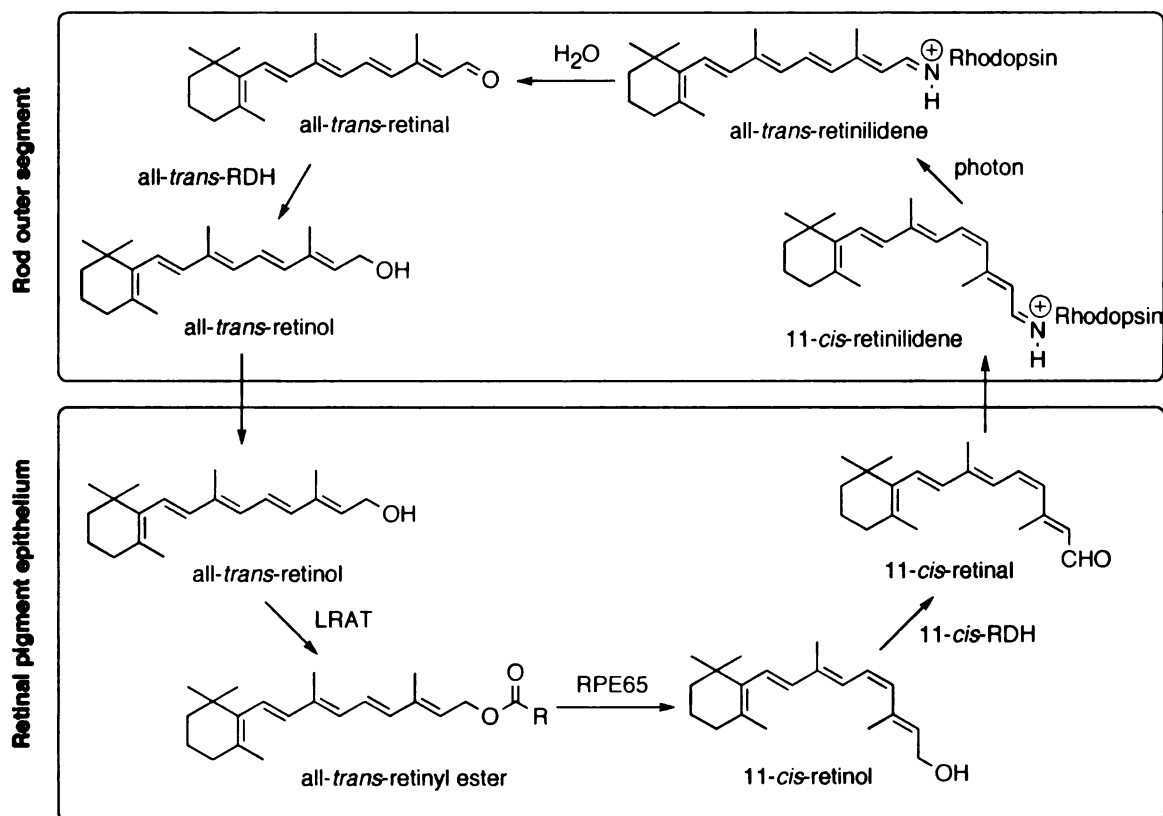


**Figure I-18. The visual cycle.**

Retinoids undergo intercellular transport and several enzymatic transformations during the course of the visual cycle (Figure I-18). *All-trans*-retinal, the product of visual cycle bleaching, is reduced to *all-trans*-retinol within photoreceptor cells and transported through an extra-cellular compartment to the retinal pigment epithelium (RPE) where it is esterified by lecithin-retinol acyltransferase (LRAT) and then isomerized to *11-cis*-retinol by the isomerohydrolase (RPE65). A dehydrogenase-mediated oxidation in RPE in mammals produces *11-cis*-retinal, which must then traverse the extracellular compartment to gain access to the photoreceptors where regeneration of visual pigments occurs. CRALBP functions in retinal pigment epithelium (RPE) as a major acceptor of *11-cis*-retinol in the isomerization step of the rod visual cycle. It also serves as a

substrate carrier for 11-*cis*-retinol dehydrogenase (RDH5), facilitating the oxidation of 11-*cis*-retinol to 11-*cis*-retinal (197, 198, 200-203). Direct CRALBP interactions have been demonstrated *in vitro* with 11-*cis*-retinol dehydrogenase and with ERM (ezrin, radixin, moesin)-binding phosphoprotein 50 (EBP50), also known as sodium hydrogen exchanger regulator factor type 1 (NHERF-1) (204). Interactions with EBP50 have been suggested as a mechanism for localizing CRALBP to the apical RPE plasma membrane for export of 11-*cis*-retinal to the adjacent rod photoreceptor cells for visual pigment regeneration. Ongoing proteomic studies also support the existence of a RPE retinoid processing protein complex containing CRALBP (205).

Due to the lack of crystal structures of this protein, the interaction of human recombinant CRALBP (rCRALBP) with retinoids has been investigated by other methods. Based on preliminary NMR studies (206), Crabb and co-workers first targeted Met and Trp residues as important sites for retinoid interaction (203). They created five mutants, M208A, M222A, M225A, W165F, W244F, and evaluated retinoid binding properties and substrate carrier functions. It turned out that all mutants bound 11-*cis*-retinal and 9-*cis*-retinal and therefore were not grossly misfolded. However, altered UV-visible spectra and lower retinoid binding affinities were observed, supporting modified ligand interactions. Altered kinetic parameters were also observed for RDH5 oxidation of 11-*cis*-retinol bound to rCRALBP mutants M222A, M225A, and W224F, suggesting impaired substrate carrier function. Heteronuclear single quantum correlation NMR analyses confirmed localized structural changes upon photoisomerization of rCRALBP-bound 11-*cis*-retinal and demonstrated ligand-dependent conformational changes for residues Met-208, Met-222, Trp-165, and Trp-244. From this study, all five residues



(Met-208, Met-222, Met-225, Trp-165, and Trp-244) have been implicated to be components of the rCRALBP ligand binding cavity.

Later, Crabb and co-workers further investigated the binding cavity using photoaffinity labeling and hydrogen/deuterium exchange (207). Photo-induced covalent labeling employing synthetic ligand 3-diazo-4-keto-11-*cis*-retinal, followed by LC-MS analysis, successfully identified eight residues being photoaffinity-modified: Tyr-179, Phe-197, Cys-198, Met-208, Lys-221, Met-222, Val-223, and Met-225. Among these eight, three of them (Met-208, Met-222, and Met-225) had already been identified in their previous investigation. In addition, topological analysis of apo- and holo-rCRALBP by hydrogen/deuterium exchange and mass spectrometry demonstrated that residues 198~255 incorporated significantly less deuterium when the retinoid binding pocket is occupied with 11-*cis*-retinal (203). This further confirmed that the identified residues were inside the retinoid binding pocket of rCRALBP.

Based on sequence information, CRALBP has been classified as a member of the CRAL-TRIO lipid-binding protein family (Pfam entry: PF00650) (208). Crystal structures have been determined for three CRAL-TRIO lipid-binding proteins, including human  $\alpha$ -tocopherol transfer protein (ATTP) (209, 210), yeast Sec14, a phosphatidylinositol-binding protein (211), and human supernatant protein factor (SPF) (212). CRALBP shares 20~33% sequence identity and ~50% homology with these three proteins. Structure models of CRALBP have been built based on the available crystal structures of the three family members (207, 213). Both open and closed conformation models have been produced (Figure I-19). The model of the closed conformation agreed well with the residues identified earlier, which are involved in interactions with retinoid.

It has also been suggested based on MD simulations of the model that the open conformation of CRALBP participates in the ligand association and dissociation processes; the closed form serves as a relatively stable carrier of retinoids, protecting them from the cellular hydrophilic environment.

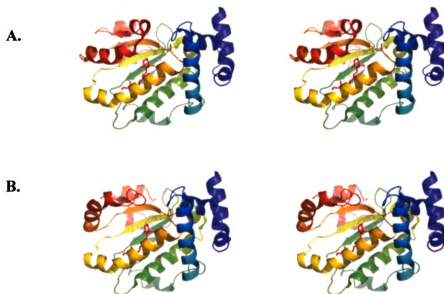


**Figure I-19. Stereoview of the structure models built for CRALBP (213).** A. Closed form; B. Open form. N-terminal starts from 66 (blue) in the rainbow presentations.

Despite all the efforts of elucidating the structural mechanism of CRALBP interacting with retinoids, the lack of a crystal structure still poses serious problems for research associated with CRALBP. More reliable answers are needed for questions like how retinoid is released from the high affinity CRALBP binding cavity, which remains an unresolved but important issue for understanding how 11-*cis*-retinal is exported from the RPE for visual pigment regeneration. Besides that, the function of CRALBP in tissues other than the RPE remain to be determined (i.e. in retinal Müller cells, ciliary

epithelium, iris, cornea, pineal gland, and a subset of oligodendrocytes of the optic nerve and brain). To answer these questions, determination of the three-dimensional structure of CRALBP will be essential.

In addition to elucidating the physiological role of CRALBP, another reason that we are interested in determining the crystal structure of CRALBP is its potential as a model for rhodopsin. As discussed earlier, the qualifications of a good rhodopsin mimic should include affinity for retinoids, ease in molecular biology manipulations, high expression levels, great solubility, and routine access to high-resolution crystal structures. CRALBP fits in almost all categories except for the crystal structures. Beyond these features, CRALBP is superior over CRABP II in mimicking rhodopsin in that retinal in CRALBP is completely buried as in rhodopsin, while in CRABP II the ionone ring of the chromophore is partially solvent-exposed. With these two reasons, we are driven to pursue the crystallization of CRALBP. Chapter V details about our effort toward obtaining the first crystal structure of CRALBP.

## Reference

1. Wade, N. J. (1998) *A Natural History of Vision*, Bradford Books.
2. Woodbridge, F. J. E. (1983) *Aristotle's Vision of Nature*, Greenwood Press Reprint.
3. Kepler, J., and Donahue, W. H. (2000) *Optics*, Green Lion Press.
4. Newton, I., Cohen, B. J., Einstein, A., and Whittaker, E. (1952) *Opticks: Or a Treatise of the Reflections, Refractions, Inflections & Colours of Light-Based on the Fourth Edition London, 1730*, Dover Publications.
5. Crescitelli, F. (1977) Friedrich Wilhelm Kuhne. The Centennial of Rhodopsin, *Arch. Ophthalmol.* 95, 1766.
6. Wald, G., and Brown, P. K. (1958) Human Rhodopsin, *Science* 127, 222-226.
7. Wald, G. (1968) Molecular Basis of Visual Excitation, *Nature* 219, 800-&.
8. Wald, G. (1968) Molecular Basis of Visual Excitation, *Science* 162, 230-&.
9. Dunne, L. J. (1974) Excitonic Coupling in Visual Pigments, *Phys Lett A A* 48, 13-13.
10. Tiffany, J. M., Noorjahan, P., Abdel-Latif, A. A., Harding, J. J., Mayne, R., Brewton, R. G., and Ren, Z. X. (1997) *Biochemistry of the Eye*, Chapman and Hall, London, UK.
11. Shirane, K. (1975) Conversion of Photoexcitation Energy in Rhodopsin, *Nature* 254, 722-723.
12. Schenkl, S., van Mourik, F., van der Zwan, G., Haacke, S., and Chergui, M. (2005) Probing the ultrafast charge translocation of photoexcited retinal in bacteriorhodopsin, *Science* 309, 917-920.
13. Crescitelli, F. (1972) The visual cells and visual pigments of the vertebrate eye., in *Handbook of Sensory Physiology* (Dartnell, H. J. A., Ed.), pp 245-363, Springer-Verlag, New York , NY.
14. Wissinger, B., and Sharpe, L. T. (1998) New aspects of an old theme: The genetic basis of human color vision, *Am J Hum Genet* 63, 1257-1262.
15. Kefalov, V., Fu, Y. B., Marsh-Armstrong, N., and Yau, K. W. (2003) Role of visual pigment properties in rod and cone phototransduction, *Nature* 425, 526-531.

16. Sakurai, K., Onishi, A., Imai, H., Chisaka, O., Ueda, Y., Usukura, J., Nakatani, K., and Shichida, Y. (2007) Physiological properties of rod photoreceptor cells in green-sensitive cone pigment knock-in mice, *J Gen Physiol* 130, 21-40.
17. Shi, G., Yau, K. W., Chen, J., and Kefalov, V. J. (2007) Signaling properties of a short-wave cone visual pigment and its role in Phototransduction, *J Neurosci* 27, 10084-10093.
18. Pugh, E. N. (2001) Rods are rods and cones cones, and (never) the twain shall meet, *Neuron* 32, 375-376.
19. Hoffmann, R. (1995) *The Same and Not the Same*, Columbia University Press, New York, NY.
20. Bennett, N., Michelvillaz, M., and Kuhn, H. (1982) Light-Induced Interaction between Rhodopsin and the Gtp-Binding Protein Metarhodopsin-Ii Is the Major Photoproduct Involved, *Eur J Biochem* 127, 97-103.
21. Borhan, B., Souto, M. L., Imai, H., Shichida, Y., and Nakanishi, K. (2000) Movement of retinal along the visual transduction path, *Science* 288, 2209-2212.
22. Emeis, D., Kuhn, H., Reichert, J., and Hofmann, K. P. (1982) Complex-Formation between Metarhodopsin-Ii and Gtp-Binding Protein in Bovine Photoreceptor-Membranes Leads to a Shift of the Photoproduct Equilibrium, *Febs Lett* 143, 29-34.
23. Kliger, D. S., and Lewis, J. W. (1995) Spectral and kinetic characterization of visual pigment photointermediates, *Israel J Chem* 35, 289-307.
24. Kliger, D. S., Lewis, J. W., and Szundi, I. (1999) Time-resolved spectroscopy of visual pigment intermediates., *Abstr Pap Am Chem S* 217, U323-U323.
25. Souto, M. L., Borhan, B., and Nakanishi, K. (2000) Low-temperature photoaffinity labeling of rhodopsin and intermediates along transduction path, *Vertebrate Phototransduction and the Visual Cycle, Pt B* 316, 425-435.
26. Collins, F. D. (1953) Rhodopsin and indicator yellow, *Nature* 171, 469-472.
27. Morton, R. A., and Pitt, G. A. J. (1955) Rhodopsin. IX. pH and the hydrolysis of indicator yellow., *Biochem. J.* 59, 128-134.
28. Palczewski, K., Kumasaka, T., Hori, T., Behnke, C. A., Motoshima, H., Fox, B. A., Le Trong, I., Teller, D. C., Okada, T., Stenkamp, R. E., Yamamoto, M., and Miyano, M. (2000) Crystal structure of rhodopsin: A G protein-coupled receptor, *Science* 289, 739-745.
29. Rando, R. R. (1996) Polyenes and vision, *Chem Biol* 3, 255-262.

30. Shichida, Y., Matuoka, S., and Yoshizawa, T. (1984) Formation of Photorhodopsin, a Precursor of Bathorhodopsin, Detected by Picosecond Laser Photolysis at Room-Temperature, *Photobioch Photobiop* 7, 221-228.
31. Shieh, T., Han, M., Sakmar, T. P., and Smith, S. O. (1997) The steric trigger in rhodopsin activation, *J Mol Biol* 269, 373-384.
32. Yan, B., Nakanishi, K., and Spudich, J. L. (1991) Mechanism of Activation of Sensory Rhodopsin-I - Evidence for a Steric Trigger, *P Natl Acad Sci USA* 88, 9412-9416.
33. Detwiler, P. (2002) Open the loop: Dissecting feedback regulation of a second messenger transduction cascade, *Neuron* 36, 3-4.
34. Graykeller, M. P., and Detwiler, P. B. (1994) The Calcium Feedback Signal in the Phototransduction Cascade of Vertebrate Rods, *Neuron* 13, 849-861.
35. Schnetkamp, P. P. M. (1995) How Does the Retinal Rod Na-Ca+K Exchanger Regulate Cytosolic-Free Ca<sup>2+</sup>, *J Biol Chem* 270, 13231-13239.
36. Abdulaev, N. G., and Ridge, K. D. (1998) Light-induced exposure of the cytoplasmic end of transmembrane helix seven in rhodopsin, *P Natl Acad Sci USA* 95, 12854-12859.
37. Farrens, D. L., Altenbach, C., Yang, K., Hubbell, W. L., and Khorana, H. G. (1996) Requirement of rigid-body motion of transmembrane helices for light activation of rhodopsin, *Science* 274, 768-770.
38. Konig, B., Welte, W., and Hofmann, K. P. (1989) Photoactivation of Rhodopsin and Interaction with Transducin in Detergent Micelles - Effect of Doping with Steroid Molecules, *Febs Lett* 257, 163-166.
39. SHI, W., Osawa, S., Dickerson, C. D., and Weiss, E. R. (1995) Rhodopsin Mutants Discriminate Sites Important for the Activation of Rhodopsin Kinase and G(T), *J Biol Chem* 270, 2112-2119.
40. Ernst, O. P., Hofmann, K. P., and Sakmar, T. P. (1995) Characterization of Rhodopsin Mutants That Bind Transducin but Fail to Induce Gtp Nucleotide Uptake - Classification of Mutant Pigments by Fluorescence, Nucleotide Release, and Flash-Induced Light-Scattering Assays, *J Biol Chem* 270, 10580-10586.
41. Franke, R. R., Sakmar, T. P., Graham, R. M., and Khorana, H. G. (1992) Structure and Function in Rhodopsin - Studies of the Interaction between the Rhodopsin Cytoplasmic Domain and Transducin, *J Biol Chem* 267, 14767-14774.
42. Onrust, R., Herzmark, P., Chi, P., Garcia, P. D., Lichtarge, O., Kingsley, C., and Bourne, H. R. (1997) Receptor and beta gamma binding sites in the alpha subunit of the retinal G protein transducin, *Science* 275, 381-384.

43. Granovsky, A. E., Natochin, M., and Artemyev, N. O. (1997) The gamma subunit of rod cGMP-phosphodiesterase blocks the enzyme catalytic site, *J Biol Chem* 272, 11686-11689.
44. Stryer, L. (1996) Vision: From photon to perception, *P Natl Acad Sci USA* 93, 557-559.
45. Leskov, I. B., Klenchin, V. A., Handy, J. W., Whitlock, G. G., Govardovskii, V. I., Bownds, M. D., Lamb, T. D., Pugh, E. N., and Arshavsky, V. Y. (2000) The gain of rod phototransduction: Reconciliation of biochemical and electrophysiological measurements, *Neuron* 27, 525-537.
46. Birge, R. R. (1990) Nature of the Primary Photochemical Events in Rhodopsin and Bacteriorhodopsin, *Biochim Biophys Acta* 1016, 293-327.
47. Pepe, I. M. (2001) Recent advances in our understanding of rhodopsin and phototransduction, *Progress in Retinal and Eye Research* 20, 733-759.
48. Rieke, F., and Baylor, D. A. (1998) Origin of reproducibility in the responses of retinal rods to single photons, *Biophys J* 75, 1836-1857.
49. Lamb, T. D. (1996) Gain and kinetics of activation in the G-protein cascade of phototransduction, *P Natl Acad Sci USA* 93, 566-570.
50. Miki, N., Keirns, J. J., Marcus, F. R., Freeman, J., and Bitensky, M. W. (1973) Regulation of Cyclic Nucleotide Concentrations in Photoreceptors - Atp-Dependent Stimulation of Cyclic Nucleotide Phosphodiesterase by Light, *P Natl Acad Sci USA* 70, 3820-3824.
51. Graykeller, M. P., and Detwiler, P. B. (1994) Intracellular Calcium Measurements in Isolated Rod Photoreceptors, *Invest Ophth Vis Sci* 35, 1486-1486.
52. Palczewski, K., Buczylo, J., Vanhooser, P., Carr, S. A., Huddleston, M. J., and Crabb, J. W. (1992) Identification of the Autophosphorylation Sites in Rhodopsin Kinase, *J Biol Chem* 267, 18991-18998.
53. Palczewski, K., Rispoli, G., and Detwiler, P. B. (1992) The Influence of Arrestin (48k Protein) and Rhodopsin Kinase on Visual Transduction, *Neuron* 8, 117-126.
54. Lamb, T. D., and Matthews, H. R. (1988) External and Internal Actions in the Response of Salamander Retinal Rods to Altered External Calcium-Concentration, *Journal of Physiology-London* 403, 473-494.
55. Sagoo, M. S., and Lagnado, L. (1997) G-protein deactivation is rate-limiting for shut-off of the phototransduction cascade, *Nature* 389, 392-395.
56. Bacigalupo, J., and Lisman, J. E. (1983) Single-Channel Currents Activated by Light in Limulus Ventral Photoreceptors, *Nature* 304, 268-270.

57. Lott, J. S., Wilde, J. I., Carne, A., Evans, N., and Findlay, J. B. C. (1999) The ordered visual transduction complex of the squid photoreceptor membrane, *Molecular Neurobiology* 20, 61-80.
58. Oday, P. M., Bacigalupo, J., Vergara, C., and Haab, J. E. (1997) Current issues in invertebrate phototransduction - Second messengers and ion conductances, *Molecular Neurobiology* 15, 41-63.
59. Hargrave, P. A. (1977) Amino-Terminal Tryptic Peptide of Bovine Rhodopsin - Glycopeptide Containing 2 Sites of Oligosaccharide Attachment, *Biochim Biophys Acta* 492, 83-94.
60. Hargrave, P. A., McDowell, J. H., Curtis, D. R., Wang, J. K., Juszczak, E., Fong, S. L., Rao, J. K. M., and Argos, P. (1983) The Structure of Bovine Rhodopsin, *Biophysics of Structure and Mechanism* 9, 235-244.
61. Okada, T., Fujiyoshi, Y., Silow, M., Navarro, J., Landau, E. M., and Shichida, Y. (2002) Functional role of internal water molecules in rhodopsin revealed by x-ray crystallography, *P Natl Acad Sci USA* 99, 5982-5987.
62. Okada, T., Sugihara, M., Bondar, A. N., Elstner, M., Entel, P., and Buss, V. (2004) The retinal conformation and its environment in rhodopsin in light of a new 2.2 angstrom crystal structure, *J Mol Biol* 342, 571-583.
63. Nathans, J. (1990) Determinants of Visual Pigment Absorbency - Identification of the Retinylidene Schiff-Base Counterion in Bovine Rhodopsin, *Biochemistry-US* 29, 9746-9752.
64. Sakmar, T. P., Franke, R. R., and Khorana, H. G. (1989) Glutamic Acid-113 Serves as the Retinylidene Schiff-Base Counterion in Bovine Rhodopsin, *P Natl Acad Sci USA* 86, 8309-8313.
65. Zhukovsky, E. A., and Oprian, D. D. (1989) Effect of Carboxylic-Acid Side-Chains on the Absorption Maximum of Visual Pigments, *Science* 246, 928-930.
66. RAO, V. R., Cohen, G. B., and Oprian, D. D. (1994) Rhodopsin Mutation G90d and a Molecular Mechanism for Congenital Night Blindness, *Nature* 367, 639-642.
67. Schertler, G. F. X. (1998) Structure of rhodopsin, *EYE* 12, 504-510.
68. Palczewski, K. (2006) G protein-coupled receptor rhodopsin, *Annu Rev Biochem* 75, 743-767.
69. Unger, V. M., Hargrave, P. A., Baldwin, J. M., and Schertler, G. F. X. (1997) Arrangement of rhodopsin transmembrane alpha-helices, *Nature* 389, 203-206.



70. Unger, V. M., and Schertler, G. F. X. (1995) Low-Resolution Structure of Bovine Rhodopsin Determined by Electron Cryomicroscopy, *Biophys J* 68, 1776-1786.
71. Nakamichi, H., and Okada, T. (2006) Local peptide movement in the photoreaction intermediate of rhodopsin, *P Natl Acad Sci USA* 103, 12729-12734.
72. Nakamichi, H., and Okada, T. (2006) Crystallographic analysis of primary visual photochemistry, *Angewandte Chemie-International Edition* 45, 4270-4273.
73. Ruprecht, J. J., Mielke, T., Vogel, R., Villa, C., and Schertler, G. F. X. (2004) Electron crystallography reveals the structure of metarhodopsin I, *Embo J* 23, 3609-3620.
74. Ridge, K. D., and Palczewski, K. (2007) Visual rhodopsin sees the light: Structure and mechanism of G protein signaling, *J Biol Chem* 282, 9297-9301.
75. Salom, D., Lodowski, D. T., Stenkamp, R. E., Le Trong, I., Golczak, M., Jastrzebska, B., Harris, T., Ballesteros, J. A., and Palczewski, K. (2006) Crystal structure of a photoactivated deprotonated intermediate of rhodopsin, *P Natl Acad Sci USA* 103, 16123-16128.
76. Spudich, J. L., Yang, C. S., Jung, K. H., and Spudich, E. N. (2000) Retinylidene proteins: Structures and functions from archaea to humans, *Annu Rev Cell Dev Bi* 16, 365-+.
77. Sharma, A. K., Spudich, J. L., and Doolittle, W. F. (2006) Microbial rhodopsins: functional versatility and genetic mobility, *Trends in Microbiology* 14, 463-469.
78. Spudich, J. L. (1998) Variations on a molecular switch: transport and sensory signalling by archaeal rhodopsins, *Mol Microbiol* 28, 1051-1058.
79. Oesterhe.D, and Stoecken.W. (1973) Functions of a New Photoreceptor Membrane, *P Natl Acad Sci USA* 70, 2853-2857.
80. Stoeckenius, W., and Bogomolni, R. A. (1982) Bacteriorhodopsin and Related Pigments of Halobacteria, *Annu Rev Biochem* 51, 587-616.
81. Luecke, H., Schobert, B., Richter, H. T., Cartailler, J. P., and Lanyi, J. K. (1999) Structure of bacteriorhodopsin at 1.55 angstrom resolution, *J Mol Biol* 291, 899-911.
82. Doukas, A. G., Pande, A., Suzuki, T., Callender, R. H., Honig, B., and Ottolenghi, M. (1981) On the Mechanism of Hydrogen-Deuterium Exchange in Bacteriorhodopsin, *Biophys J* 33, 275-279.
83. Ehrenberg, B., Lewis, A., Porta, T. K., Nagle, J. F., and Stoeckenius, W. (1980) Exchange Kinetics of the Schiff-Base Proton in Bacteriorhodopsin, *P Natl Acad Sci-Biol* 77, 6571-6573.

84. Degroot, H. J. M., Harbison, G. S., Herzfeld, J., and Griffin, R. G. (1989) Nuclear Magnetic-Resonance Study of the Schiff-Base in Bacteriorhodopsin - Counterion Effects on the N-15 Shift Anisotropy, *Biochemistry-Us* 28, 3346-3353.
85. Frigaard, N. U., Martinez, A., Mincer, T. J., and DeLong, E. F. (2006) Proteorhodopsin lateral gene transfer between marine planktonic Bacteria and Archaea, *Nature* 439, 847-850.
86. Balashov, S. P., Imasheva, E. S., Boichenko, V. A., Anton, J., Wang, J. M., and Lanyi, J. K. (2005) Xanthorhodopsin: A proton pump with a light-harvesting carotenoid antenna, *Science* 309, 2061-2064.
87. Beja, O., Aravind, L., Koonin, E. V., Suzuki, M. T., Hadd, A., Nguyen, L. P., Jovanovich, S., Gates, C. M., Feldman, R. A., Spudich, J. L., Spudich, E. N., and DeLong, E. F. (2000) Bacterial rhodopsin: Evidence for a new type of phototrophy in the sea, *Science* 289, 1902-1906.
88. Matsunoyagi, A., and Mukohata, Y. (1977) 2 Possible Roles of Bacteriorhodopsin - Comparative-Study of Strains of Halobacterium-Halobium Differing in Pigmentation, *Biochemical and Biophysical Research Communications* 78, 237-243.
89. Mongodin, E. F., Nelson, K. E., Daugherty, S., DeBoy, R. T., Wister, J., Khouri, H., Weidman, J., Walsh, D. A., Papke, R. T., Perez, G. S., Sharma, A. K., Nesbo, C. L., MacLeod, D., Baptiste, E., Doolittle, W. F., Charlebois, R. L., Legault, B., and Rodriguez-Valera, F. (2005) The genome of *Salinibacter ruber*: Convergence and gene exchange among hyperhalophilic bacteria and archaea, *P Natl Acad Sci USA* 102, 18147-18152.
90. Spudich, J. L. (2006) The multitasking microbial sensory rhodopsins, *Trends in Microbiology* 14, 480-487.
91. Bogomolni, R. A., and Spudich, J. L. (1982) Identification of a 3rd-Rhodopsin-Like Pigment in Phototactic Halobacterium-Halobium, *P Natl Acad Sci-Biol* 79, 6250-6254.
92. Spudich, J. A., Kuczmariski, E. R., Pardee, J. D., Simpson, P. A., Yamamoto, K., and Stryer, L. (1981) Control of Assembly of Dictyostelium Myosin and Actin-Filaments, *Cold Spring Harbor Symposia on Quantitative Biology* 46, 553-561.
93. Ren, L., Martin, C. H., Wise, K. J., Gillespie, N. B., Luecke, H., Lanyi, J. K., Spudich, J. L., and Birge, R. R. (2001) Molecular mechanism of spectral tuning in sensory rhodopsin II, *Biochemistry-Us* 40, 13906-13914.
94. Bergo, V., Spudich, E. N., Spudich, J. L., and Rothschild, K. J. (2003) Conformational changes detected in a sensory rhodopsin II-transducer complex, *J Biol Chem* 278, 36556-36562.

95. Furutani, Y., Kamada, K., Sudo, Y., Shimono, K., Kamo, N., and Kandori, H. (2005) Structural changes of the complex between pharaonis phoborhodopsin and its cognate transducer upon formation of the m photointermediate, *Biochemistry-Us* 44, 2909-2915.
96. Hein, M., Radu, I., Klare, J. P., Engelhard, M., and Siebert, F. (2004) Consequences of counterion mutation in sensory rhodopsin II of *Natronobacterium pharaonis* for photoreaction and receptor activation: An FTIR study, *Biochemistry-Us* 43, 995-1002.
97. Sudo, Y., Furutani, Y. J., Shimono, K., Kamo, N., and Hidekori, K. (2003) Hydrogen bondin alteration of Thr-204 in the complex between pharaonis phoborhodopsin and its transducer protein, *Biochemistry-Us* 42, 14166-14172.
98. Jung, K. H., Trivedi, V. D., and Spudich, J. L. (2003) Demonstration of a sensory rhodopsin in eubacteria, *Mol Microbiol* 47, 1513-1522.
99. Vogeley, L., Sineshchekov, O. A., Trivedi, V. D., Sasaki, J., Spudich, J. L., and Luecke, H. (2004) *Anabaena* sensory rhodopsin: A photochromic color 0 sensor at 2.0 angstrom, *Science* 306, 1390-1393.
100. Sudo, Y., and Spudich, J. L. (2006) Three strategically placed hydrogen-bonding residues convert a proton pump into a sensory receptor, *P Natl Acad Sci USA* 103, 16129-16134.
101. Bowmaker, J. K., and Dartnall, H. J. A. (1980) Visual Pigments of Rods and Cones in a Human Retina, *Journal of Physiology-London* 298, 501-511.
102. Asenjo, A. B., Rim, J., and Oprian, D. D. (1994) Molecular Determinants of Human Red/Green Color Discrimination, *Neuron* 12, 1131-1138.
103. Merbs, S. L., and Nathans, J. (1992) Absorption-Spectra of Human Cone Pigments, *Nature* 356, 433-435.
104. Oprian, D. D., Asenjo, A. B., Lee, N., and Pelletier, S. L. (1991) Design, Chemical Synthesis, and Expression of Genes for the 3 Human Color-Vision Pigments, *Biochemistry-Us* 30, 11367-11372.
105. Stockman, A., Sharpe, L. T., Merbs, S., and Nathans, J. (2000) Spectral sensitivities of human cone visual pigments determined in vivo and in vitro, *Vertebrate Phototransduction and the Visual Cycle, Pt B* 316, 626-650.
106. Dawson, T. L. (2006) Colour and colour vision of creatures great and small, *Coloration Technology* 122, 61-73.
107. Bowmaker, J. K. (1991) *The evolution of vertebrate visual pigments and photoreceptors*, The Macmillan Press, Houndsmills, Basingstoke, Hampshire, UK.

108. Kelber, A., Vorobyev, M., and Osorio, D. (2003) Animal colour vision - behavioural tests and physiological concepts, *Biological Reviews* 78, 81-118.
109. Wald, G. (1933) Vitamin A in the retina., *Nature* 132, 316-317.
110. Morton, R. A., and Goodwin, T. W. (1944) Preparation of retinene *in vitro.*, *Nature* 153, 405-406.
111. Wald, G., and Brown, P. K. (1950) The Synthesis of Rhodopsin from Retinene, *P Natl Acad Sci USA* 36, 84-92.
112. Akhtar, M., Blosse, D., and Dewhurst, P. (1968) Studies on vision. The nature of the retinal-opsin linkage., *Biochem. J.* 110, 693-702.
113. Bownds, D. (1967) Site of attachment of retinal in rhodopsin., *Nature* 216, 1178-1181.
114. Oseroff, A. R., and Callende, R. H. (1974) Resonance Raman-Spectroscopy of Rhodopsin in Retinal Disk Membranes, *Biochemistry-Us* 13, 4243-4248.
115. Blatz, P. E., Baumgartner, N., Balasubramaniyan, B., Balasubramaniyan, P., and Stedman, F. (1971) Wavelength regulation in visual pigment chromophore. Large induced bathochromic shifts in retinol and related polyenes., *Photochem. Photobiol.* 14, 531-549.
116. Pitt, G. A. J., Collins, F. D., Morton, R. A., and Stok, P. (1955) Rhodopsin. VIII. N-Retinyldenemethylamine, an indicator yellow analog., *Biochem. J.* 59, 122-128.
117. Blatz, P. E., Mohler, J. H., and Ahmed, W. (1991) Spectroscopic Observation of Solvent Interaction with Selected Retinal Schiff-Bases, *Photochem Photobiol* 54, 255-264.
118. Erickson, J. O., and Blatz, P. E. (1968) N-retinylidene-1-amino-2-propanol: a Schiff base analog for rhodopsin., *Vision Res.* 8, 1367-1375.
119. Motto, M. G., Sheves, M., Tsujimoto, K., Baloghnaier, V., and Nakanishi, K. (1980) Opsin Shifts in Bovine Rhodopsin and Bacteriorhodopsin - Comparison of 2 External Point-Charge Models, *J Am Chem Soc* 102, 7947-7949.
120. Nakanishi, K., Baloghnaier, V., Arnaboldi, M., Tsujimoto, K., and Honig, B. (1980) An External Point-Charge Model for Bacteriorhodopsin to Account for Its Purple Color, *J Am Chem Soc* 102, 7945-7947.
121. Hubbard, R. E. (1958) Paper 4, in *Proc. Nat. Phys. Lab. Symp. No. 8*, London.

122. Blatz, P. E., and Mohler, J. H. (1975) Effect of Selected Anions and Solvents on Electronic Absorption, Nuclear Magnetic-Resonance, and Infrared-Spectra of N-Retinylidene-N-Butylammonium Cation, *Biochemistry-Us* 14, 2304-2309.
123. Honig, B., Greenberg, A. D., Dinur, U., and Ebrey, T. G. (1976) Visual-Pigment Spectra - Implications of Protonation of Retinal Schiff-Base, *Biochemistry-Us* 15, 4593-4599.
124. Kliger, D. S., Milder, S. J., and Dratz, E. A. (1977) Solvent Effects on Spectra of Retinal Schiff-Bases .1. Models for Bathochromic Shift of Chromophore Spectrum in Visual Pigments, *Photochem Photobiol* 25, 277-286.
125. Suzuki, H., Komatsu, T., and Kitajima, H. (1974) Theory of Optical Property of Visual Pigment, *Journal of the Physical Society of Japan* 37, 177-185.
126. Waddell, W. H., Schaffer, A. M., and Becker, R. S. (1977) Visual Pigments .7. Experimental and Theoretical Investigations of Absorption Spectral Properties of Protonated Retinal Schiff-Bases and Implications for Bathochromic Shift in Visual Pigments, *J Am Chem Soc* 99, 8456-8460.
127. Arnaboldi, M., Motto, M. G., Tsujimoto, K., Baloghnaïr, V., and Nakanishi, K. (1979) Hydro-Retinals and Hydro-Rhodopsins, *J Am Chem Soc* 101, 7082-7084.
128. Mollevanger, L. C. P. J., Kentgens, A. P. M., Pardoën, J. A., Courtin, J. M. L., Veeman, W. S., Lugtenburg, J., and Degrip, W. J. (1987) High-Resolution Solid-State C-13-Nmr Study of Carbons C-5 and C-12 of the Chromophore of Bovine Rhodopsin - Evidence for a 6-S-Cis Conformation with Negative-Charge Perturbation near C-12, *Eur J Biochem* 163, 9-14.
129. Nakanishi, K. (1985) Bioorganic Studies with Rhodopsin, *Pure Appl Chem* 57, 769-776.
130. Nathans, J., Thomas, D., and Hogness, D. S. (1986) Molecular-Genetics of Human Color-Vision - the Genes Encoding Blue, Green, and Red Pigments, *Science* 232, 193-202.
131. Gat, Y., and Sheves, M. (1993) A Mechanism for Controlling the Pk(a) of the Retinal Protonated Schiff-Base in Retinal Proteins - a Study with Model Compounds, *J Am Chem Soc* 115, 3772-3773.
132. Blatz, P. E., Mohler, J. H., and Navangul, H. V. (1972) Anion-Induced Wavelength Regulation of Absorption Maxima of Schiff-Bases of Retinal, *Biochemistry-Us* 11, 848-&.
133. Livnah, N., and Sheves, M. (1993) The Schiff-Base Bond Configuration in Bacteriorhodopsin and in Model Compounds, *Biochemistry-Us* 32, 7223-7228.

134. Livnah, N., and Sheves, M. (1993) Model Compounds Can Mimic Spectroscopic Properties of Bovine Rhodopsin, *J Am Chem Soc* 115, 351-353.
135. Blatz, P. E., and Liebman, P. A. (1973) Wavelength regulation in visual pigments., *Exp. Eye Res.* 17, 573-580.
136. Tan, Q., Lou, J. H., Borhan, B., Karnaukhova, E., Berova, N., and Nakanishi, K. (1997) Absolute sense of twist of the C12-C13 bond of the retinal chromophore in bovine rhodopsin based on exciton-coupled CD spectra of 11,12-dihydroretinal analogues, *Angew Chem Int Edit* 36, 2089-2093.
137. Verdegem, P. J. E., Bovee-Geurts, P. H. M., de Grip, W. J., Lugtenburg, J., and de Groot, H. J. M. (1999) Retinylidene ligand structure in bovine rhodopsin, metarhodopsin-I, and 10-methylrhodopsin from internuclear distance measurements using C-13-labeling and 1-D rotational resonance MAS NMR, *Biochemistry-Us* 38, 11316-11324.
138. Honig, B., Hudson, B., Sykes, B. D., and Karplus, M. (1971) Ring Orientation in Beta-Ionone and Retinals (Theoretical/Nmr/Semi-Empirical Approach/Overhauser Effect/S-Cis Conformation), *P Natl Acad Sci USA* 68, 1289-&.
139. Rafferty, C. N. (1979) Light-Induced Perturbation of Aromatic Residues in Bovine Rhodopsin and Bacteriorhodopsin, *Photochem Photobiol* 29, 109-120.
140. Stenkamp, R. E., Filipek, S., Driessen, C. A. G. G., Teller, D. C., and Palczewski, K. (2002) Crystal structure of rhodopsin: a template for cone visual pigments and other G protein-coupled receptors, *Bba-Biomembranes* 1565, 168-182.
141. Yokoyama, R., and Yokoyama, S. (1990) Convergent Evolution of the Red-Like and Green-Like Visual Pigment Genes in Fish, *Astyanax-Fasciatus*, and Human, *P Natl Acad Sci USA* 87, 9315-9318.
142. Chan, T., Lee, M., and Sakmar, T. P. (1992) Introduction of Hydroxyl-Bearing Amino-Acids Causes Bathochromic Spectral Shifts in Rhodopsin - Amino-Acid Substitutions Responsible for Red-Green Color Pigment Spectral Tuning, *J Biol Chem* 267, 9478-9480.
143. Altun, A., Yokoyama, S., and Morokuma, K. (2008) Quantum mechanical/molecular mechanical studies on spectral tuning mechanisms of visual pigments and other photoactive proteins, *Photochem Photobiol* 84, 845-854.
144. Fujimoto, K., Hasegawa, J. Y., Hayashi, S., and Nakatsuji, H. (2006) On the color-tuning mechanism of Human-Blue visual pigment: SAC-CI and QM/MM study, *Chem Phys Lett* 432, 252-256.

145. Fujimoto, K., Hasegawa, J. Y., and Nakatsuji, H. (2008) Origin of color tuning in human red, green, and blue cone pigments: SAC-CI and QM/MM study, *Chem Phys Lett* 462, 318-320.
146. Birge, R. R., Murray, L. P., Pierce, B. M., Akita, H., Baloghnaier, V., Findsen, L. A., and Nakanishi, K. (1985) 2-Photon Spectroscopy of Locked-11-Cis-Rhodopsin - Evidence for a Protonated Schiff-Base in a Neutral Protein-Binding Site, *P Natl Acad Sci USA* 82, 4117-4121.
147. Mathies, R., and Stryer, L. (1976) Retinal Has a Highly Dipolar Vertically Excited Singlet-State - Implications for Vision, *P Natl Acad Sci USA* 73, 2169-2173.
148. Wanko, M., Hoffmann, M., Frauenheim, T., and Elstner, M. (2006) Computational photochemistry of retinal proteins, *J Comput Aid Mol Des* 20, 511-518.
149. Trabanino, R. J., Vaidehi, N., and Goddard, W. A. (2006) Exploring the molecular mechanism for color distinction in humans, *J Phys Chem B* 110, 17230-17239.
150. Houjou, H., Inoue, Y., and Sakurai, M. (2001) Study of the opsin shift of bacteriorhodopsin: Insight from QM/MM calculations with electronic polarization effects of the protein environment, *J Phys Chem B* 105, 867-879.
151. Warshel, A., and Chu, Z. T. (2001) Nature of the surface crossing process in bacteriorhodopsin: Computer simulations of the quantum dynamics of the primary photochemical event, *J Phys Chem B* 105, 9857-9871.
152. Yan, E. C. Y., Kazmi, M. A., Ganim, Z., Hou, J. M., Pan, D. H., Chang, B. S. W., Sakmar, T. P., and Mathies, R. A. (2003) Retinal counterion switch in the photoactivation of the G protein-coupled receptor rhodopsin, *P Natl Acad Sci USA* 100, 9262-9267.
153. Kholmurodov, K. T., Fel'dman, T. B., and Ostrovsky, M. A. (2007) Interaction of chromophore, 11-cis-retinal, with amino acid residues of the visual pigment rhodopsin in the region of protonated Schiff base: A molecular dynamics study, *Russ Chem B+* 56, 20-27.
154. Martinez-Mayorga, K., Pitman, M. C., Grossfield, A., Feller, S. E., and Brown, M. F. (2006) Retinal counterion switch mechanism in vision evaluated by molecular simulations, *J Am Chem Soc* 128, 16502-16503.
155. Giguere, V. (1994) Retinoic Acid Receptors and Cellular Retinoid-Binding Proteins - Complex Interplay in Retinoid Signaling, *Endocrine Reviews* 15, 61-79.
156. Chambon, P. (1996) A decade of molecular biology of retinoic acid receptors, *Faseb J* 10, 940-954.

157. Lotan, R. (1980) Effects of Vitamin-a and Its Analogs (Retinoids) on Normal and Neoplastic-Cells, *Biochimica Et Biophysica Acta* 605, 33-91.
158. DeLuca, L. M. (1991) Retinoids and their receptors in differentiation, embryogenesis, and neoplasia., *Faseb J* 5, 2924-2933.
159. Chomienne, C., Fenaux, P., and Degos, L. (1996) Retinoid differentiation therapy in promyelocytic leukemia, *Faseb J* 10, 1025-1030.
160. Delva, L., Bastie, J. N., Rochette-Egly, C., Kraiba, R., Balitrand, N., Despouy, G., Chambon, P., and Chomienne, C. (1999) Physical and functional interactions between cellular retinoic acid binding protein II and the retinoic acid-dependent nuclear complex, *Molecular and Cellular Biology* 19, 7158-7167.
161. Fisher, G. J., and Voorhees, J. J. (1996) Molecular mechanisms of retinoid actions in skin, *Faseb J* 10, 1002-1013.
162. Tallman, M. S. (1996) Differentiating therapy in acute myeloid leukemia, *Leukemia* 10, 1262-1268.
163. Hong, W. K., Itri, L. M. (1994) Retinoids and human cancer, in *The Retinoids: Biology, Chemistry, and Medicine* (Sporn, M. B., Roberts, A. B., Goodman, D. S., Ed.) 2nd ed., pp 597-630, Raven Press, New York.
164. Vaezeslami, S., Mathes, E., Vasilelou, C., Borhan, B., and Geiger, J. H. (2006) The structure of apo-wild-type cellular retinoic acid binding protein II at 1.4 Å and its relationship to ligand binding and nuclear translocation, *J Mol Biol* 363, 687-701.
165. Kliewer, S. A., Umesono, K., Mangelsdorf, D. J., and Evans, R. M. (1992) Retinoid X-Receptor Interacts with Nuclear Receptors in Retinoic Acid, Thyroid-Hormone and Vitamin-D3 Signaling, *Nature* 355, 446-449.
166. Kreutz, M., Fritsche, J., Andreesen, R., and Krause, S. W. (1998) Regulation of cellular retinoic acid binding protein (CRABP II) during human monocyte differentiation in vitro, *Biochem Biophys Res Commun* 248, 830-834.
167. Leid, M., Kastner, P., Lyons, R., Nakshatri, H., Saunders, M., Zacharewski, T., Chen, J. Y., Staub, A., Garnier, J. M., Mader, S., and Chambon, P. (1992) Purification, Cloning, and RAR Identity of the HeLa-Cell Factor with Which RAR or TR Heterodimerizes to Bind Target Sequences Efficiently, *Cell* 68, 377-395.
168. Leroy, P., Krust, A., Kastner, P., Mendelsohn, C., Zelent, A., Chambon, P. (1992) Retinoic acid receptors, in *Retinoids in Normal Development and Teratogenesis* (Morris-Kay, G., ed., Ed.), pp 7-25, Oxford University Press, Oxford.



169. Mangelsdorf, D. J., Thummel, C., Beato, M., Herrlich, P., Schutz, G., Umesono, K., Blumberg, B., Kastner, P., Mark, M., Chambon, P., and Evans, R. M. (1995) The Nuclear Receptor Superfamily - the 2nd Decade, *Cell* 83, 835-839.
170. Morrisskay, G. (1993) Retinoic Acid and Craniofacial Development - Molecules and Morphogenesis, *Bioessays* 15, 9-15.
171. Bailey, J. S., and SIU, C. H. (1988) Purification and Partial Characterization of a Novel Binding-Protein for Retinoic Acid from Neonatal Rat, *J Biol Chem* 263, 9326-9332.
172. ONG, D. E., and Chytil, F. (1975) Retinoic Acid-Binding Protein in Rat Tissue - Partial-Purification and Comparison to Rat Tissue Retinol-Binding Protein, *J Biol Chem* 250, 6113-6117.
173. Sani, B. P. H., D.L. (1974) Retinoic acid-binding-protein in chick-embryo metatarsal skin, *Biochem. Biophys. Res. Commun.* 61, 1276-1282.
174. Willmert, L. J., and Noy, N. (2003) Involvement of CRABP-II in transcriptional activity of RAR, *Faseb J* 17, A315-A316.
175. Ong, D. E., Newcomer, M. E., & Chytil, F. (1994) Cellular retinoid-binding proteins, in *The Retinoids: Biology, Chemistry, and Medicine* (Sporn, M. B., Roberts, A. B., Goodman, D. S., Ed.) 2nd ed., pp 283-318, Raven Press, New York.
176. Bertucci, F., Houlgatte, R., Benziene, A., et al. (2000) Gene expression profiling of primary breast carcinomas using arrays of candidate genes, *Hum. Mol. Genet.* 9, 2981-2991.
177. Bertucci, F., Van Hulst, S., Bernard, K., Lorigod, B., Granjeaud, S., Tagett, R., Starkey, M., Nguyen, C., Jordan, B., and Birnbaum, D. (1999) Expression scanning of an array of growth control genes in human tumor cell lines, *Oncogene* 18, 3905-3912.
178. Delva, L., Cornic, M., Balitrand, N., Guidez, F., Miclea, J. M., Delmer, A., Teillet, F., Fenaux, P., Castaigne, S., Degos, L., and Chomienne, C. (1993) Resistance to All-Trans-Retinoic Acid (Atra) Therapy in Relapsing Acute Promyelocytic Leukemia - Study of in-Vitro Atra Sensitivity and Cellular Retinoic Acid-Binding Protein-Levels in Leukemic-Cells, *Blood* 82, 2175-2181.
179. Hibbs, K., Skubitz, K. M., Pambuccian, S. E., Casey, R. C., Burleson, K. M., Oegema, T. R., Thiele, J. J., Grindle, S. M., Bliss, R. L., and Skubitz, A. P. N. (2004) Differential gene expression in ovarian carcinoma - Identification of potential biomarkers, *American Journal of Pathology* 165, 397-414.
180. Li, C. M., Guo, M. R., Borczuk, A., Powell, C. A., Wei, M., Thaker, H. M., Friedman, R., Klein, U., and Tycko, B. (2002) Gene expression in Wilms' tumor

mimics the earliest committed stage in the metanephric mesenchymal-epithelial transition, *American Journal of Pathology* 160, 2181-2190.

181. Tsibris, J. C. M., Segars, J., Coppola, D., Mane, S., Wilbanks, G. D., O'Brien, W. F., and Spellacy, W. N. (2002) Insights from gene arrays on the development and growth regulation of uterine leiomyomata, *Fertility and Sterility* 78, 114-121.
182. Vo, H. P., and Crowe, D. L. (1998) Transcriptional regulation of retinoic acid responsive genes by cellular retinoic acid binding protein-II modulates RA mediated tumor cell proliferation and invasion, *Anticancer Research* 18, 217-224.
183. Zhou, D. C., Hallam, S. J., Lee, S. J., Klein, R. S., Wiernik, P. H., Tallman, M. S., and Robert, E. (1998) Constitutive expression of cellular retinoic acid binding protein II and lack of correlation with sensitivity to all-trans retinoic acid in acute promyelocytic leukemia cells, *Cancer Research* 58, 5770-5776.
184. Budhu, A. S., and Noy, N. (2002) Direct channeling of retinoic acid between cellular retinoic acid-binding protein II and retinoic acid receptor sensitizes mammary carcinoma cells to retinoic acid-induced growth arrest, *Molecular and Cellular Biology* 22, 2632-2641.
185. Dong, D., Ruuska, S. E., Levinthal, D. J., and Noy, N. (1999) Distinct roles for cellular retinoic acid-binding proteins I and II in regulating signaling by retinoic acid, *J Biol Chem* 274, 23695-23698.
186. Sessler, R. J., and Noy, N. (2005) A ligand-activated nuclear localization signal in cellular retinoic acid binding protein-II, *Molecular Cell* 18, 343-353.
187. Vaezeslami, S., Mathes, E., Vasileiou, C., Borhan, B., and Geiger, J. H. (2006) The Structure of Apo-wild-type Cellular Retinoic Acid Binding Protein II at 1.4 Å and its Relationship to Ligand Binding and Nuclear Translocation, *J Mol Biol.*
188. Kleywegt, G. J., Bergfors, T., Senn, H., Lemotte, P., Gsell, B., Shudo, K., and Jones, T. A. (1994) Crystal-Structures of Cellular Retinoic Acid-Binding Protein-I and Protein-II in Complex with All-Trans-Retinoic Acid and a Synthetic Retinoid, *Structure* 2, 1241-1258.
189. Chen, X., Tordova, M., Gilliland, G. L., Wang, L. C., Li, Y., Yan, H. G., and Ji, X. H. (1998) Crystal structure of apo-cellular retinoic acid-binding protein type II (R111M) suggests a mechanism of ligand entry, *J Mol Biol* 278, 641-653.
190. Thompson, J. R., Bratt, J. M., and Banaszak, L. J. (1995) Crystal-Structure of Cellular Retinoic Acid-Binding Protein-I Shows Increased Access to the Binding Cavity Due to Formation of an Intermolecular Beta-Sheet, *J. Mol. Biol.* 252, 433-446.

191. Scapin, G., Gordon, J. I., and Sacchettini, J. C. (1992) Refinement of the Structure of Recombinant Rat Intestinal Fatty Acid-Binding Apoprotein at 1.2-Å Resolution, *J. Biol. Chem.* 267, 4253-4269.
192. Wang, L. C., and Yan, H. G. (1998) NMR study suggests a major role for Arg111 in maintaining the structure and dynamical properties of type II human cellular retinoic acid binding protein, *Biochemistry-US* 37, 13021-13032.
193. Chaudhuri, B. N., Kleywegt, G. J., Broutin-L'Hermite, I., Bergfors, T., Senn, H., Le Motte, P., Partouche, O., and Jones, T. A. (1999) Structures of cellular retinoic acid binding proteins I and II in complex with synthetic retinoids, *Acta Crystallogr D* 55, 1850-1857.
194. Kleywegt, G. J., Bergfors, T., Senn, H., Le Motte, P., Gsell, B., Shudo, K., and Jones, T. A. (1994) Crystal structures of cellular retinoic acid binding proteins I and II in complex with all-*trans* retinoic acid and a synthetic retinoid., *Structure* 2, 1241-1258.
195. Crist, R. M., Vasileiou, C., Rabago-Smith, M., Geiger, J. H., and Borhan, B. (2006) Engineering a rhodopsin protein mimic, *J Am Chem Soc* 128, 4522-4523.
196. Vasileiou, C., Vaezslami, S., Crist, R. M., Rabago-Smith, M., Geiger, J. H., and Borhan, B. (2007) Protein design: Reengineering Cellular Retinoic Acid Binding Protein II into a rhodopsin protein mimic, *J Am Chem Soc* 129, 6140-6148.
197. Saari, J. C., Bredberg, L., and Garwin, G. G. (1982) Identification of the Endogenous Retinoids Associated with 3 Cellular Retinoid-Binding Proteins from Bovine Retina and Retinal-Pigment Epithelium, *J Biol Chem* 257, 3329-3333.
198. Saari, J. C., and Bredberg, D. L. (1987) Photochemistry and Stereoselectivity of Cellular Retinaldehyde-Binding Protein from Bovine Retina, *J Biol Chem* 262, 7618-7622.
199. Saari, J. C., Nawrot, M., Kennedy, B. N., Garwin, G. G., Hurley, J. B., Huang, J., Possin, D. E., and Crabb, J. W. (2001) Visual cycle impairment in cellular retinaldehyde binding protein (CRALBP) knockout mice results in delayed dark adaptation, *Neuron* 29, 739-748.
200. Golovleva, I., Bhattacharya, S., Wu, Z. P., Shaw, N., Yang, Y. W., Andrabi, H., West, K. A., Burstedt, M. S. I., Forsman, K., Holmgren, G., Sandgren, O., Noy, N., Qin, J., and Crabb, J. W. (2003) Disease-causing mutations in the cellular retinaldehyde binding protein tighten and abolish ligand interactions, *J Biol Chem* 278, 12397-12402.
201. Stecher, H., Gelb, M. H., Saari, J. C., and Palczewski, K. (1999) Preferential release of 11-*cis*-retinol from retinal pigment epithelial cells in the presence of cellular retinaldehyde-binding protein, *J Biol Chem* 274, 8577-8585.

202. Winston, A., and Rando, R. R. (1998) Regulation of isomerohydrolase activity in the visual cycle, *Biochemistry-Us* 37, 2044-2050.
203. Wu, Z. P., Yang, Y. W., Shaw, N., Bhattacharya, S., Yan, L., West, K., Roth, K., Noy, N., Qin, J., and Crabb, J. W. (2003) Mapping the ligand binding pocket in the cellular retinaldehyde binding protein, *J Biol Chem* 278, 12390-12396.
204. Nawrot, M., West, K., Huang, J., Possin, D. E., Bretscher, A., Crabb, J. W., and Saari, J. C. (2004) Cellular retinaldehyde-binding protein interacts with ERM-binding phosphoprotein 50 in retinal pigment epithelium, *Invest Ophth Vis Sci* 45, 393-401.
205. Bhattacharya, S. K., Wu, Z., Jin, Z., Yan, L., Miyagi, M., West, K., Nawrot, M., Saari, J. C., and Crabb, J. W. (2002) Proteomic approach to identification of a mammalian visual cycle protein complex., *Faseb J* 16, A14-A14.
206. Crabb, J. W., Carlson, A., Chen, Y., Goldflam, S., Intres, R., West, K. A., Hulmes, J. D., Kapron, J. T., Luck, L. A., Horwitz, J., and Bok, D. (1998) Structural and functional characterization of recombinant human cellular retinaldehyde-binding protein, *Protein Sci* 7, 746-757.
207. Wu, Z. P., Hasan, A., Liu, T. Y., Teller, D. C., and Crabb, J. W. (2004) Identification of CRALBP ligand interactions by photoaffinity labeling, hydrogen/deuterium exchange, and structural modeling, *J Biol Chem* 279, 27357-27364.
208. Panagabko, C., Morley, S., Hernandez, M., Cassolato, P., Gordon, H., Parsons, R., Manor, D., and Atkinson, J. (2003) Ligand specificity in the CRAL-TRIO protein family, *Biochemistry-Us* 42, 6467-6474.
209. Meier, R., Tomizaki, T., Schulze-Briese, C., Baumann, U., and Stocker, A. (2003) The molecular basis of vitamin E retention: Structure of human alpha-tocopherol transfer protein, *J Mol Biol* 331, 725-734.
210. Min, K. C., Kovall, R. A., and Hendrickson, W. A. (2003) Crystal structure, of human alpha-tocopherol transfer protein bound to its ligand: Implications for ataxia with vitamin E deficiency, *P Natl Acad Sci USA* 100, 14713-14718.
211. Sha, B. D., Phillips, S. E., Bankaitis, V. A., and Luo, M. (1998) Crystal structure of the *Saccharomyces cerevisiae* phosphatidylinositol-transfer protein, *Nature* 391, 506-510.
212. Stocker, A., and Baumann, U. (2003) Supernatant protein factor in complex with RRR-alpha-tocopherylquinone: A link between oxidized vitamin E and cholesterol biosynthesis, *J Mol Biol* 332, 759-765.

213. Liu, T. Y., Jenwitheesuk, E., Teller, D. C., and Samudrala, R. (2005) Structural insights into the cellular retinaldehyde-binding protein (CRALBP), *Proteins-Structure Function and Bioinformatics* 61, 412-422.

## **CHAPTER II. Crystal Structures of Ligand-bound Cellular Retinoic Acid Binding Protein II Mutants**

### **2.1. Introduction.**

#### **2.1.1. Need for a ligand that can be totally buried inside the CRABP II mutants.**

The triple mutant KLE-CRABP II was a successful design in that it proved that the protonated Schiff base and the stabilizing counter anion are two essential factors in inducing the red shift of the bound retinal (1). However, there are still limitations of the KLE-CRABP II-all-*trans*-retinal system in terms of its application towards investigation of the point charge theory. According to the point charge theory, the placement of counter anions along the polyene chain would potentially stabilize the positive charge of the bound ligand at different positions and therefore lead to stabilization of different resonance structures, which would result in differed red shift abilities. To test this theory, the ideal situation is that the ligand is fully buried inside the protein and able to experience various protein-ligand interactions generated by binding site mutations. However, as shown in Figure II-1, the all-*trans*-retinal-bound CRABP II mutants all feature a binding mode with the ionone ring of the retinoid partially solvent-exposed. To circumvent this less-than-ideal situation associated with the Rt-bound CRABP II model systems, we decided to explore the possibility of introducing a shorter ligand into the CRABP II mutants. By docking simulations, we have identified a shorter retinal analog,

C<sub>15</sub>-aldehyde (Figure II-2), which is predicted to be totally buried inside the protein once bound to the CRABP<sub>II</sub> mutants.



**Figure II-1. Retinoic acid bound in wild-type-CRABP<sub>II</sub>.**

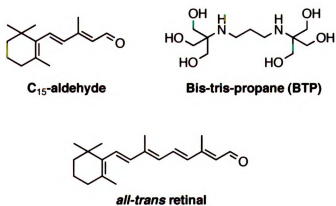


**Figure II-2. Structures of the related compounds.**

**Table II-1. CRABP II mutants bound with C<sub>15</sub>-aldehyde.**

	Mutant	$\lambda_{\max}$ <sup>a</sup>	red. am. <sup>b</sup>	quen. fluor. <sup>c</sup>
1	C <sub>15</sub> -aldehyde (buffer)	340	N/A	N/A
2	C <sub>15</sub> -aldehyde PSB (EtOH)	380	N/A	N/A
3	R132K:R111L:L121E	380	yes	0.80
4	R132K:R111L:L121E:R59W	404	yes	0.81
5	R132K:R111L:L121E:R59E	424	yes	0.81
6	R132K:R111L:L121E:R59D	414	yes	0.87
7	R132K:R111L:L121E:A36E	410	yes	0.89
8	R132K:R111L:L121E:V76Y	388	yes	0.85
9	R132K:R111L:L121Q	413	yes	0.80
10	R132K:R111L:A32E	407	yes	0.61
11	R132K:R111L:T54E	402	yes	0.67
12	R132K:Y134F:R111L:L121D:T54V	415	yes	0.78
13	R132K:R111L:R59L	406	yes	0.57
14	R132K:R111L:F15D	390	yes	0.69

<sup>a</sup> Deconvolution of overlapping UV-vis spectra is detailed in reference (1). <sup>b</sup> Yes/no refer to the results obtained from MALDI-TOF analysis (presence of  $[M+204]^+$ ) of protein-C<sub>15</sub>-aldehyde complex that has been subjected to reductive amination conditions. <sup>c</sup> End fluorescence level after fluorescence titration.

The C<sub>15</sub>-aldehyde was then synthesized by Kin-Sing Lee and subsequently used for binding assays with different CRABP II mutants. Some of the results are shown in Table II-1 (results from Kin-Sing Lee). The C<sub>15</sub>-aldehyde itself absorbs at 340 nm as a free ligand in buffer. Red shift to 380 nm is observed upon formation of the protonated Schiff base when C<sub>15</sub>-aldehyde is incubated with tributylamine. Further red shift is observed when the protonated Schiff base is formed between the CRABP II mutants and the C<sub>15</sub>-aldehyde, which is referred to as "opsin shift" since it is induced by protein-chromophore interactions. The most dramatic opsin shift is observed in the CRABP II mutant, KLE-R59E, where an opsin shift of 44 nm is obtained. Compared to the Rt-



KLE-CRABPII complex where the opsin shift is ~7 nm, the C<sub>15</sub>-aldehyde-bound CRABPII mutants seem to possess a better wavelength red shift ability.

The focus now shifts toward understanding of the details of how C<sub>15</sub>-aldehyde is bound in the CRABPII mutants in order to further explain the observed binding data as well as to guide our future rational re-engineering of CRABPII. The determination of the C<sub>15</sub>-aldehyde-bound CRABPII mutant structures was therefore pursued.

### **2.1.2. Engineered CRABPII mutants as switchable colorimetric fusion proteins.**

The ability of the CRABPII mutants to form protonated Schiff bases with the aldehydic ligands and afford a red shift of the ligand's  $\lambda_{\text{max}}$  suggests a natural advantage of the system in terms of generating ligand-dependent fluorescence. By introducing highly conjugated chromophores to the designed CRABPII mutants, we could envision a situation where a particular protein-ligand complex is able to produce fluorescence. Such a scenario, combined with the fact that CRABPII is a small and soluble cellular protein, suggests a potential of the designed CRABPII mutants being used as ligand-inducible fluorescent fusion tags.

Green Fluorescence Protein (GFP) has been the top choice in the recent decade (2-8). GFP is a spontaneously fluorescent protein from the jelly fish *Aequorea victoria*. The wide usage of GFP and its genetic variants as fusion tags has addressed many important biological questions (5, 6). The small size and the solubility of GFP are two

other important factors that make GFP suitable as fusion tags. However, despite the popularity of GFP as fluorescence fusion tags, there are some limitations with GFP. First of all, molecular oxygen is required for the formation of the chromophore. This also leads to the formation of the by-product,  $\text{H}_2\text{O}_2$ , which could be toxic during the overexpression of GFP in the organisms (7). Second of all, the formation of GFP is slow (up to 2 hrs) and is problematic for the study of proteins with short half-lives (9, 10). Thirdly, raising the growth temperature always results in reduced fluorescence levels in GFP. Finally, although GFP variants featuring different excitation and emission spectra has provided the possibility of simultaneous detections, problems still exist both in the high photobleaching rates and instability of some mutants and in the overlapping excitation and emission spectra of the mutants (9, 11-14).

Our approach in using the CRABPII or possibly other lipocalin family proteins could potentially provide an alternative option of fluorescence tagging. One of the advantages of designing CRABPII into fluorescence fusion tags is its tolerance toward multiple mutations. It is proven that the lipocalin family proteins are highly amenable toward substantial modifications without destroying their structural integrity (15-18). Family members of the lipocalins share less than 10% sequence identity and yet all have a highly conserved overall fold. Other advantages that CRABPII has in terms of being used as a fusion tag include its even smaller size (137 aa vs ~240 aa for GFP) as well as its great solubility. The binding cavity of the CRABPII is huge ( $600 \text{ \AA}^3$ ), which possibly allows adopting chromophores in a decent range of sizes and conformations. The combination of different mutations and different chromophores introduced can be expected to lead to color tuning of the fusion tags and therefore simultaneous detection of

multiple proteins of interests. The most attractive feature of the CRABP<sub>II</sub> fluorescence fusion tags is its tunable nature using small molecules, which could potentially provide a temporal control of the fluorescence signal that can not be achieved using GFP and its variants.

## **2.2. *C<sub>15</sub>-aldehyde-bound CRABP<sub>II</sub> mutant structures.***

### **2.2.1. Two distinctively different binding orientations of C<sub>15</sub>-aldehyde in different CRABP<sub>II</sub> mutants.**

The crystal structure of CRABP<sub>II</sub> mutant R132K:R111L:L121E:R59W (KLE-R59W) bound to C<sub>15</sub>-aldehyde was determined at 1.95 Å. This mutant was designed based on the determinants of PSB formation in CRABP<sub>II</sub> mutants derived from our previous work. These determinants include three aspects: (1) the nucleophilic Lys must be properly positioned for proper nucleophilic attack; (2) the aldehyde carbonyl must also be properly oriented and activated for nucleophilic attack; (3) a counter ion must be provided to stabilize the positively charged protonated form of the Schiff base. As stated, the first three mutations in the KLE-R59W mutant, R132K:R111L:L121E, turned out to be key for the formation of a stable PSB from Retinal (Rt) in CRABP<sub>II</sub>. The fourth mutation is at a position where the corresponding residue is presumably within contact distance of the ionone ring of the bound C<sub>15</sub>-aldehyde based on our energy minimized model (19).

By looking at the overlay of the crystal structures of the C<sub>15</sub>-aldehyde-bound KLE-R59W complex and the Rt-bound R132K:R111L:L121E (KLE) complex, it is clear that the C<sub>15</sub>-aldehyde adopts a similar trajectory to Rt in KLE (Figure II-3). There are also distinct differences between the two structures. Besides C<sub>15</sub>-aldehyde being shorter in length, the two structures also differ in that the PSB formed in the C<sub>15</sub>-aldehyde-bound structure is a *trans* imine, whereas in the KLE-Rt complex a *cis* double bond is formed. The 2Fo-Fc electron density map for the C<sub>15</sub>-aldehyde in KLE-R59W is shown in Figure II-4A and the detailed binding site is portrayed in Figure II-5A. Glu121, which was established as the counter anion stabilizing the PSB in the KLE-Rt complex, is now 4.8 Å away from the PSB nitrogen. A buffer molecule, bis-tris-propane (BTP, Figure II-2), is also present inside the binding pocket. The -OH hydroxy group of BTP makes a 2.9 Å hydrogen bond with the Schiff base nitrogen, which turns out to be the only interaction that the PSB makes. BTP also interacts with Glu121 through four hydrogen bonding interactions, with two of them involving the same hydroxy that interacts with the PSB. In other words, the stabilizing effect of Glu121 for the PSB is now indirect and mediated by the hydroxy group of BTP through hydrogen bonding interactions. These hydrogen bonding interactions further secure the position of BTP inside the pocket. BTP is important in obtaining ligand-bound crystals of this KLE-R59W mutant. Crystals of this mutant obtained from co-crystallization experiments without having BTP in the growing conditions all turned out to be *apo*, with no electron density for ligand evident after refinement of the structures.

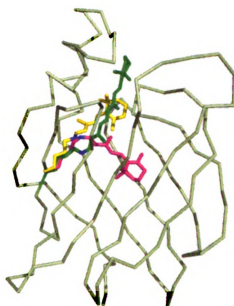
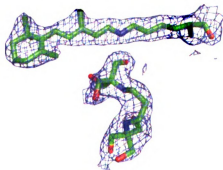


**Figure II-3. Overlay of the ligands bound in different binding orientations.** Green: *all-trans*-retinal in KLE; Yellow: C<sub>15</sub>-aldehyde in KLE-R59W; Magenta: C<sub>15</sub>-aldehyde in KL-A32E; KLE-CRABP II C $\alpha$  trace is shown in lime.

**A.**



**B.**

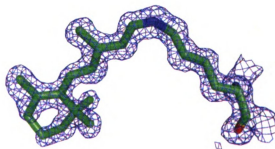


**Figure II-4. 2Fo-Fc electron density map calculated at 1.0  $\sigma$  for bound ligands.** A. C<sub>15</sub>-aldehyde bound to Lys132 (upper) and bis-tris-propane (lower) in KLE-R59W; B. C<sub>15</sub>-aldehyde bound to Lys132 in KL-A32E.

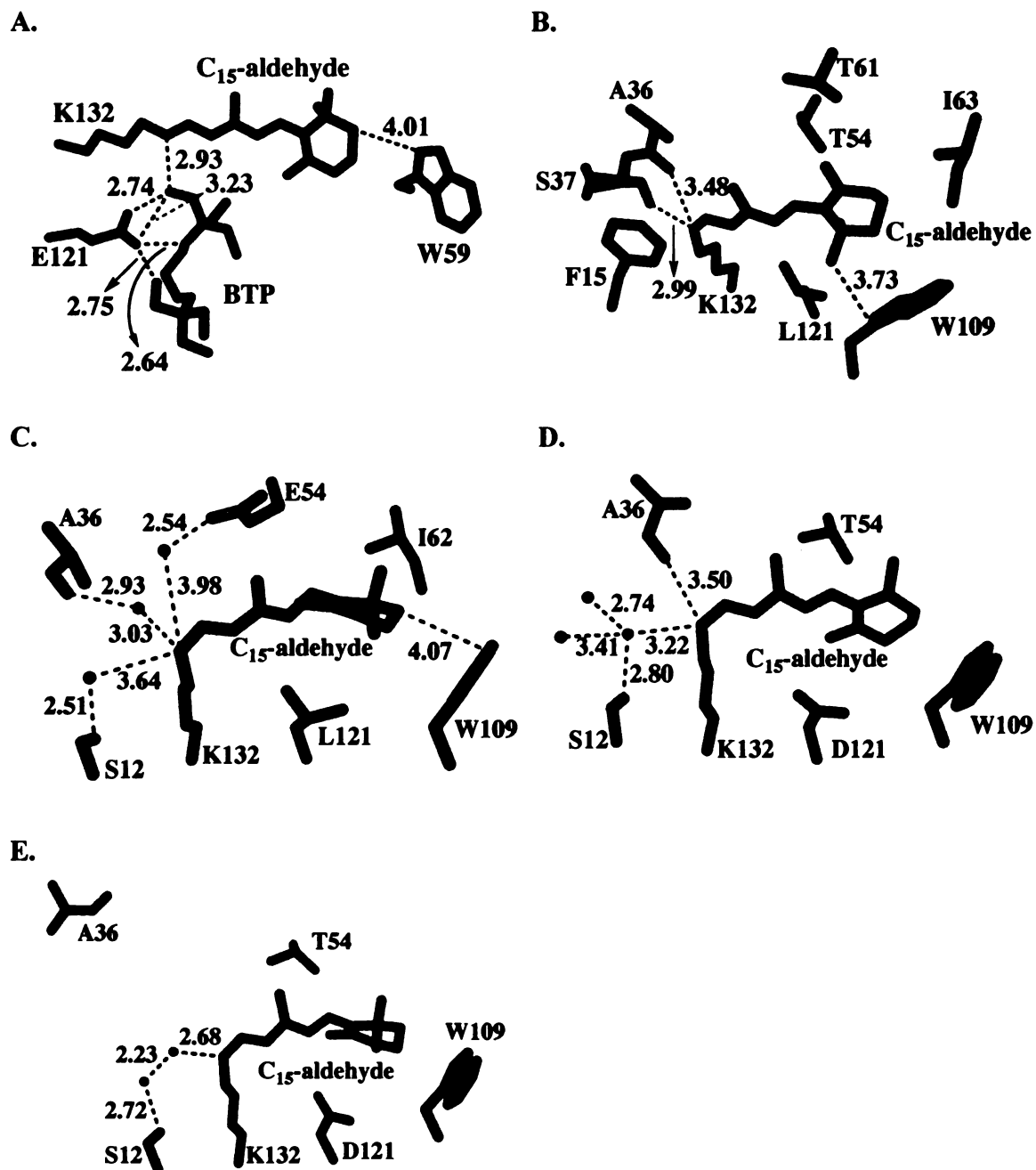


**Figure II-5. Interactions between the PSB and the residues nearby in different  $C_{15}$ -aldehyde-bound CRABPII mutants.** A. KLE-R59W; B. KL-A32E; C. KL-T54E, MolA; D. KFLDV, MolA; E. KFLDV, MolB. Distances are in Ångström (Å).

As expected,  $C_{15}$ -aldehyde is now totally buried inside the protein. Trp59 is sitting right on top of the ionone ring with its shortest distance to the ligand just over 4 Å.

This binding mode provided us with the possibility of engineering around any part of the bound C<sub>15</sub>-aldehyde analog.

The structure of the C<sub>15</sub>-aldehyde-bound R132K:R111L:A32E CRABPII mutant (KL-A32E) at 1.22 Å resolution revealed a very surprising result. As shown in the overlay between *holo*-KLE-R59W and *holo*-KL-A32E, the C<sub>15</sub>-aldehyde in KL-A32E swings about 90° away from the C<sub>15</sub>-aldehyde binding site seen in the KLE-R59W mutant and all other retinal-binding mutants as well (Figure II-3). The ligand is now buried even further within the binding pocket (Figure II-4B), approximately where the BTP was bound in the KLE-R59W structure. In this “alternative” binding trajectory, the Schiff base adopts a *cis* conformation and is stabilized through hydrogen bonding with two backbone carbonyl oxygens, Ala36 and Ser37 (Figure II-5B). The C<sub>15</sub>-aldehyde resides in a very hydrophobic environment in this structure. Note that the wild-type Leu, instead of Glu as in KLE-R59W, resides at the 121 position. Mutation at this position turns out to be key in determining the binding orientation. Mutation A32E was meant to introduce a negatively charged residue next to the ligand bound in the orthogonal orientation, but is indeed far away from the ligand due to the new binding mode.

### **2.2.2. A single mutation at position 121 is key in determining the binding orientation of C<sub>15</sub>-aldehyde.**

By overlaying the C<sub>15</sub>-aldehyde binding site in KL-A32E with that in the KLE-Rt complex, it is clear that the L121E mutation sterically interferes with the alternative

binding trajectory of C<sub>15</sub>-aldehyde (Figure II-6A), while Leu121 in KL-A32E allows the alternative binding mode. Two additional C<sub>15</sub>-aldehyde-bound crystal structures were obtained, which confirmed that smaller residues at 121 result in the ligand binding to this alternative, more hydrophobic cavity. The two mutants are R132K:R111L:T54E (KL-T54E) and R132K:Y134F:R111L:L121D:T54V (KFLDV). In these two mutants, either a Leu (KL-T54E) or an Asp (KFLDV) is present at the 121 position. Despite the fact that Leu is neutral and Asp is negatively charged, mutants containing either of the two residues at 121 all allow the ligand to bind in the alternative orientation (Figure II-6B).

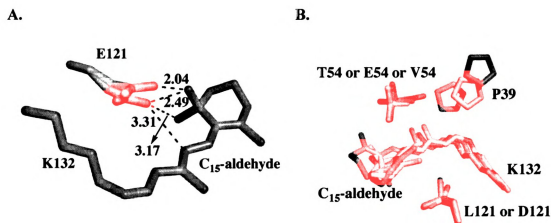


**Figure II-6.** A. The structures of KLE-Rt and C<sub>15</sub>-aldehyde-KL-A32E are overlaid. Glu121 from KLE-Rt (magenta) and C<sub>15</sub>-aldehyde from *holo*-KL-A32E (green) are shown; B. Overlay of the C<sub>15</sub>-aldehyde bound in three CRABP II mutants: KL-A32E (magenta), KL-T54E (green), and KFLDV (yellow).

In addition to the crystal structures, we have another line of evidence to support the role of residue 121 in directing the ligand binding orientation. Fluorescence titration experiments were used to measure the C<sub>15</sub>-aldehyde binding affinity of the CRABP II



mutants by measuring ligand-induced fluorescence quenching of protein tryptophan residues. The quenching efficiency at saturation of the various mutants fell into two categories (19). The fluorescence of mutants containing Glu or Gln at 121 levels off between 0.8 and 0.9, while that of mutants having smaller residues (Leu, Asp, etc.) at 121 levels off usually between 0.5 and 0.7 (Table II-1). This observation again suggests two different types of binding for C<sub>15</sub>-aldehyde. If we compare the two binding orientations in terms of their relative distances to the nearby tryptophan(s), we can see that the new binding orientation positions the ionone ring of the C<sub>15</sub>-aldehyde right next to Trp109 with the shortest distance between the two residues being only 3.7 Å in KL-A32E (Figure II-5B). In the orthogonal binding trajectory, except for the introduced Trp at 59 in KLE-R59W, all of the three native Trp's are far away from the C<sub>15</sub>-aldehyde, with the closest one being over 10 Å. The alternative binding trajectory features a much closer distance to Trp and therefore should lead to more efficient fluorescence quenching, which should result in decreased fluorescence levels at saturation. Our fluorescence titration results are consistent with the observation in our crystal structures, both indicating that the single mutation at 121 is key in determining the different binding orientations of C<sub>15</sub>-aldehyde bound in CRABP II mutants. Glu121 forces the ligand to bind in the orthogonal orientation and smaller residues at 121 prefer the ligand to go into the alternative binding cavity.

### 2.2.3. Protonated Schiff base stabilization.

The PSB in bovine rhodopsin is stabilized by the carboxylate oxygen of Glu113 3.4 Å away (20-22). The counterion interaction has been shown to be responsible for the majority of the red shift of the chromophore upon binding in the protein's active site (23). We have previously established a similar counterion interaction in our CRABPII model, the KLE-Rt complex, where the carboxylate of Glu121 is positioned 2.6 Å away from the PSB nitrogen (1). Stabilization of the PSB through hydrogen bonding has also been seen in certain rhodopsin crystal structures. In the sensory rhodopsin II, two Asp residues are sitting 3.8 Å and 4.0 Å away from the PSB nitrogen, respectively, and a water molecule makes contacts with both the PSB nitrogen (2.6 Å) and the two Asp residues (24). Very similar arrangements have been observed in both bacteriorhodopsin (25) and halorhodopsin (26) where, besides weak counterion interactions, the PSB is also stabilized by polarized water molecules through hydrogen bonding.

For our C<sub>15</sub>-aldehyde-bound CRABPII mutants, the formation of the PSB and Schiff base has been confirmed by the shift of the chromophore's  $\lambda_{\text{max}}$  and by reductive amination followed by MALDI analysis, respectively (Table II-1) (19). Each of the four mutant structures displays a unique mechanism for PSB stabilization. As described earlier, the PSB in KLE-R59W (Figure II-5A) is stabilized only by the hydroxy group of BTP through hydrogen bonding and the same hydroxy group is polarized through hydrogen bonding interactions with the carboxylate of Glu121. This is an arrangement similar to that seen in sensory rhodopsin II, bacteriorhodopsin and halorhodopsin where the carboxylate can indirectly interact with the PSB through water-mediated hydrogen bonding.

In the case of KL-A32E, however, the PSB stabilization involves hydrogen bonding of the PSB nitrogen with two carbonyl oxygens from the helix backbone (Figure II-5B). This stabilization mechanism is interesting in that it is the very opposite of the classical “oxyanion hole” interactions present in many enzymes where the negatively charged oxygen of the tetrahedral intermediate is hydrogen bonded with two backbone amide -NH groups (27-30).

In the crystal structure of mutant KL-T54E, there are two molecules in the asymmetric unit and they share the same mechanism for PSB stabilization. The PSB nitrogen makes hydrogen bonding interactions with a nearby water molecule (3.0 Å distance) (Figure II-5C). For the C<sub>15</sub>-aldehyde-bound KFLDV mutant, the two molecules in the asymmetric unit exhibit slightly different binding situations. In molecule A, the PSB nitrogen makes hydrogen bonds with two nearby residues, a water molecule at 3.2 Å and the carbonyl group of Ala36 at 3.5 Å (Figure II-5D). In molecule B, a sole hydrogen bonding interaction between the PSB and a non-polarized water 2.7 Å away is stabilizing the PSB. Ala36 is moved away due to the crystal-packing-induced partial unwinding of the  $\alpha$ 2 helix at its C-terminus (Figure II-5E). What is unique in our system is that the PSB can be stabilized by interacting only with water molecules as shown in both molecules of the *holo*-KL-T54E mutant and Mol B of the *holo*-KFLDV mutant.

The pK<sub>a</sub> values of known rhodopsins have been reported to be between 9.3 and ~16 (31-35). The pK<sub>a</sub> values of the PSB in the C<sub>15</sub>-aldehyde-bound CRABPII mutants, KLE-R59W, KL-A32E, KL-T54E and KFLDV, were measured to be 7.7, 8.6, 7.8 and

8.4, respectively (19). Overall, these values are much lower than that of the bovine rhodopsin ( $pK_a > 16$ ) (35) and that of the bacteriorhodopsin ( $pK_a$  13.3) (31). The striking difference might be contributed to whether negatively charged residues are placed in the vicinity of the PSB. In all of the rhodopsin structures solved so far, one or two negatively charged residues are always present in the vicinity of the PSB and interact with the PSB nitrogen either directly (Glu113 in bovine rhodopsin and Asp238 in halorhodopsin) or through water-mediated hydrogen bonding (Asp85, Asp212 in bacteriorhodopsin and Asp75 in sensory rhodopsin). Although having a negatively charged residue next to the PSB does not guarantee a greatly enhanced  $pK_a$  as demonstrated in the all-*trans*-retinal-bound KLE-CRABPII mutant ( $pK_a$  8.7), it is reasonable to rationalize that the lack of negatively charged residues next to the PSB could possibly make the protonation of the Schiff base harder and therefore results in a lower  $pK_a$  of the PSB. Among the four C<sub>15</sub>-aldehyde-bound CRABPII mutants, KL-A32E, KL-T54E and KFLDV all lack negatively charged residues in the vicinity of the PSB and are therefore not surprising to have much lower  $pK_a$  values compared to the rhodopsins.

In the C<sub>15</sub>-aldehyde-bound KLE-R59W-CRABPII mutant, the counterion, Glu121, is close to the PSB (4.8 Å) and is making indirect hydrogen bonding with the PSB. However, similar to the all-*trans*-retinal-bound KLE-CRABPII mutant, the C<sub>15</sub>-aldehyde-bound KLE-R59W-CRABPII also shows relatively lower  $pK_a$  (7.7). It has been proven that distances between the PSB nitrogen and the counter ion as well as the geometry of the hydrogen bonding also play important roles in determining the  $pK_a$  of

the PSB (36-38). Having a negatively charged residue next to the PSB is therefore not a guarantee for increased  $pK_a$ . While the relatively short distance between the counterion and the PSB (2.6 Å) in the Rt-bound KLE-CRABP II is probably responsible for its relatively lower  $pK_a$  (8.7), the apparent  $pK_a$  of the C<sub>15</sub>-aldehyde-bound KLE-R59W-CRABP II (7.7) is harder to interpret. The  $pK_a$  of the C<sub>15</sub>-aldehyde-bound KLE-R59W-CRABP II was measured in the absence of BTP. Attempts to measure the  $pK_a$  in the presence of 100 mM BTP were not successful due to precipitation of the protein probably caused by the high concentration of BTP.

#### **2.2.4. *Cis* versus *trans* protonated Schiff base.**

As revealed in the crystal structures of different rhodopsins, the PSB always adopts a *trans* conformation (20, 21, 24-26). In our KLE-R59W-C<sub>15</sub>-aldehyde complex, a *trans* double bond is also observed for the PSB. However, in all three of the CRABP II mutants where the C<sub>15</sub>-aldehyde adopts the alternative binding mode, a *cis* double bond was observed. A *cis* imine double bond has also been observed in our KLE-Rt complex previously reported (1). Given the fact that *trans* double bonds are thermodynamically more favored in solution, the formation of the *cis* PSB is apparently due to the positioning of the ligand by specific residues inside the binding cavities of these particular proteins.

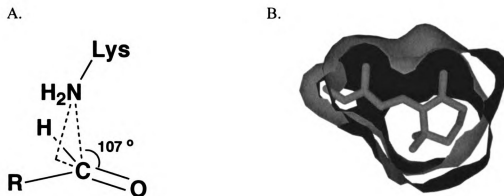


**Figure II-7. A. Proposed nucleophilic attack of lysine amino group to the aldehyde following the Bürgi-Dunitz model; B. Surface representation of C<sub>15</sub>-aldehyde (yellow) bound in KL-A32E (gray).**

In an overly simplified model, let us first assume that the nucleophilic attack happens following the Bürgi-Dunitz trajectory (39, 40), where the lysine nitrogen adopts a favorable 107° attacking angle with the terminal C=O bond of the chromophore and the N-C-O plane bisects the H-C(O)-C angle (Figure II-7A). We could also assume that the C<sub>15</sub>-aldehyde is not moving much from its original binding position due to the tight interactions of the residues around it (Figure II-7B), which is supported by the three CRABPII mutant crystal structures with C<sub>15</sub>-aldehyde bound in the alternative binding pocket (Figure II-6B). Under these two assumptions we would see that during the reaction the lysine side chain would have to either swing in a way to facilitate the formation of a *cis* double bond or swing in another way facilitating formation of a *trans* PSB. Given that the energy difference between a *cis* and a *trans* protonated Schiff base is 7-12 kJ mol<sup>-1</sup> (15-17 kJ mol<sup>-1</sup> for the unprotonated imine) (41), if the energy gained by the lysine swinging into the “*cis*” conformation versus “*trans*” is greater than 12 kJ mol<sup>-1</sup>

<sup>1</sup>, the PSB formed would be *cis*. Otherwise, a *trans* double might be preferred. In the case where the chromophore is less tightly packed, the increased freedom of the ligand would probably favor the more thermodynamically stable *trans* double bond, as seen in the C<sub>15</sub>-aldehyde-bound KLE-R59W mutant structure.

### 2.2.5. Flexibility of the helix-turn-helix lid.

When overlaying different CRABPII mutant structures, one can clearly see that the  $\beta$ -barrel portion of the protein is very rigid, whereas the helix-turn-helix shows flexibility. The flexibility of the helix-turn-helix portion of CRABPII has been previously observed (42). Based on the comparison of the crystal structures we have obtained for CRABPII mutants, the largest movement is observed between the C<sub>15</sub>-aldehyde-bound KL-A32E mutant and the C<sub>15</sub>-aldehyde-bound KLE-R59W mutant, with the longest distance being over 10 Å between the same Ala35 C $\alpha$  in the two different structures (Figure II-8).

As shown in *holo*-KLE-R59W, where the largest outward movement of  $\alpha$ 2 is observed, the C-terminal of this helix (blue color) loses one helical turn and becomes a loop-like structure. Similar unwinding has been observed in several *apo* mutants as well and therefore is not induced by ligand binding. Unfortunately, up to this point, the *apo* structure of KLE-R59W has not been obtained probably due to the decreased structural stability of this protein when there is no ligand bound. This partial unwinding in the C<sub>15</sub>-aldehyde-bound KLE-R59W results in the biggest outward movement among all our

CRABPII mutant crystal structures. Overlay of the C<sub>15</sub>-aldehyde-bound KLE-R59W and the *apo* structure of KLE-R59E that shares the same partial unwinding shows that the ligand would bump into the unwound portion of *apo*-KLE-R59E (Figure II-9A). In *holo*-KLE-R59W the bound C<sub>15</sub>-aldehyde indeed pushed out the unwound C-terminal portion of the  $\alpha 2$  helix even more (Figure II-9B). In other words, the flexible helix lid allows the ligand to bind in this particular trajectory.

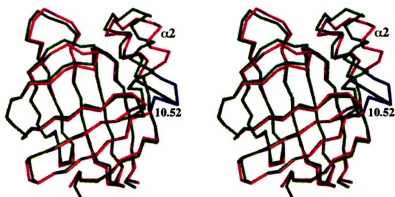


**Figure II-8.** Stereoview of the overlay between *holo*-KL-A32E (green) and *holo*-KLE-R59W (magenta). Blue portion indicates the unwinding of the  $\alpha 2$  helix. Distance (Å) is measured between the C $\alpha$  of Ala35 in the two structures.

The same partial unwinding has been observed in Mol B of the C<sub>15</sub>-aldehyde-bound KFLDV mutant. However, the outward movement is more moderate compared to the *holo*-KLE-R59W. In Mol A of *holo*-KFLDV, the  $\alpha 2$  helix is well maintained and adopts a “median” position in terms of movement by comparison with all the other CRABPII mutant structures solved so far. The fact that the two molecules in the same



asymmetric unit are displaying fairly large structural differences indicates that crystal packing could be playing a role in this partial unwinding of the helix. Both molecules in the asymmetric unit of the *holo*-KL-T54E mutant exhibit well-maintained helices. The positions of the helices in both molecules could also be described as “median” in the context of all the known CRABP II mutant structures.

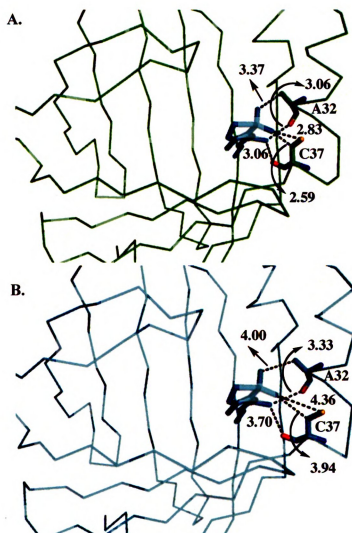


**Figure II-9.** Overlay between C<sub>15</sub>-aldehyde-bound KLE-R59W (blue) and *apo*-KLE-R59E (green). A. Model of C<sub>15</sub>-aldehyde in *apo*-KLE-R59E; B. Crystal structure of C<sub>15</sub>-aldehyde bound in KLE-R59W.

The most inward movement of the  $\alpha 2$  helix is observed in the KL-A32E mutant, where the helical structure is well maintained (Figure II-8). The inward movement of the helix is possibly achieved through hydrogen bonding interactions between the two backbone carbonyl oxygen atoms on the helix and the PSB nitrogen (Figure II-5B). Crystal packing effects from the tight arrangement of neighboring molecules in this crystal, which is not observed in the other three *holo*-CRABPII mutant structures, could also contribute to the movement in the structure of the C<sub>15</sub>-aldehyde-bound KL-A32E mutant. Nevertheless, the results from our crystal structures confirm and clearly demonstrate the great flexibility of the helix-turn-helix motif in CRABPII.

#### **2.2.6. An evolutionary correlation between CRABPII and plasma retinol-binding protein?**

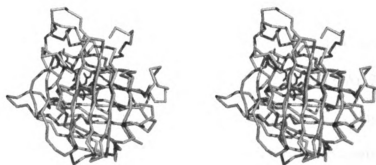
Plasma retinol-binding protein (RBP) is a 21kD protein with 184 amino acid residues and is the first structurally characterized lipocalin protein (16, 17, 43-47). RBP is synthesized in hepatocytes and transports vitamin A (retinol) from the liver, its storage site, to a variety of target tissues (44, 48-50). After being secreted out of the liver and into the extracellular fluid, RBP circulates the plasma by forming a complex with transthyretin (TTR), a thyroid-hormone-transporting protein (51, 52). The complexation protects the relatively small RBP from being lost through glomerular filtration. RBP exhibits a typical lipocalin scaffold (43, 45-47, 53). A hydrophobic binding cavity is formed within an 8-strand  $\beta$ -barrel. Two helices are attached at each terminus of the polypeptide. Unlike CRABPs, the RBP helices are not positioned at the entrance of the

binding site, but instead swing outward into an almost parallel orientation with neighbouring  $\beta$ -barrel strands.

Both CRABPs and RBP belong to the calycin superfamily, which includes fatty acid binding proteins, lipocalins, avidin, metalloproteinase inhibitors, and triabin (17). The calycin proteins all contain a basic  $\beta$ -barrel scaffold to form the binding cavity, which binds small, lipophilic ligands. An evolutionary correlation between cellular retinoid-binding proteins and RBP has been previously suggested, though the sequence homology between the two is very low (10% identity). Through site-directed mutagenesis, Schmidt and co-workers have created a point mutation, Q117I, deep inside the binding pocket of RBP (54). This Gln to Ile mutation established a better hydrophobic interaction with the ionone ring of retinol, which resulted in more than three-fold increase of the expression of the recombinant protein. The conversion into a hydrophobic residue from a hydrophilic one in a hydrophobic environment was believed to lead to further stability of the protein and therefore higher expression level. The same mutant also showed slightly enhanced binding affinity for retinol due to a higher association rate. The authors then raised the question of why nature would place a hydrophilic Gln residue at that critical position when it has better choices. They then compared RBP with cellular retinol-binding protein (CRBP). In CRBP, retinol binds in a completely opposite orientation and a Gln is also present inside the hydrophobic binding pocket, interacting with the hydroxy group of the ligand (55, 56). Interestingly, replacement of Gln with Arg in CRBP has been shown to diminish retinol affinity (57). They therefore speculated that “the Gln117 residue in RBP constitutes an evolutionary

remnant from ancient times when vitamin A might have been bound to the  $\beta$ -barrel in a different manner” (54).

A.



B.

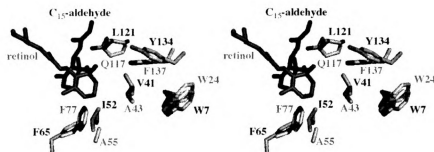


**Figure II-10. Stereoview of the overlay of  $C_{15}$ -aldehyde-bound KL-A32E (green) and retinol-bound RBP (pink). A. Overall scaffold; B. Binding sites overlay.**

What we have observed in our  $C_{15}$ -aldehyde-bound CRABP II system favors the same argument. Although both CRABPs and RBP are retinoid-binding proteins, they differ dramatically in the way that ligands sit inside the  $\beta$ -barrel pockets. Like its iLBP family member CRBP, WT-CRABP II positions its retinoid ligand, RA, with the carboxylate end going inside the cavity and the ionone ring portion solvent-exposed at the entrance. RBP, however, positions retinol in the opposite way with the ionone ring totally buried inside the cavity and the hydroxy group pointing outside, exposed to the

solvent. With the discovery of the alternative binding trajectory of C<sub>15</sub>-aldehyde in KL-A32E and the other two CRABP<sub>II</sub> mutants, we noticed the similarity between the way that C<sub>15</sub>-aldehyde is bound in KL-A32E and the retinol in RBP.

By overlaying the two structures together through secondary structure alignment using the online program “secondary-structure matching” (SSM) (58), 70% of RBP and 58% of CRABP<sub>II</sub> are aligned, respectively, with an rmsd of 2.62 Å (Figure II-10A). In the  $\beta$ -barrel region, the overall folds of the two proteins very much resemble one another. Helical portions of the two, however, do not overlay at all. When looking into the binding cavities of the two, we were happy to find that the ionone ring of C<sub>15</sub>-aldehyde and that of retinol occupy relatively similar positions (Figure II-10). Certain residues around the ionone rings seem to be conserved (Figure II-10B and Table II-2). Phe65 in CRABP<sub>II</sub> and Phe77 in RBP are close to each other in space and both are relatively close to the ionone rings of the ligands (6.2 Å and 4.4 Å, respectively). Tyr134 in CRABP<sub>II</sub> and Phe137 are also close (6.2 Å and 4.6 Å, respectively), approaching the ionone rings from another direction. Trp7 in CRABP<sub>II</sub> and Trp24 in RBP are further away (beyond 8 Å), but are very well conserved. Several other nearby residues, mostly hydrophobic, are also listed in Table 3, with each pair making similar interactions with the ionone rings. Based on this observation, we propose that an evolutionarily conserved, hydrophobic, yet under-used binding cavity is present in CRABP<sub>II</sub>. This observation favors the argument that an evolutionary correlation exists between the intracellular Lipid-Binding Proteins (iLBPs) and the lipocalin protein family.

**Table II-2. Residues around the ionone rings.**

Entry	CRABPII	RBP
1	F65 (6.21)	F77 (4.44)
2	Y134 (6.25)	F137 (4.62)
3	W7 (9.64)	W24 (8.40)
4	T54 (3.74)	A57 (3.45)
5	I52 (3.66)	A55 (3.99)
6	L121 (3.67)	Q117 (4.60)
7	V41 (4.86)	A43 (4.69)

Numbers in parenthesis refer to the closest distances (Å) between the specific residues to the corresponding ionone rings of the ligands.

### **2.2.7. Testing the point charge theory based on the C<sub>15</sub>-aldehyde-bound KLE-R59W-CRABPII structure.**

The high-resolution crystal structures of the C<sub>15</sub>-aldehyde-bound CRABPII mutants revealed detailed binding interactions between the chromophore and the nearby residues. Such information not only gave us confidence in interpreting the wavelength shifts results, but also helped us to identify options for further rational design. We then set out to design out experiments to test the wavelength shifts upon placing negative charged residues next to the polyene chain, referred to as the “point charge theory” (59).

Table II-3 shows a series of KLE-X-CRABPII mutants. As shown in discussed earlier, the three mutations, KLE, not only ensure formation of the PSB between C<sub>15</sub>-aldehyde and Lys132, but also render the ligand to adopt only one binding mode. In addition to the KLE mutations, these mutants were designed in a way that a negatively charged residue was introduced as a fourth mutation at places close to the polyene chain of the chromophore (Figure II-11). As shown in Table II-3, the greatest red shift was observed when a Glu is placed at position 59, which is right next to the ionone ring. As the negative charge moves gradually toward the PSB, the absorption maxima also drop

gradually to about 400 nm. This observation agrees well with the proposed theory in that negative charges placed further away from the PSB should stabilize the positive charge more remotely, leading to more extended conjugation and therefore greater red shift of the absorption maxima.

**Table II-3. Absorption maxima observed for the KLE-X-CRABPII series of mutants**

Mutant	$\lambda_{\text{max}}$ (nm)
C <sub>15</sub> -aldehyde (buffer)	340
C <sub>15</sub> -aldehyde PSB (EtOH)	380
R132K:R111L:L121E	380
R132K:R111L:L121E:R59E	424
R132K:R111L:L121E:A32E	416
R132K:R111L:L121E:A36E	410
R132K:R111L:L121E:F15D	397
R132K:R111L:L121E:V76D	399

\* Results from Kin-Sing Lee.

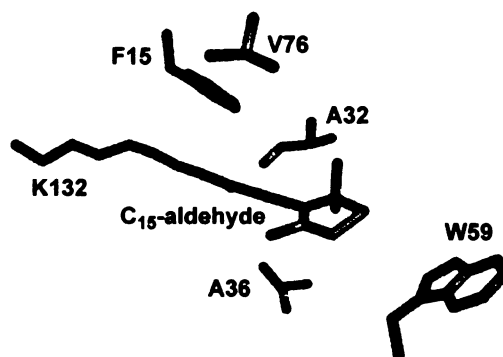


**Figure II-11. C<sub>15</sub>-aldehyde bound in the KLE-R59W-CRABPII mutant.**

## 2.2.8. Conclusion

The crystal structures of four different C<sub>15</sub>-aldehyde-bound CRABPII mutants were determined. Protonated Schiff base formation was observed between the active site

Lys at position 132 and the chromophore. Each of the four mutants contains a unique hydrogen bonding pattern that stabilizes the PSB. Two dramatically different binding orientations were observed in the different mutants with a single mutation at position 121 being key in determining which binding pocket the ligand occupies. Through steric interactions, Glu or Gln at position 121 forces the C<sub>15</sub>-aldehyde into the orthogonal binding mode where the ionone ring of the ligand extends towards the entrance of the cavity. A smaller residue (Leu or Asp) at position 121 allows the ligand to swing into an alternative, deeper, and more hydrophobic cavity. The constrained binding interactions in the alternative binding mode prefers the formation of a *cis* PSB, while the less tightly packed ligand environment in the orthogonal binding mode results in *trans* imine formation. Flexibility of the helix-turn-helix motif was also observed, featuring a dramatic 10 Å movement of Ala35 C $\alpha$  in two C<sub>15</sub>-aldehyde-bound CRABPII mutants. By overlaying the alternative binding mode in the mutant CRABPII with the retinol-bound RBP through secondary structure alignment, we have observed structural resemblances between the two proteins both in the overall  $\beta$ -barrel fold and in the binding environments around the ionone rings of the ligands. Taken together with the previous literature, we proposed that a conserved, yet underused binding pocket is present in CRABPII and that an evolutionary correlation exists between the intracellular Lipid-Binding Proteins (iLBP) and the lipocalin protein family.

A series of KLE-X-CRABPII mutants featuring negatively charged residues placed next to the polyene chain of the chromophore displayed interesting wavelength regulation properties. Negative charge placed further away from the PSB led to a greater red shift of the absorption maximum of the bound chromophore. This result agrees well



with the proposed point charge theory and presumably shed more light to the wavelength regulation mechanism in color vision.

### 2.3. Merocyanin-bound CRABPII mutant structure.

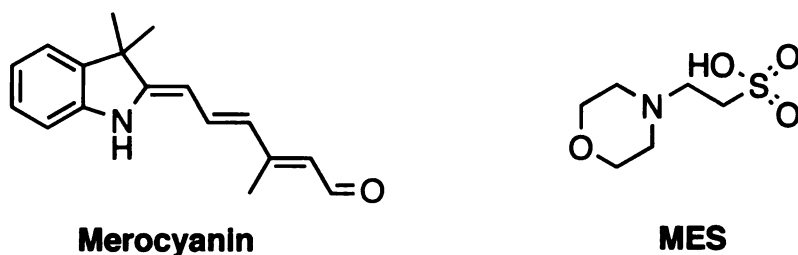


**Figure II-12. Structures of merocyanin and MES.**

**Table II-4. UV maximum absorption of the merocyanin-bound CRABPII mutants.**

	Mutant	$\lambda_{\text{max}}$
1	Merocyanin in EtOH	461
2	Merocyanin in buffer	493
3	Merocyanin PSB in EtOH	578
4	Merocyanin PSB in buffer	573
5	R132K:R111L:L121E	588
6	R132K:R111L:L121E:R59E	596
7	R132K:R111L:L121E:R59W	596
8	R132K:R111L:L121E:T56W	591
9	R132K:R111L:L121E:T56R	591
10	R132K:R111L:L121E:V76E	593
11	R132K:R111L:L121E:V76W	570
12	R132K:R111L:L121E:V76R	586

\* Results from Kin-Sing Lee.

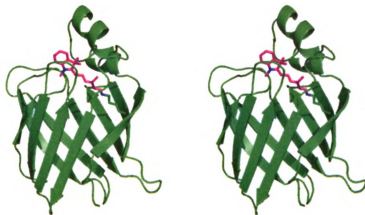
As an effort toward designing CRABPII mutants as fluorescence tags, Kin-Sing Lee and Calvin Grant in the Borhan lab have been working on synthesizing putative

chromophores. An interesting compound, merocyanin, was synthesized and showed excellent spectroscopic properties (Table II-4). By feeding this molecule to a series of CRABP II mutants, red shift of the  $\lambda_{\text{max}}$  was observed in almost all mutants tested. The largest shifts were observed in mutants KLE-R59E and KLE-R59W, both affording an opsin shift of over 20 nm. However, the binding of merocyanin into CRABP II mutants appeared to be much slower compared to C<sub>15</sub>-aldehyde or all-*trans*-retinal.

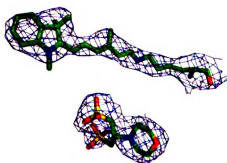
The crystallization of merocyanin-CRABP II mutant complexes was pursued. Structure of the KLE-R59W CRABP II mutant bound with merocyanin was determined at 2.60 Å. The merocyanin is bound the orthogonal way with its aromatic ring extending toward the entrance and positioning itself right under the Trp59 (Figure II-13). The Schiff base formed appears to be in a *trans* conformation and is stabilized by a weak hydrogen bonding interaction from a water molecule that is 3.4 Å away (Figure II-13C). It is interesting to see the *trans* imine formation in this mutant especially when we compare this mutant to the C<sub>15</sub>-aldehyde-bound-KLE-R59W-CRABP II where the ligand binds also in the orthogonal way and also in *trans* imine form. The similarity of binding in the two complexes seems to suggest that shorter chromophores that bind the orthogonal way in CRABP II tends to favor a *trans* imine formation probably due to the ligands' freedom in this spacious binding cavity. A buffer molecule, 2-(*N*-morpholino)ethanesulfonic acid (MES), is found to be bound inside the cavity as well (Figure II-13B), occupying a space approximately where BTP molecules are found in some other CRABP II mutant structures. The overall fold of this merocyanin-bound-

KLE-R59W-CRABPII resembles the C<sub>15</sub>-aldehyde-bound-KLE-R59W-CRABPII structure, with similar partial unwinding at the C-terminal end of the  $\alpha$ 2 helix.

A.



B.



C.

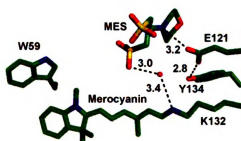


**Figure II-13. Merocyanin bound in KLE-R59W-CRABPII mutant.** A. Stereoview of the overall fold of the protein; B. 2Fo-Fc map calculated at 1  $\sigma$ ; C. Detailed binding interactions between merocyanin and the protein.

This merocyanin molecule shows excellent fluorescence ability after being complexed with CRABPII mutants. In particular, the complex between merocyanin and KLE-R59W-CRABPII is capable to emit fluorescence at 614 nm after being excited at

570 nm (to be published by Kin-Sing Lee). This serves as the proof-of-concept for designing CRABP<sub>II</sub> mutants as ligand-inducible fluorescence fusion tags. The structural information obtained from this complex will also be instructional for directing our future ligand design and protein engineering efforts.

## References

1. Vasileiou, C., Vaezeslami, S., Crist, R. M., Rabago-Smith, M., Geiger, J. H., and Borhan, B. (2007) Protein design: Reengineering Cellular Retinoic Acid Binding Protein II into a rhodopsin protein mimic, *J Am Chem Soc* 129, 6140-6148.
2. Gerisch, G., and Muller-Taubenberger, A. (2003) GFP-fusion proteins as fluorescent reporters to study organelle and cytoskeleton dynamics in chemotaxis and phagocytosis, *Method Enzymol* 361, 320-337.
3. Hoffman, R. M. (2005) The multiple uses of fluorescent proteins to visualize cancer in vivo, *Nat Rev Cancer* 5, 796-806.
4. Lippincott-Schwartz, J., Snapp, E., and Kenworthy, A. (2001) Studying protein dynamics in living cells, *Nat Rev Mol Cell Bio* 2, 444-456.
5. Muller-Taubenberger, A., and Anderson, K. I. (2007) Recent advances using green and red fluorescent protein variants, *Appl Microbiol Biot* 77, 1-12.
6. Shaner, N. C., Patterson, G. H., and Davidson, M. W. (2007) Advances in fluorescent protein technology, *J Cell Sci* 120, 4247-4260.
7. Tsien, R. Y. (1998) The green fluorescent protein, *Annu Rev Biochem* 67, 509-544.
8. VanEngelenburg, S. B., and Palmer, A. E. (2008) Fluorescent biosensors of protein function, *Curr Opin Chem Biol* 12, 60-65.
9. Heim, R., Prasher, D. C., and Tsien, R. Y. (1994) Wavelength Mutations and Posttranslational Autoxidation of Green Fluorescent Protein, *P Natl Acad Sci USA* 91, 12501-12504.
10. Phillips, G. J. (2001) Green fluorescent protein - a bright idea for the study of bacterial protein localization, *Fems Microbiol Lett* 204, 9-18.
11. Baumann, C. T., Lim, C. S., and Hager, G. L. (1998) Simultaneous visualization of the yellow and green forms of the green fluorescent protein in living cells, *J Histochem Cytochem* 46, 1073-1076.
12. Chalfie, M., Tu, Y., Euskirchen, G., Ward, W. W., and Prasher, D. C. (1994) Green Fluorescent Protein as a Marker for Gene-Expression, *Science* 263, 802-805.
13. Cormack, B. P., Valdivia, R. H., and Falkow, S. (1996) FACS-optimized mutants of the green fluorescent protein (GFP), *Gene* 173, 33-38.

14. Hein, R., and Tsien, R. Y. (1996) Engineering green fluorescent protein for improved brightness, longer wavelengths and fluorescence resonance energy transfer, *Curr Biol* 6, 178-182.
15. Akerstrom, B., Flower, D. R., and Salier, J. P. (2000) Lipocalins: unity in diversity, *Bba-Protein Struct M* 1482, 1-8.
16. Flower, D. R. (2000) Experimentally determined lipocalin structures, *Bba-Protein Struct M* 1482, 46-56.
17. Flower, D. R., North, A. C. T., and Sansom, C. E. (2000) The lipocalin protein family: structural and sequence overview, *Bba-Protein Struct M* 1482, 9-24.
18. Skerra, A. (2000) Lipocalins as a scaffold, *Bba-Protein Struct M* 1482, 337-350.
19. Lee, K. S., Jia, X., Vasileiou, C., Geiger, J. H., and Borhan, B., To be published.
20. Okada, T., Sugihara, M., Bondar, A. N., Elstner, M., Entel, P., and Buss, V. (2004) The retinal conformation and its environment in rhodopsin in light of a new 2.2 angstrom crystal structure, *Journal of Molecular Biology* 342, 571-583.
21. Palczewski, K., Kumasaka, T., Hori, T., Behnke, C. A., Motoshima, H., Fox, B. A., Le Trong, I., Teller, D. C., Okada, T., Stenkamp, R. E., Yamamoto, M., and Miyano, M. (2000) Crystal structure of rhodopsin: A G protein-coupled receptor, *Science* 289, 739-745.
22. Kholmurodov, K. T., Fel'dman, T. B., and Ostrovsky, M. A. (2007) Interaction of chromophore, 11-cis-retinal, with amino acid residues of the visual pigment rhodopsin in the region of protonated Schiff base: A molecular dynamics study, *Russian Chemical Bulletin* 56, 20-27.
23. Sekharan, S., Sugihara, M., and Buss, V. (2007) Origin of spectral tuning in rhodopsin - It is not the binding pocket, *Angewandte Chemie-International Edition* 46, 269-271.
24. Luecke, H., Schobert, B., Lanyi, J. K., Spudich, E. N., and Spudich, J. L. (2001) Crystal structure of sensory rhodopsin II at 2.4 angstroms: Insights into color tuning and transducer interaction, *Science* 293, 1499-1503.
25. Facciotti, M. T., Rouhani, S., Burkard, F. T., Betancourt, F. M., Downing, K. H., Rose, R. B., McDermott, G., and Glaeser, R. M. (2001) Structure of an early intermediate in the M-state phase of the bacteriorhodopsin photocycle, *Biophys J* 81, 3442-3455.
26. Kolbe, M., Besir, H., Essen, L. O., and Oesterhelt, D. (2000) Structure of the light-driven chloride pump halorhodopsin at 1.8 angstrom resolution, *Science* 288, 1390-1396.

27. Brady, L., Brzozowski, A. M., Derewenda, Z. S., Dodson, E., Dodson, G., Tolley, S., Turkenburg, J. P., Christiansen, L., Hugejensen, B., Norskov, L., Thim, L., and Menge, U. (1990) A Serine Protease Triad Forms the Catalytic Center of a Triacylglycerol Lipase, *Nature* 343, 767-770.
28. Jaeger, K. E., Dijkstra, B. W., and Reetz, M. T. (1999) Bacterial biocatalysts: Molecular biology, three-dimensional structures, and biotechnological applications of lipases, *Annual Review of Microbiology* 53, 315-+.
29. Kraut, J. (1977) Serine Proteases - Structure and Mechanism of Catalysis, *Annu Rev Biochem* 46, 331-358.
30. Menard, R., and Storer, A. C. (1992) Oxyanion Hole Interactions in Serine and Cysteine Proteases, *Biological Chemistry Hoppe-Seyler* 373, 393-400.
31. Druckmann, S., Ottolenghi, M., Pande, A., Pande, J., and Callender, R. H. (1982) Acid-Base-Equilibrium of the Schiff-Base in Bacteriorhodopsin, *Biochemistry-US* 21, 4953-4959.
32. Koutalos, Y. (1992) High-Ph Form of Bovine Rhodopsin, *Biophys J* 61, 272-275.
33. Koutalos, Y., Ebrey, T. G., Gilson, H. R., and Honig, B. (1990) Octopus Photoreceptor-Membranes - Surface-Charge Density and Pk of the Schiff-Base of the Pigments, *Biophys J* 58, 493-501.
34. Liang, J., Steinberg, G., Livnah, N., Sheves, M., Ebrey, T. G., and Tsuda, M. (1994) The Pk(a) of the Protonated Schiff-Bases of Gecko Cone and Octopus Visual Pigments, *Biophys J* 67, 848-854.
35. Steinberg, G., Ottolenghi, M., and Sheves, M. (1993) Pk(a) of the Protonated Schiff-Base of Bovine Rhodopsin - a Study with Artificial Pigments, *Biophys J* 64, 1499-1502.
36. GAT, Y., and Sheves, M. (1993) A Mechanism for Controlling the Pk(a) of the Retinal Protonated Schiff-Base in Retinal Proteins - a Study with Model Compounds, *J Am Chem Soc* 115, 3772-3773.
37. Scheiner, S., and Hillenbrand, E. A. (1985) Modification of Pk Values Caused by Change in H-Bond Geometry, *P Natl Acad Sci USA* 82, 2741-2745.
38. Taylor, R., Kennard, O., and Versichel, W. (1983) Geometry of the N-H= $\pi$ C Hydrogen-Bond .1. Lone-Pair Directionality, *J Am Chem Soc* 105, 5761-5766.
39. Burgi, H. B., and Dunitz, J. D. (1983) From Crystal Statics to Chemical-Dynamics, *Accounts of Chemical Research* 16, 153-161.

40. Burgi, H. B., Dunitz, J. D., and Shefter, E. (1973) Geometrical Reaction Coordinates .2. Nucleophilic Addition to a Carbonyl Group, *J Am Chem Soc* 95, 5065-5067.
41. Hammerum, S., and Solling, T. I. (1999) The proton affinities of imines and the heats of formation of immonium ions investigated with composite ab initio methods, *J Am Chem Soc* 121, 6002-6009.
42. Wang, L. C., Li, Y., Abildgaard, F., Markley, J. L., and Yan, H. G. (1998) NMR solution structure of type II human cellular retinoic acid binding protein: Implications for ligand binding, *Biochemistry-Us* 37, 12727-12736.
43. Cowan, S. W., Newcomer, M. E., and Jones, T. A. (1990) Crystallographic Refinement of Human Serum Retinol Binding-Protein at 2a Resolution, *Proteins* 8, 44-61.
44. Kanai, M., Raz, A., and Goodman, D. S. (1968) Retinol-Binding Protein - Transport Protein for Vitamin a in Human Plasma, *Journal of Clinical Investigation* 47, 2025-&.
45. Newcomer, M. E., Jones, T. A., Aqvist, J., Sundelin, J., Eriksson, U., Rask, L., and Peterson, P. A. (1984) The 3-Dimensional Structure of Retinol-Binding Protein, *Embo Journal* 3, 1451-1454.
46. Zanotti, G., Berni, R., and Monaco, H. L. (1993) Crystal-Structure of Liganded and Unliganded Forms of Bovine Plasma Retinol-Binding Protein, *J Biol Chem* 268, 10728-10738.
47. Zanotti, G., Ottonello, S., Berni, R., and Monaco, H. L. (1993) Crystal-Structure of the Trigonal Form of Human Plasma Retinol-Binding Protein at 2.5-Angstrom Resolution, *Journal of Molecular Biology* 230, 613-624.
48. Blomhoff, R. (1994) Transport and Metabolism of Vitamin-A, *Nutrition Reviews* 52, 13-23.
49. Blomhoff, R., Green, M. H., Berg, T., and Norum, K. R. (1990) Transport and Storage of Vitamin-A, *Science* 250, 399-404.
50. Quadro, L., Blaner, W. S., Salchow, D. J., Vogel, S., Piantedosi, R., Gouras, P., Freeman, S., Cosma, M. P., Colantuoni, V., and Gottesman, M. E. (1999) Impaired retinal function and vitamin A availability in mice lacking retinol-binding protein, *Embo Journal* 18, 4633-4644.
51. Goodman, D. S., and RAZ, A. (1972) Extraction and Recombination Studies of Interaction of Retinol with Human Plasma Retinol-Binding Protein, *Journal of Lipid Research* 13, 338-&.



52. Monaco, H. L., Rizzi, M., and Coda, A. (1995) Structure of a Complex of 2 Plasma-Proteins - Transthyretin and Retinol-Binding Protein, *Science* 268, 1039-1041.
53. Grzyb, J., Latowski, D., and Strzalka, K. (2006) Lipocalins - a family portrait, *Journal of Plant Physiology* 163, 895-915.
54. Schmidt, A. M., Bloss, I., and Skerra, A. (1998) Improved folding of apo-retinol-binding protein in the periplasm of *Escherichia coli*: positive influences of dsbC coexpression and of an amino acid exchange in the vitamin A binding site, *Protein Engineering* 11, 601-607.
55. Calderone, V., Folli, C., Marchesani, A., Berni, R., and Zanotti, G. (2002) Identification and structural analysis of a zebrafish apo and holo cellular retinol-binding protein, *Journal of Molecular Biology* 321, 527-535.
56. Cowan, S. W., Newcomer, M. E., and Jones, T. A. (1993) Crystallographic Studies on a Family of Cellular Lipophilic Transport Proteins - Refinement of P2 Myelin Protein and the Structure Determination and Refinement of Cellular Retinol-Binding Protein in Complex with All-Trans-Retinol, *Journal of Molecular Biology* 230, 1225-1246.
57. Stump, D. G., Lloyd, R. S., and Chytil, F. (1991) Site-Directed Mutagenesis of Rat Cellular Retinol-Binding Protein - Alteration in Binding-Specificity Resulting from Mutation of Glutamine-108 to Arginine, *J Biol Chem* 266, 4622-4630.
58. Krissinel, E., and Hendrick, K. Protein structure comparison service SSM at European Bioinformatic Institute (<http://www.ebi.ac.uk/msd-srv/ssm>).
59. Nathans, J., Thomas, D., and Hogness, D. S. (1986) Molecular-Genetics of Human Color-Vision - the Genes Encoding Blue, Green, and Red Pigments, *Science* 232, 193-202.

## **CHAPTER III. Crystal Structures of the Apo-CRABPII Mutants**

### **3.1. Introduction**

Retinoic acid (RA) is the most important metabolite of vitamin A (retinol) in vertebrates. It has been proven to play indispensable roles during cell growth and differentiation by regulating the transcription of a variety of target genes (1-4). RA also possesses antitumor activity. RA and other retinoid analogs have been successfully employed in treatment against several types of cancers, including acute promyelocytic leukemia (2), skin cancer (5) and cervical cancer (6).

The transcription effects of RA are exerted through binding of RA to the retinoic acid receptor (RAR). RAR is a nuclear transcriptional activator, which forms a heterodimer with retinoids X receptor (RXR) upon association with RA (7-10). The RAR/RXR dimer then recognizes the RA-response elements on specific target genes and regulates their transcription.

The delivery of RA to RAR is facilitated by cellular retinoic acid binding proteins (CRABPs), members of the intracellular lipid-binding protein family (iLBP) (11-13). CRABPs are cytosolic, small (~16 kD), and soluble proteins that are found in all vertebrates (14). There are two types of CRABPs, CRABPI and CRABPII. CRABPI and II are highly conserved (both >90% identity) across species, respectively (15, 16). The identity between CRABPI and CRABPII in the same species, however, is relatively lower (74% in human). Therefore, the two proteins probably diverged at a fairly early stage during evolution and have distinct cellular functions. CRABPs modulate the RA

effective concentration through multiple ways, including binding to excess RA and/or metabolizing the excess RA in the cell through interaction with metabolizing enzymes. CRABPI and II deliver RA to RAR through different mechanisms (17-19). While CRABPI shows no interaction with RAR, CRABPII has been shown to localize into the nucleus upon RA complexation and delivers RA to RAR through protein/protein interactions (16, 20).

The crystal structures of the wild-type CRABPI and II have been solved earlier (21, 22). Both proteins adopt a typical iLBP fold with a rigid " $\beta$ -barrel" forming a huge binding cavity and a flexible helix-turn-helix motif functioning as a "lid" at the entrance (Figure III-1). Interestingly, water-mediated interactions are observed in the cavity of apo-WT-CRABPII MolA, connecting the Arg111 deep inside the cavity through Arg132 to the Ala36 and Val33 on the  $\alpha$ 2 helix. The water-mediated network is not observed in MolB probably due to the crystal packing. The difference in crystal packing environments between MolA and MolB at the  $\alpha$ 2 helix region is dramatic, which is apparent from the number of the intermolecular interactions that each  $\alpha$ 2 helix makes with the neighboring molecules: MolA has 0 hydrogen bond and 8 vdw contacts and MolB has 7 hydrogen bonds and 43 vdw contacts.

Similar water-mediated networks have been observed in other members of the iLBP family, such as CRABPI (23) and intestinal fatty acid-binding protein (24), and suggested to play important roles in maintaining the stability of these proteins. In the rat intestinal fatty acid-binding protein (FABP) structure (1IFC, 1.2 Å), the water-mediated network connects the Arg106 (conserved residue of Arg111 in CRABPII) through Arg126 (conserved residue of Arg132 in CRABPII) to Asp34 and Ala32 on the  $\alpha$ 2 helix

at the portal. In the CRABPI structure (1CBI), the network is observed, but not in a continuous manner. This is probably a result of certain water molecules not being observed due to the relatively low resolution of the structure (2.7 Å). In the high resolution structure of cellular retinol-binding protein II (CRBP<sub>II</sub>, 1.2 Å, PDB ID: 2RCQ), which is also an iLBP family member, the water-mediated network is again observed, which also resembles the one in apo-WT-CRAB<sub>II</sub>. In the apo-CRBP<sub>II</sub> structure, the network starts at the Glu108 (conserved residue of Arg111 in CRAB<sub>II</sub> based on similarity) and extends to Ala36 and Val33 (both conserved in CRAB<sub>II</sub> based on identity). These observations further emphasize the structural importance of these water-mediated networks for the iLBP family proteins.

In the course of our study, we have generated many different CRAB<sub>II</sub> mutants. The crystallization trials of these mutants have resulted in both ligand-bound and apo-structures of certain mutants. In this chapter, the apo-CRAB<sub>II</sub> mutant structures will be reported. Interesting structural information that is obtained from these structures will be discussed.

## **3.2. Results**

### **3.2.1. Mutations of conserved and non-conserved residues**

Through site-directed mutagenesis, we have created a series of CRAB<sub>II</sub> mutants, each of which carry multiple mutations involving both conserved and non-conserved residues (25). All of the mutation sites that are involved in these mutants are shown in Figure III-1.

Arg132 resides deep inside the binding pocket and is a fully conserved residue in the basis of identity in the intracellular binding protein family. In the WT-CRABP<sub>II</sub>, Arg132 directly interacts with the incoming carboxylate group of the retinoic acid (RA). The R132K mutation therefore greatly decreases the binding affinity of CRABP<sub>II</sub> toward RA.

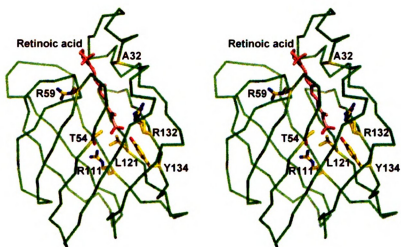


**Figure III-1. Stereoview of the mutation sites involved in these CRABP<sub>II</sub> mutants.** Tertiary structure of CRABP<sub>II</sub> is represented by retinoic acid-bound CRABP<sub>II</sub> (PDB code: 2FR3).

Tyr134 and Arg111 are also positioned deep in the pocket and are conserved residues based on similarity. Y134F is a very conserved mutation and ~20% of the iLBP family members actually have Phe at 134 as the native residue. R111L mutation, however, introduces a dramatic change from the hydrophilic Arg to a hydrophobic Leu, which enhances the hydrophobicity of the cavity and also creates an extra space due to the size differences of the two residues.

Arg59, Ala32 and Thr54 are also conserved residues based on similarity. Among the three, Arg59 and Ala32 are fully conserved residues and Thr54 is conserved in 46 out

of 52 iLBP family members. These three residues are not deep inside the cavity and are instead at positions where the linear part of RA interacts with. R59E mutation, which happens at the entrance, switches the positively charged Arg to a negatively charged Glu. T54E or T54V mutations meant to decrease or increase the hydrophobicity of the cavity, respectively. A32E mutation is unique in that it is the only mutation listed here that involves a mutation of a residue on the helix. The change induced by this mutation is also unique in that the whole  $\alpha 2$  helix in MolB of apo-KL-A32E mutant is completely disordered.

The Leu121 is not a conserved residue. The mutations, L121E or L121D, both introduce negatively charged residues deep inside the cavity replacing a neutral residue, which decreases the hydrophobicity of the cavity.

Generally, combinations of these mutations do not change the overall fold of the CRABP II greatly, except for the R132K:R111L:A32E (KL-A32E) mutant where the  $\alpha 2$  helix is completely disordered in MolB.

### **3.2.2. The structure of apo-R132K:R111L:L121E:R59E-CRABP II (apo-KLE-R59E)**

The structure of apo-KLE-R59E is solved at 1.85 Å with final  $R_{\text{work}}$  and  $R_{\text{free}}$  of 18.6% and 24.8%, respectively. The Ramachandran plot indicated that all of the residues except Asp126 are in the favored/allowed region. Asp126 in both MolA and MolB is in the disallowed region. However, the electron density map suggests the correct assignment of the residue. The same residue has always been found in the disallowed region in previously solved CRABP II structures (22), which added to our confidence for

the assignment for this residue. The overall fold of this mutant is approximately the same as WT-CRABP II (PDB ID: 1CBS, 2FR3) with RMSD of 1.117 for MolA (Figure III-2A) and 0.463 for MolB (Figure III-2B). The MolBs of the two molecules are very similar which is also obvious from the RMSD value of 0.463. The two MolAs are, however, experiencing greater differences. The main difference lies in the region where the C-terminal of the  $\alpha 2$  helix meets the  $\beta C$ - $\beta D$  loop. A partial unwinding of the  $\alpha 2$  helix is clearly observed in MolA of the apo-KLE-R59E mutant structure, which is not observed in MolB and in either of the molecules of the WT-CRABP II structure. To accommodate this movement, the  $\beta C$ - $\beta D$  loop in apo-KLE-R59E correspondingly adopts an outward movement, compared to the WT-CRABP II MolA. Similar movements have been observed in previously solved apo-KLE-CRABP II mutant structure (PDB ID: 3D97).

The Arg59 in the WT-CRABP II resides on the  $\beta C$ - $\beta D$  loop and guards the entrance of the protein. In the WT-CRABP II structure, Arg59 interacts with Gln74 through two water-mediated hydrogen bonding (Figure III-2C), which is disrupted upon the R59E mutation in the apo-KLE-R59E mutant (Figure III-2D). Clearly, the disruption of this interaction does not affect the overall rigidity of the CRABP II. The other three mutations, R132K:R111L:L121E, are all deep inside the active site. A buffer molecule, bis-tris-propane (BTP), is present inside the binding cavity in both MolA and MolB (Figure III-2E). In both molecules, BTP is close to Trp109 and partly fills the hydrophobic hole created by R111L mutation as the overlay between this mutant and the WT-CRABP II shows that Arg111 side chain would compete with the BTP for the same space. The atomic positions of BTP in MolA are well defined with an average B factor of  $37.8 \text{ \AA}^2$ , reasonably higher than the overall B factor ( $28.9 \text{ \AA}^2$ ). The BTP in MolB,

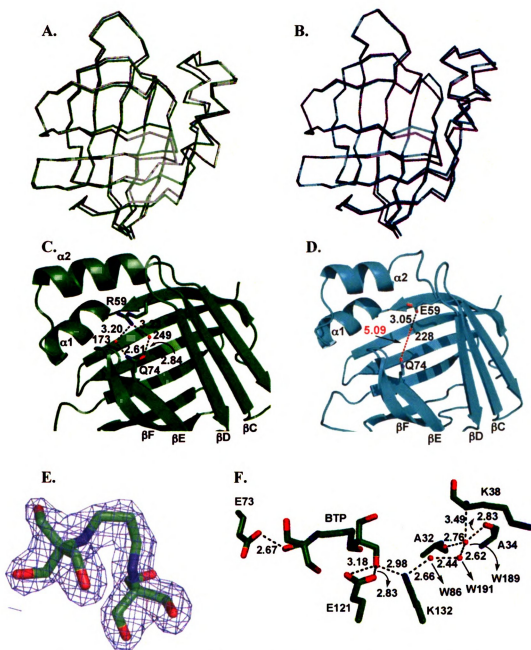


**Figure III-2. Structure of the apo-KLE-R59E-CRABPII.** (a) Overlay of MolA of apo-KLE-R59E-CRABPII (gray) and MolA of apo-WT-CRABPII (green); (b) Overlay of MolB of apo-KLE-R59E-CRABPII (purple) and MolB of apo-WT-CRABPII (cyan); (c) Salt bridge between Arg59 and Gln74 in apo-WT-CRABPII MolA; (d) Disrupted salt bridge in apo-KLE-R59E-CRABPII MolA; (e) 2Fo-Fc map calculated at 1.0  $\sigma$  for bis-tris-propane bound in apo-KLE-R59E-CRABPII MolA; (f) Water-mediated interactions in MolA of apo-KLE-R59E-CRABPII.



however, is poorly defined (average B: 65.2 Å<sup>2</sup>) even though the bulk electron density clearly suggests its presence. Overlaying the MolA and MolB shows that the two BTP molecules do not overlap with each other. In MolA, the BTP makes three hydrogen bonding interactions with the nearby protein residues. In MolB, however, the hydrogen bonding interactions are harder to assign due to our lack of confidence for each atomic position of the molecule.

A water-mediated network is clearly shown, involving polar residues, BTP and the ordered water molecules and extending from deep down in the cavity to the  $\alpha$ 2 helix at the entrance (Figure III-2F). Similar water-mediated interactions have been observed in previously solved CRABP II mutant structures and have been proposed to be important in maintaining the structural integrity of CRABP II by acting as a pillar inside the huge, hydrophobic binding cavity of CRABP II.

### **3.2.3. The structure of apo-R132K:Y134F:R111L:L121E-CRABP II (apo-KFLE)**

The structure of apo-KFLE was solved at a resolution of 1.78 Å with  $R_{\text{work}}$  and  $R_{\text{free}}$  of 18.0% and 23.8%, respectively. The Ramachandran plot indicates again that Asp126 is the only residue sitting outside of the allowed region in both molecules of the asymmetric unit. The protein also maintains the rigid overall structure. Overlay of this mutant structure with the WT-CRABP II gives RMSD of 1.137 for MolA (Figure III-3A) and 0.450 for MolB (Figure III-3B), which is similar to the ones observed for KLE-

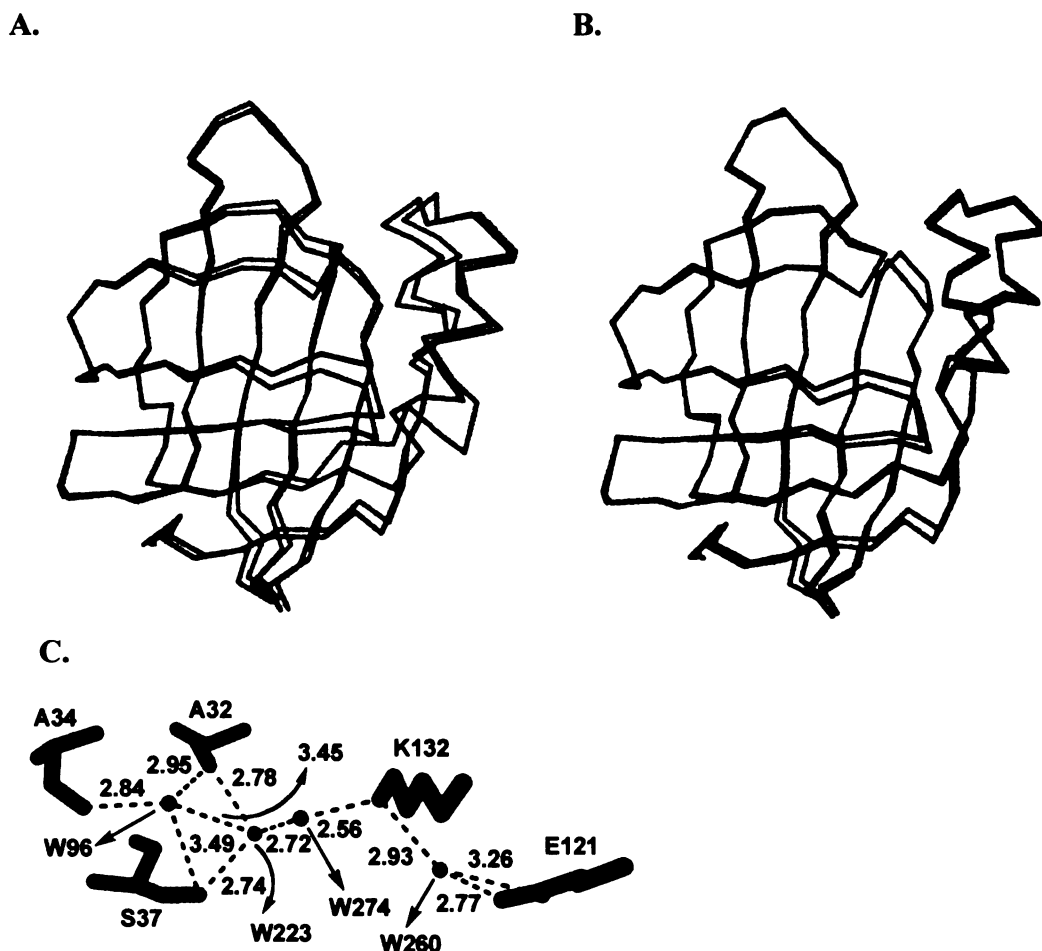


**Figure III-3. Structure of the apo-KFLE-CRABPII.** (a) Overlay of MolA of apo-KFLE-CRABPII (purple) and MolA of apo-WT-CRABPII (green); (b) Overlay of MolB of apo-KFLE-CRABPII (orange) and MolB of apo-WT-CRABPII (cyan); (c) Water-mediated interaction in apo-KFLE-CRABPII MolA.

R59E. In fact, this apo-KFLE mutant structure greatly resembles that of the KLE-R59E mutant including the same partial unwinding at the  $\alpha 2$  helix region in MolA. The RMSD between the two structures is 0.200 for MolA and 0.276 for MolB. This resemblance is not very surprising. Except for the three common mutations, R132K:R111L:L121E, that are shared between KFLE and KLE-R59E, the fourth mutation in the KFLE mutant, Y134F, is a conserved mutation inside the binding site. Therefore, minimal overall

structural changes should be expected upon this mutation. There is no BTP bound in either of the molecules even though the growth condition for the crystal also contains BTP. In MolA of apo-KFLE, the water-mediated interactions are as follows: Glu121-W260-Lys132-W274-W223-carbonyl group of Ala32/carbonyl group of Ser37 (Figure III-3C).

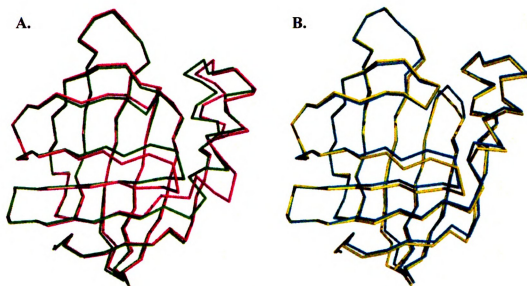


**Figure III-4. Structure of the apo-KFLD-CRABPII.** (a) Overlay of MolA of apo-KFLD-CRABPII (magenta) and MolA of apo-WT-CRABPII (green); (b) Overlay of MolB of apo-KFLD-CRABPII (yellow) and MolB of apo-WT-CRABPII (cyan).

#### 3.2.4. The structure of apo-R132K:Y134F:R111L:L121D-CRABPII (apo-KFLD)

The structure of apo-KFLD was solved at 1.94 Å with  $R_{\text{work}}$  and  $R_{\text{free}}$  of 21.0% and 27.7%, respectively. Again, the overall structure of this mutant resembles those of KLE-R59E (0.271 for MolA and 0.256 for MolB) and KFLE (0.210 for MolA and 0.188 for MolB). The same partial unwinding is also observed at the C-terminal of the  $\alpha 2$  helix

region in MolA (Figure III-4). The helical structures are well maintained in MolB. The crystal was also grown in conditions with BTP as the buffer and yet no BTP was found in the crystal structure of this mutant. Surprisingly, the water-mediated interactions are not observed in this mutant.

### **3.2.5. The structure of apo-R132K:Y134F:R111L:L121D:T54V-CRABP II (apo-KFLD-T54V)**

The structure of apo-KFLD-T54V was solved at 1.51 Å. Final  $R_{\text{work}}$  and  $R_{\text{free}}$  after refinement are 17.1% and 21.2%, respectively. The Ramachandran plot showed again that Asp126 is the only residue that is outside of the favored/allowed region. There is no buffer molecule bound inside the binding cavity. Interestingly, no partial unwinding is observed for the  $\alpha 2$  helix in MolA of this mutant (Figure III-5A,B). Since this KFLD-T54V mutant only differs from the KFLD mutant by a single mutation, T54V, and this mutation did not change the size, shape or conformation of the residue, it may suggest that the appearance of the partial unwinding of the  $\alpha 2$  helix C-terminal is random. Due to the fully maintained helical turns, the structure of this mutant now shares more structural similarity with the apo-WT-CRABP II structure (RMSD: 0.302 for MolA and 0.363 for MolB) than with that of the apo-KFLD mutant (RMSD: 1.136 for MolA and 0.344 for MolB). The water-mediated interactions are shown in Figure III-5C.

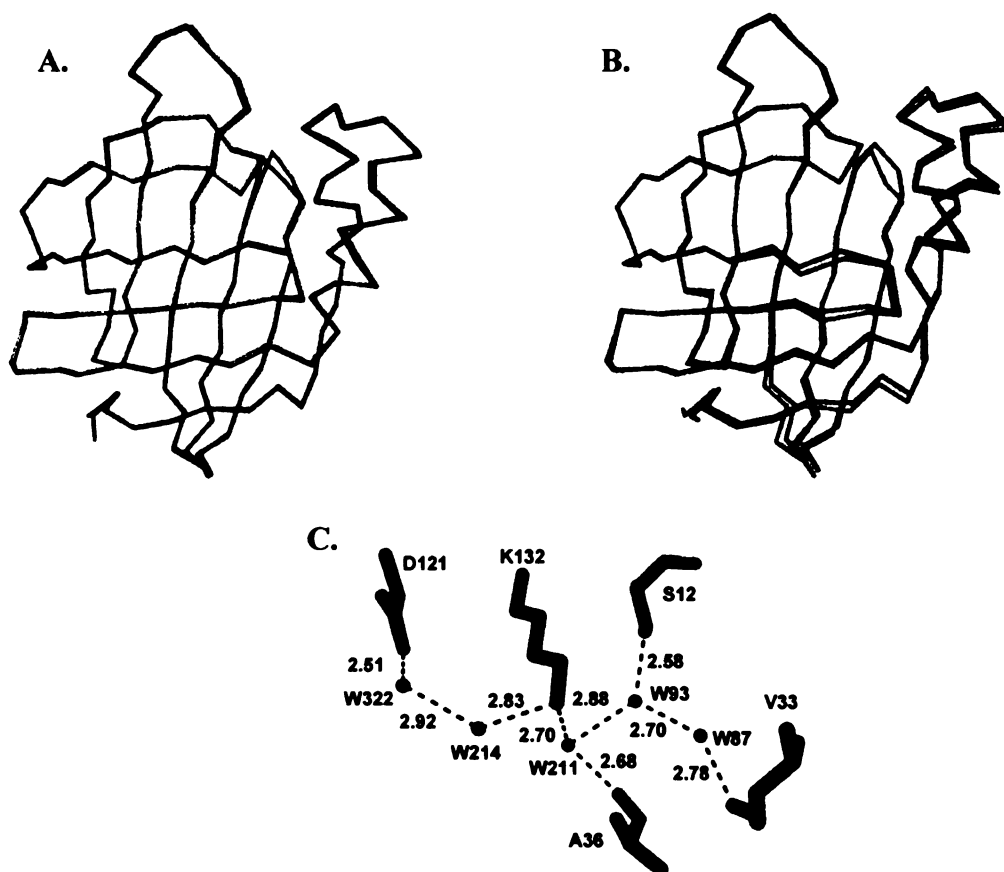


**Figure III-5. Structure of the apo-KFLD-T54V-CRABP II.** (a) Overlay of MolA of apo-KFLD-T54V-CRABP II (pink) and MolA of apo-WT-CRABP II (green); (b) Overlay of MolB of apo-KFLD-T54V-CRABP II (purple) and MolB of apo-WT-CRABP II (cyan); (c) Water-mediated interactions in the apo-KFLD-T54V-CRABP II.

### 3.2.6. The structure of apo-R132K:R111L:T54E-CRABP II (apo-KL-T54E)

The structure of apo-KL-T54E was solved at 1.85 Å resolution. Final  $R_{\text{work}}$  and  $R_{\text{free}}$  after refinement are 18.8% and 24.4%, respectively. Asp126 is still the only residue that sits outside of the favored/allowed region in the Ramachandran plot. There is no partial unwinding on the  $\alpha 2$  helix in MolA. The RMSD values between this mutant structure and that of the WT-CRABP II are 0.369 for MolA (Figure III-6A) and 0.344 for MolB (Figure III-6B). BTP molecules are found in the cavities of both MolA and MolB

of this mutant structure (Figure III-6C). It need to be pointed out that the B factors for both BTP molecules in this structure (56.3 Å<sup>2</sup> in MolA and 84.0 in MolB) are much higher than the average B factor of the whole structure (24.0 Å<sup>2</sup>). Long-range water-mediated interactions are absent in this mutant probably due to the absence of charged residues (Arg111 or Glu121) deep inside the cavity. Short-ranged water-mediated interactions are found between the Glu54 and the α2 helix: carboxylate group of Glu54-W187-W172-carbonyl group of Ala36 (Figure III-6D). The Glu54 also forms hydrogen bonds with the bound BTP.

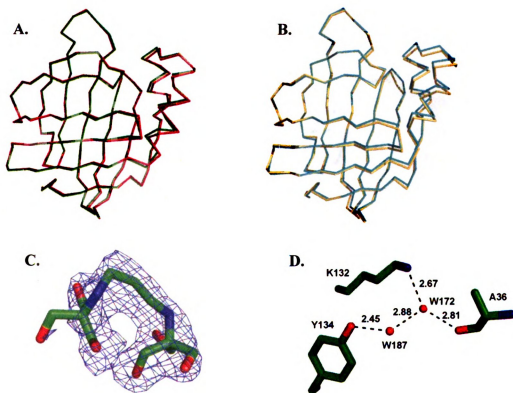


**Figure III-6. Structure of the apo-KL-T54E-CRABPII.** (a) Overlay of MolA of apo-KL-T54E-CRABPII (hot pink) and MolA of apo-WT-CRABPII (green); (b) Overlay of MolB of apo-KL-T54E-CRABPII (yellow) and MolB of apo-WT-CRABPII (cyan); (c) 2Fo-Fc map of the BTP bound calculated at 1.0  $\sigma$ ; (d) Water-mediated interactions in MolA of the apo-KL-T54E-CRABPII.

### 3.2.7. The structure of apo-R132K:R111L:A32E-CRABP II (apo-KL-A32E)

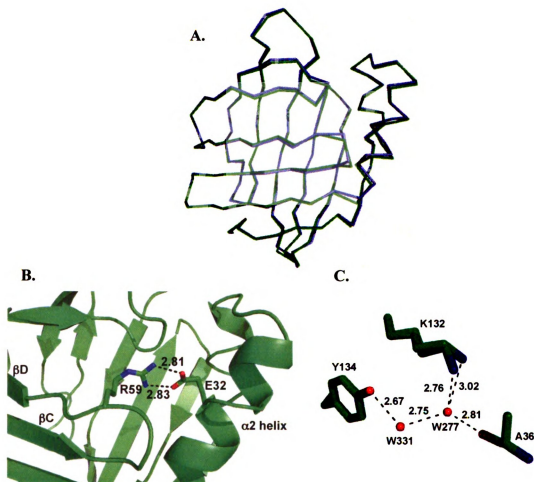


**Figure III-7. Structure of the apo-KL-A32E-CRABP II.** (a) Overlay of MolA of apo-KL-A32E-CRABP II (purpleblue) and MolA of apo-WT-CRABP II (green); (b) Salt bridge between Arg59 and Glu32 in the apo-KL-A32E-CRABP II MolA; (c) Water-mediated interactions in MolA of the apo-KL-A32E-CRABP II.

The crystal structure of apo-KL-A32E was solved at 1.56 Å resolution. Final  $R_{\text{work}}$  and  $R_{\text{free}}$  after refinement are 15.3% and 19.9%, respectively. The Ramachandran plot showed that Asp126 is the only residue outside of the favored/allowed region as observed before. The helical structure in MolA is well maintained with no partial

unwinding at the C-terminal of the  $\alpha 2$  helix. The RMSD between this MolA and MolA of the WT-CRABPII is calculated to be 0.414, consistent with the observation that these two structures are very similar (Figure III-7A). The introduced Glu32 on the  $\alpha 2$  helix forms a salt bridge with Arg59 on the  $\beta C$ - $\beta D$  loop (Figure III-7B). In MolB of the apo-KL-A32E, however, the  $\alpha 2$  helix is completely disordered. The rest of the KL-A32E MolB still folds normally and overlays perfectly with MolB of other apo-CRABPII mutants. Given the fact that the structures listed earlier all contain R132K:R111L mutations and are all capable of maintaining the structural integrity of the protein, A32E mutation in KL-A32E is clearly detrimental to the helical structure of the  $\alpha 2$  helix. No buffer molecule is found in the cavity in either MolA or MolB. The water-mediated network in MolA is shown in Figure III-7C.

### **3.3. Discussion**

#### **3.3.1. Rigid overall fold of the apo-CRABPII mutant structures**

By overlaying all six apo-CRABPII mutant structures together (Figure III-8), it is evident that most of the  $\beta$ -barrel portion of the protein remains rigid in every structure (red structures in Figure III-8). The flexibility can be seen for the helix-turn-helix region, which serves as a lid governing the entry and exit of the ligand, and the  $\beta C$ - $\beta D$  loop that is next to the  $\alpha 2$  helix. This is consistent with what have been observed in the NMR solution structure (26) of apo-WT-CRABPII and in the crystal structures of other CRABPII mutants (27).



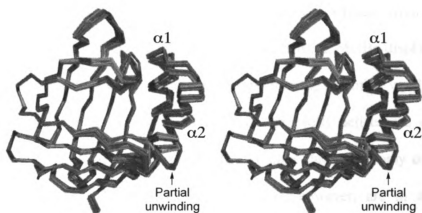


**Figure III-8. Stereoview of the overlay of all apo structures together.** Red: MolBs of WT, KLE-R59E, KFLE, KFLD, KFLD-T54V, and KL-T54E; green: MolAs of WT, KFLD-T54V, KL-T54E, and KL-A32E; blue: MolAs of KLE-R59E, KFLE, and KFLD.

Three different conformations of the helices are present in different molecules. The first conformation is shared by all of the MolBs, except for that of the apo-KL-A32E mutant structure which lost its  $\alpha 2$  helix completely. The MolBs are shown in red colors in Figure III-8. All of these MolB molecules adopt almost an identical conformation with the RMSD against WT-CRABP II MolB between 0.347 and 0.484.

Some of the MolAs adopt the second conformation (WT, KFLD-T54V, KL-A32E and KL-T54E), which is shown in the green structures in Figure III-8. In this conformation, the helices are clearly shifted compared to the MolB structures, together with the neighboring  $\beta$ -turn regions.

The third conformation is present in the rest of the MolA molecules (KLE-R59E, KFLE, KFLD, blue colors in Figure III-8). The interesting feature of this conformation is the partial unwinding at the C-terminal of the  $\alpha 2$  helix. Similar unwinding has also been observed in crystal structures of other CRABP II mutants, such as apo-KLE-CRABP II (PDB ID: 3D97) mutant and apo-KE-CRABP II.

The occurrence of multiple conformations of the helices results from their unique flexibility as discussed previously. The reason that all these MolBs display a uniform conformation is probably because of the tight crystal packing. In other words, the tighter interactions from the neighboring molecules that the MolB helices are experiencing probably constrain the helices in these MolBs and leave them with only one favorable conformation to adopt. The helices of the MolAs, however, are in a much less constrained environment in the crystals and therefore are able to adopt different and more relaxed conformations given their flexible nature.

It is not certain what causes the partial unwinding at the C-terminal of the  $\alpha 2$  helix. It seems that the R132K and L121E/D mutations are present in all of the structures that share the unwinding (KE, KLE, KLE-R59E, KFLE, and KFLD). However, at the same time there are other mutants that share the same two mutations and yet do not have the unwinding, such as KFLD-T54V and KFLE-T54V (PDB ID: 2FS0). Therefore the partial unwinding is probably favored by the combination of R132K and L121E/D mutations, but not guaranteed. Also, the T54V mutation seems to be able to reverse the unwinding through some unclear interactions.

### **3.3.2. A32E mutation is detrimental to the $\alpha 2$ helix in apo-KL-A32E**

Considering that the  $\alpha 2$  helices in the apo-CRABP II mutant structures reported here are all well ordered except for the KL-A32E mutant, we are able to see that the A32E mutation is probably responsible for the loss of helical structure in MolB of the apo-KL-A32E CRABP II mutant. Similarly, the  $\alpha 2$  helix has been seen to be disordered in a previously solved CRABP II mutant structure, apo-F15W-CRABP II (PDB ID: 2FRS)

(22). Phe15 is located at the  $\alpha 1$  helix. The F15W mutation clearly destabilizes the  $\alpha 2$  helix and results in a totally disordered  $\alpha 2$  helix in MolA of the apo-F15W-CRABPII mutant. Steric hindrance between Trp15 and the neighboring  $\alpha 2$  helix residues is believed to be responsible for the structural loss of the helix. When it comes to the KL-A32E mutant, the loss of ordered helical structural is probably not because of steric reasons since the Glu32 is close to the entrance and can clearly swing its side chains to avoid bumping into neighboring residues. More possibly, the difference in favored *phi* angles between Glu and Ala might be the reason for the detrimental effects of Glu32.

It is also interesting to notice that the  $\alpha 2$  helix in MolA of the apo-KL-A32E mutant is well preserved and the average B factor for the MolA  $\alpha 2$  helix is  $20.6 \text{ \AA}^2$ , which is even lower than the overall B factor of  $26.3 \text{ \AA}^2$ . In MolA, a salt bridge is established between Glu32 and Arg59 (Figure III-7B). The same salt bridge is maintained in another crystal structure of the same KL-A32E mutant when complexed with a retinoid analog, suggesting a preference of this salt bridge of this mutant. When overlaying the MolA and MolB of different apo mutant structures together, we can see that the  $\beta C$ - $\beta D$  loop in MolB is shifted further away from the  $\alpha 2$  helix than that in MolA (Figure III-8), which causes the Arg59 to move away from the  $\alpha 2$  helix. In the structure of MolB of KL-A32E, this movement might cause disruption of the salt bridge between A32E and Arg59. We then speculate that, while the A32E mutation is detrimental to the structural integrity of the  $\alpha 2$  helix, the salt bridge between Arg59 and Glu32 observed in MolA of apo-KL-A32E possibly compensate for the reduced structural integrity introduced by having Glu32 on the  $\alpha 2$  helix and hold the ordered structure of the helix.

The disruption of the salt bridge in MolB due to crystal packing then lead to the disordered  $\alpha 2$  helix.

### **3.3.3. Water-mediated network acts as a pillar inside the cavity**

The water-mediated interactions have been observed in other apo-CRABP II mutant structures and were suggested to play an essential role in preserving the structural integrity of the protein. Similar situations are seen in the apo-mutant structures reported here. Water-mediated interactions are observed in all six apo structures, except for apo-KFLD. The appearance of these ordered waters that constitute these hydrogen bonding networks in all of these crystal structures again suggest their possible structural roles. If we overlay the water-mediated interactions together, we are able to see that these different network patterns do not overlap with each other. This is due to the different mutations that each mutant is carrying. However, at places where no mutation is involved, we could be able to see some "conserved" water molecules in different mutant structures.

However, contrary to what have been suggested before, the lack of the continuous water-mediated network in apo-KFLD does not seem to break down the overall fold of the mutant. Similarly, the lack of long-range water-mediated interactions in apo-KL-A32E and apo-KL-T54E due to the absence of charged residues inside the cavities of the two mutants does not lead to collapsed structures either. It is therefore more reasonable to postulate that the ordered water molecules appear due to the stabilizing effect of the polar residues inside the cavity of CRABP II.

### **3.3.4. The hydrophobic cavity allows binding of BTP**

BTP contains six hydroxy groups with three on each end of the molecule, which are linked through a hydrocarbon chain. Out of the total of six apo-CRABPII mutant structures reported here, two of them, apo-KLE-R59E and apo-KL-T54E, showed binding of BTP in the cavity of the protein. These binding situations differ in their average B factors, indicating a difference in terms of how comfortable the molecule is bound inside a specific mutant. By overlaying the structures that have BTP in the binding sites, it is clear that these BTP molecules do not overlap. The freedom of binding for BTP is due to lack of highly specific interactions between BTP and the binding environment, which is consistent with the relatively high B-factors observed for some of the bound BTPs. All BTP molecules occupy approximately the same hydrophobic hole created by the R111L mutation and at the same time tend to adopt multiple conformations with no particular preference energetically. That could possibly explain the less definitive electron densities of specific atoms of BTP in apo-KL-T54E. There are also cases where there is no BTP bound even when the crystal also grew in conditions that contain BTP, indicating a low binding affinity of BTP toward CRABPII mutants. Binding of BTP is not believed to alter the conformation of the protein, which is apparent from the fact that different mutants display minimal structural changes with or without BTP in the binding sites, such as BTP-bound KL-T54E vs. WT-CRABPII and BTP-bound KLE-R59E vs KFLE-CRABPII.

### **3.5. Conclusion**

The structural information deduced from six high resolution apo-CRABP II mutant structures are presented and discussed. The  $\beta$ -barrel portion of CRABP II is again demonstrated to be very rigid and resistant to multiple mutations involving either conserved or non-conserved residues. The helix-turn-helix is proven to be very flexible, with three conformations observed in different mutants. A partial unwinding at the C-terminal of the  $\alpha 2$  helix is seen in three mutant structures. This unwinding is believed to be caused by a combination of helices' flexibility as well as mutations of R132K and L121E/D. Water-mediated interactions linking residues deep inside the cavity with the ones at the helical entrance are found in almost all mutants, indicating their important roles in maintaining the overall fold of these apo-CRABP II mutants.

## Reference

1. Chambon, P. (1996) A decade of molecular biology of retinoic acid receptors, *Faseb J* 10, 940-954.
2. Chomienne, C., Fenaux, P., and Degos, L. (1996) Retinoid differentiation therapy in promyelocytic leukemia, *Faseb J* 10, 1025-1030.
3. DeLuca, L. M. (1991) Retinoids and their receptors in differentiation, embryogenesis, and neoplasia., *Faseb J* 5, 2924-2933.
4. Lotan, R. (1980) Effects of Vitamin-a and Its Analogs (Retinoids) on Normal and Neoplastic-Cells, *Biochimica Et Biophysica Acta* 605, 33-91.
5. Fisher, G. J., and Voorhees, J. J. (1996) Molecular mechanisms of retinoid actions in skin, *Faseb J* 10, 1002-1013.
6. Hong, W. K., Itri, L. M. (1994) Retinoids and human cancer, in *The Retinoids: Biology, Chemistry, and Medicine* (Sporn, M. B., Roberts, A. B., Goodman, D. S., Ed.) 2nd ed., pp 597-630, Raven Press, New York.
7. Giguere, V. (1994) Retinoic Acid Receptors and Cellular Retinoid-Binding Proteins - Complex Interplay in Retinoid Signaling, *Endocrine Reviews* 15, 61-79.
8. Kliewer, S. A., Umesono, K., Mangelsdorf, D. J., and Evans, R. M. (1992) Retinoid X-Receptor Interacts with Nuclear Receptors in Retinoic Acid, Thyroid-Hormone and Vitamin-D3 Signaling, *Nature* 355, 446-449.
9. Mangelsdorf, D. J., Thummel, C., Beato, M., Herrlich, P., Schutz, G., Umesono, K., Blumberg, B., Kastner, P., Mark, M., Chambon, P., and Evans, R. M. (1995) The Nuclear Receptor Superfamily - the 2nd Decade, *Cell* 83, 835-839.
10. Morrisskay, G. (1993) Retinoic Acid and Craniofacial Development - Molecules and Morphogenesis, *Bioessays* 15, 9-15.
11. Bailey, J. S., and SIU, C. H. (1988) Purification and Partial Characterization of a Novel Binding-Protein for Retinoic Acid from Neonatal Rat, *J Biol Chem* 263, 9326-9332.
12. ONG, D. E., and Chytil, F. (1975) Retinoic Acid-Binding Protein in Rat Tissue - Partial-Purification and Comparison to Rat Tissue Retinol-Binding Protein, *J Biol Chem* 250, 6113-6117.
13. Sani, B. P. H., D.L. (1974) Retinoic acid-binding-protein in chick-embryo metatarsal skin, *Biochem. Biophys. Res. Commun.* 61, 1276-1282.

14. Ong, D. E., Newcomer, M. E., & Chytil, F. (1994) Cellular retinoid-binding proteins, in *The Retinoids: Biology, Chemistry, and Medicine* (Sporn, M. B., Roberts, A. B., Goodman, D. S., Ed.) 2nd ed., pp 283-318, Raven Press, New York.
15. Budhu, A., Gillilan, R., and Noy, N. (2001) Localization of the RAR interaction domain of cellular retinoic acid binding protein-II, *Journal of Molecular Biology* 305, 939-949.
16. Budhu, A. S., and Noy, N. (2002) Direct channeling of retinoic acid between cellular retinoic acid-binding protein II and retinoic acid receptor sensitizes mammary carcinoma cells to retinoic acid-induced growth arrest, *Molecular and Cellular Biology* 22, 2632-2641.
17. Boylan, J. F., and Gudas, L. J. (1991) Overexpression of the Cellular Retinoic Acid Binding Protein-I (Crabp-I) Results in a Reduction in Differentiation-Specific Gene-Expression in F9 Teratocarcinoma Cells, *J Cell Biol* 112, 965-979.
18. Boylan, J. F., and Gudas, L. J. (1992) The Level of Crabp-I Expression Influences the Amounts and Types of All-Trans-Retinoic Acid Metabolites in F9 Teratocarcinoma Stem-Cells, *J Biol Chem* 267, 21486-21491.
19. Napoli, J. L. (2000) Retinoic acid: Its biosynthesis and metabolism, *Prog Nucleic Acid Re* 63, 139-188.
20. Dong, D., Ruuska, S. E., Levinthal, D. J., and Noy, N. (1999) Distinct roles for cellular retinoic acid-binding proteins I and II in regulating signaling by retinoic acid, *J Biol Chem* 274, 23695-23698.
21. Kleywegt, G. J., Bergfors, T., Senn, H., Lemotte, P., Gsell, B., Shudo, K., and Jones, T. A. (1994) Crystal-Structures of Cellular Retinoic Acid-Binding Protein-I and Protein-II in Complex with All-Trans-Retinoic Acid and a Synthetic Retinoid, *Structure* 2, 1241-1258.
22. Vaezeslami, S., Mathes, E., Vasilelou, C., Borhan, B., and Geiger, J. H. (2006) The structure of apo-wild-type cellular retinoic acid binding protein II at 1.4 Å and its relationship to ligand binding and nuclear translocation, *Journal of Molecular Biology* 363, 687-701.
23. Thompson, J. R., Bratt, J. M., and Banaszak, L. J. (1995) Crystal-Structure of Cellular Retinoic Acid-Binding Protein-I Shows Increased Access to the Binding Cavity Due to Formation of an Intermolecular Beta-Sheet, *J. Mol. Biol.* 252, 433-446.
24. Scapin, G., Gordon, J. I., and Sacchettini, J. C. (1992) Refinement of the Structure of Recombinant Rat Intestinal Fatty Acid-Binding Apoprotein at 1.2-Å Resolution, *J. Biol. Chem.* 267, 4253-4269.



25. Gunasekaran, K., Hagler, A. T., and Gierasch, L. M. (2004) Sequence and structural analysis of cellular retinoic acid-binding proteins reveals a network of conserved hydrophobic interactions, *Proteins* 54, 179-194.
26. Wang, L. C., Li, Y., Abildgaard, F., Markley, J. L., and Yan, H. G. (1998) NMR solution structure of type II human cellular retinoic acid binding protein: Implications for ligand binding, *Biochemistry-Us* 37, 12727-12736.
27. Wang, L. C., Li, Y., and Yan, H. G. (1997) Structure-function relationships of cellular retinoic acid-binding proteins - Quantitative analysis of the ligand binding properties of the wild-type proteins and site-directed mutants, *J Biol Chem* 272, 1541-1547.

## CHAPTER IV. Investigation of the Interaction between Cellular Retinoic Acid Binding Protein II and Retinoic Acid Receptor Gamma Ligand Binding Domain

### 4.1. Background

As stated earlier, the effects of retinoic acid (RA) are mediated by at least two families of proteins, nuclear hormone receptors and cellular retinoic acid binding proteins (CRABPs). The transcriptional activities of RA are mediated by two members of the nuclear hormone receptor superfamily: Retinoic Acid Receptor (RAR) and Retinoid X Receptor (RXR). This superfamily is composed of nuclear ligand-activated transcriptional regulators that also include steroid hormone, thyroid hormone and vitamin D<sub>3</sub> receptors. The RARs and the RXRs each consist of three isotypes ( $\alpha$ ,  $\beta$ , and  $\gamma$ ) encoded by separate genes. Each isotype has several isoforms, arising from the differential usage of two promoters and alternative splicing (1, 2). The RAR family (RAR $\alpha$ ,  $\beta$ , and  $\gamma$ ) binds to and is therefore activated by *all-trans* (tRA) and 9-*cis* RA (9cRA), whereas the RXR family (RXR $\alpha$ ,  $\beta$ , and  $\gamma$ ) is activated only by 9cRA (Figure IV-1).

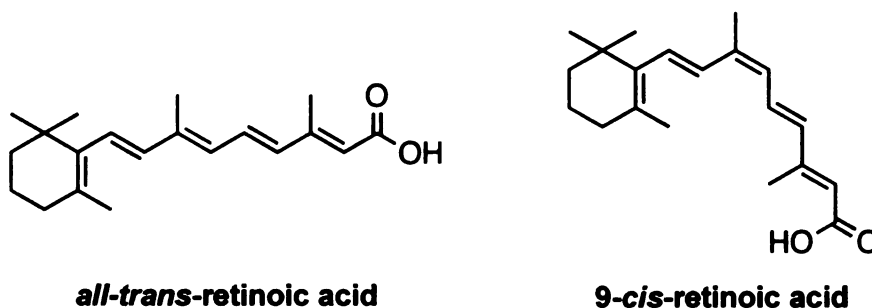
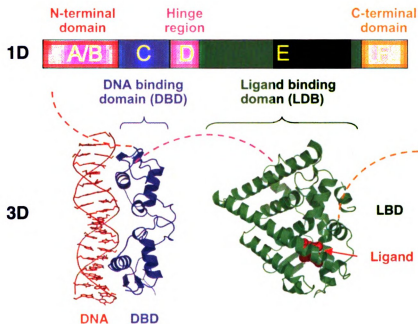


Figure IV-1. *All-trans* retinoic acid and 9-*cis* retinoic acid.



**Figure IV-2. Structural organization of nuclear receptors (3).**

The RARs and the RXRs exhibit the conserved modular structure of nuclear receptors and their amino acid sequence can be divided into six regions (A-F) based on homology among themselves and with other members of the nuclear receptor superfamily (Figure IV-2) (4). Region C, consisting of 66 amino acids, contains two zinc finger motifs and is the sequence specific DNA binding domain (DBD). Within a given species, region C is highly conserved between the three RAR isotypes (94-97%) and between the three RXR isotypes (91-97%). Region E consists of 220 amino acids and is the ligand binding domain (LBD) which is also highly conserved between RAR isotypes (84-90%) and RXR isotypes (88-95%). This region is functionally complex, including the ligand binding domain, the ligand-inducible transcriptional activation function AF-2, and a dimerization surface. The interspecies conservation of the DBD and the LBD of a given RAR type or of a given RXR type is even greater than the similarity found when

comparing the three RAR types or the three RXR types within a given species, which suggests that the DNA and ligand binding properties of the various RARs and RXRs could exhibit subtle functional differences.

Region D is located as a hinge between the DBD and the LBD and is conserved both among RARs or RXRs within a given species and is conserved between species for a given RAR or RXR. The C-terminal F domain, which exists in the RARs, is missing in the RXRs and its function is still unknown. However, the amino end A/B regions of RARs and RXRs have both been shown to contain a second transcriptional activation function AF-1.

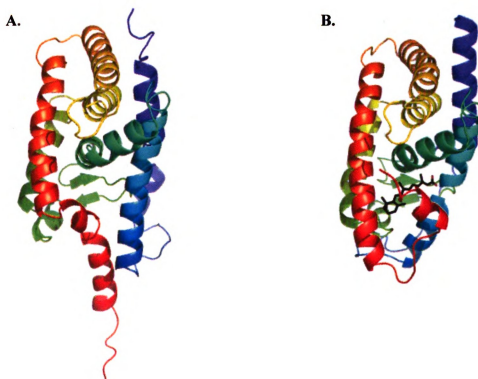


**Figure IV-3. Comparison of the crystal structures of the apo-RXR $\alpha$  (A, PDB: 1LBD; (5)) and holo-RAR $\gamma$  (B, PDB: 2LBD; (6)) ligand-binding domains reveals the ligand-induced conformational change. N-terminal is labeled in blue and C-terminal in red in the rainbow representation in both structures.**

The crystal structures of the LBDs of both RARs and RXRs have been determined (Figure 3) (5, 6). The LBDs are formed by 12 conserved alpha-helices and a beta-turn (between H5 and H6) which are folded into a three-layered, anti-parallel helical sandwich with H4, H5, H8, H9 and H11 situated between H1, H2 and H3 on one side and H6, H7 and H10 on the other. In this structure, the C-terminal helix H12, which encompasses the AF-2 activation domain, points away from the LBD core. By comparing the crystal structures of apo-RXR $\alpha$  LBD and holo-RAR $\gamma$  LBD, the major conformational change before and after ligand binding seems to be the relocation of H12, which after ligand binding folds back towards the LBD core and “seals” the ligand entry site.

In the absence of the ligand, retinoic acid receptors are found primarily in the nucleus. They bind as asymmetric, oriented RAR/RXR heterodimers to specific DNA sequences, RA response elements (RAREs), composed typically of two direct repeats of a core hexameric motif, (A/G)G(G/T)TCA (2, 7). The classical RARE is a 5-bp-spaced direct repeat (DR5). However, RAR/RXR heterodimers also bind to direct repeats separated by 1 bp (DR1) or 2 bp (DR2). Unliganded and DNA-bound retinoid receptors repress transcription through recruitment of the corepressors NcoR and SMRT (8, 9). After ligand binding, the resulting conformational changes cause the release of the corepressors and recruit coactivators which upon association with larger complexes with chromatin modifying and remodeling activities will decompact repressive chromatin and facilitate the positioning of the transcriptional machinery at the promoter region (9-11).

CRABP I and II, are the other family of proteins that mediate the biological effects of RA (12-15). CRABPs belong to a family of proteins called intracellular lipid-

binding proteins (iLBP), including fatty acid-binding proteins, lipid-binding proteins, and cellular retinoid-binding proteins (16). CRABPs are responsible for modulating the intracellular existence of RA. The sequences of CRABPs are highly conserved in vertebrates (17, 18). CRABP I and II are closely related, with an identity of 76% in human. CRABPs are believed to act as carriers of RA, serving to solubilize and protect RA in the aqueous environment of the cytosol. In addition to this general role, CRABPs have also been shown to facilitate RA modification upon interaction with other proteins (12-15).

Despite the sequence similarity between CRABPI and CRABPII, the two proteins have been shown to have distinct roles in regulating RA (17). Professor Noy and colleagues demonstrated that the rate constant for movement of RA from CRABPII, but not CRABPI, to RAR strongly depends on the concentration of RAR (19). They therefore suggested that transfer of RA from CRABPI to RAR involves dissociation of RA from CRABPI, followed by association of RA with the acceptor. In contrast, movement of RA from CRABPII to RAR is facilitated by a mechanism involving direct interactions between CRABPII and RAR. However, the interaction between the two is short-lived according to their observation as no stable complex could be trapped in spite of several attempts including chemical crosslinking, electrophoresis under denaturing conditions, fluorescence anisotropy titrations and electrophoretic mobility shift assays.

Their later investigations revealed three spatially aligned residues E75Q, K81P, and E102K (CRABPI/CRABPII), displaying dramatic changes in electrostatic surface potential of the two proteins (17). Substituting the corresponding CRABPII residues onto CRABPI conferred upon the protein the ability to channel RA to RAR and to enhance the

transcriptional activity of RAR in cells. Conversely, substituting the three residues on CRABP II into their CRABP I counterparts resulted in loss of the ability to interact with RAR and to enhance the activity of the receptor.

Professor Chomienne and co-workers also worked on the interaction between RAR and CRABP II. By attaching CRABP II with fluorescence proteins they have demonstrated the distribution of CRABP II in the nucleus (20). However, contradictory to what had been suggested by Professor Noy, they have shown that CRABP II was associated with RAR $\alpha$  and RXR $\alpha$  in a ligand-independent manner through a GST pull-down assay using GST-tagged RAR $\alpha$  or RXR $\alpha$ . Moreover, they have demonstrated that, in the presence of retinoids that bind both the nuclear receptors and CRABP II, transcription by RAR $\alpha$ -RXR $\alpha$  heterodimers is enhanced by the presence of CRABP II, suggesting CRABP II as a novel transcriptional regulator involved in RA signaling.

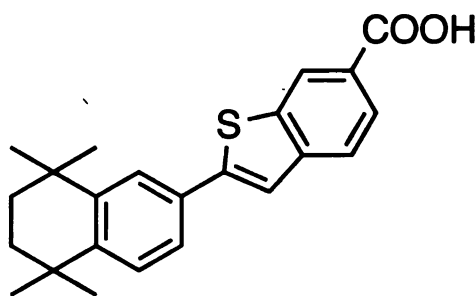


**Figure IV-4. The synthetic retinoid analog CD270.**

To further investigate the problem, Budhu and Noy performed a similar *in vitro* pull-down assay using immobilized His-tagged RAR $\alpha$ -LBD incubated with CRABP II in the presence of RA or a synthetic analog CD270 (Figure IV-4) which had been reported to interact with CRABP II with a high affinity but to be a poor ligand for RAR $\alpha$  (18).

The results are consistent with their earlier statement that CRABP<sub>II</sub> interacts with RAR in a ligand-dependent manner and that the complex is not stable. No CRABP<sub>II</sub> was found to co-precipitate with RAR $\alpha$ -LBD in the absence of ligand or in the presence of RA. However, CD270 stabilized the complex in a dose-dependent manner and CRABP<sub>II</sub> was co-precipitated with RAR $\gamma$ -LBD in the presence of CD270.

As we have shown earlier, among our mutants of CRABP<sub>II</sub>, the triple mutant KLE-CRABP<sub>II</sub> shows an excellent retinal-binding property ( $K_d = 1.4 \pm 4.9$  nM). In this particular protein, retinal forms a protonated Schiff base with the lysine residue in position 132, which can be followed by the UV red shift from 380 nm (free retinal) to 447 nm (protonated Schiff base). This covalent protein-ligand complex gave us an opportunity that resembles the situation in Noy's research involving the synthetic CD270. In both cases, ligands prefer to stay with the CRABP<sub>II</sub> proteins instead of being transferred into RAR, which has been suggested by Noy and colleagues as key in order to achieve a stable complex between the two proteins. We therefore set out to detect the protein-protein interaction between CRABP<sub>II</sub> and RAR employing the all-*trans*-retinal-bound KLE-CRABP<sub>II</sub> mutant.

## **4.2 Results and discussion**

### **4.2.1. *In vitro* binding assay.**

With both RAR $\gamma$ -LBD and CRABP<sub>II</sub>s (WT-CRABP<sub>II</sub> and KLE-CRABP<sub>II</sub>) in hand, the binding assay was performed. His-tagged RAR $\gamma$ -LBD was first immobilized on Ni-NTA resin. WT-CRABP<sub>II</sub> and KLE-CRABP<sub>II</sub> were then incubated with the



immobilized RAR $\gamma$ -LBD either in the absence of ligand or in the presence of either RA (for wild type) or retinal (for triple mutant) at 4°C for 1 h. The resin was then washed three times with Tris buffer (10 mM Tris, 100 mM NaCl, pH 8.0). SDS gel loading buffer was then added to the beads and proteins attaching to the resin were analyzed by SDS electrophoresis. The results are shown in Figure IV-5. For wild-type CRABP II, no interaction between RAR $\gamma$ -LBD and WT-CRABP II was observed either in the absence (lane 6) or in the presence of RA (lane 7). The same results were obtained for the triple mutant CRABP II: no KLE-CRABP II was co-precipitated with RAR $\gamma$ -LBD either in the absence (lane 8) or in the presence of RA (lane 9) or retinal (lane 10).

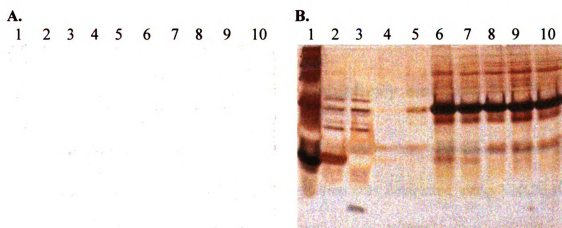


**Figure IV-5. *In vitro* binding assay.** 1. MW; 2. WT-CRABP II; 3. KLE-CRABP II; 4. Ni-NTA beads + WT-CRABP II; 5. Ni-NTA beads + KLE-CRABP II; 6. Ni-NTA beads + His<sub>6</sub>-RAR-LBD + WT-CRABP II; 7. Ni-NTA beads + His<sub>6</sub>-RAR-LBD + WT-CRABP II + RA; 8. Ni-NTA beads + His<sub>6</sub>-RAR-LBD + KLE-CRABP II; 9. Ni-NTA beads + His<sub>6</sub>-RAR-LBD + KLE-CRABP II + RA; 10. Ni-NTA beads + His<sub>6</sub>-RAR-LBD + KLE-CRABP II + retinal. **A.** Coomassie blue stain; **B.** Silver stain.

#### **4.2.2. Following the protonated Schiff base formation by UV.**

As mentioned before, there is a major red shift in the UV spectrum from 380 nm to 447 nm before and after retinal binds to KLE-CRABP II. In order to investigate whether RAR $\gamma$ -LBD will prevent the formation of the protonated Schiff base, RAR $\gamma$ -LBD was added into the complex between KLE-CRABP II and retinal. A UV scan was performed and it turned out that the protonated Schiff base is no longer existent after RAR-LBD was added, based on the fact that the UV absorbance went back to around 375 nm. Two possibilities were proposed: one is that the Schiff base might have been hydrolyzed and retinal was transferred into RAR $\gamma$ -LBD; the other possibility is that the Schiff base is not completely hydrolyzed, but instead of being protonated, the Schiff base is now unprotonated, which could also lead to an absorption at 375 nm.

#### **4.2.3. *In vitro* binding assay using reductively aminated Schiff base complex.**

Since a secondary amine base is much more stable than a protonated Schiff base in the aqueous environment, a reductive amination was conducted using Na(CN)BH<sub>3</sub>. The excess of retinal in the reaction was removed from the reduced protein-ligand complex by buffer exchange using a concentrator. Similar *in vitro* binding assay was performed. However, again, no co-precipitation with RAR $\gamma$ -LBD was observed for reduced KLE-CRABP II-retinal complex.

#### **4.2.4. Presence of Tween20 leads to hydrolysis of the protonated Schiff base.**

Tween20 (0.1%) was present in the purified RAR $\gamma$ -LBD solution. It was introduced during the dialysis after Ni-NTA purification (see detailed procedures in Chapter VI). The function of this detergent is to prevent aggregation of the protein. Since detergent is well known to be able to change the solubility of proteins in buffers, it is suspected that the presence of Tween20 might lead to certain conformational change of CRABP II, which will eventually lead to the hydrolysis of the PSB.

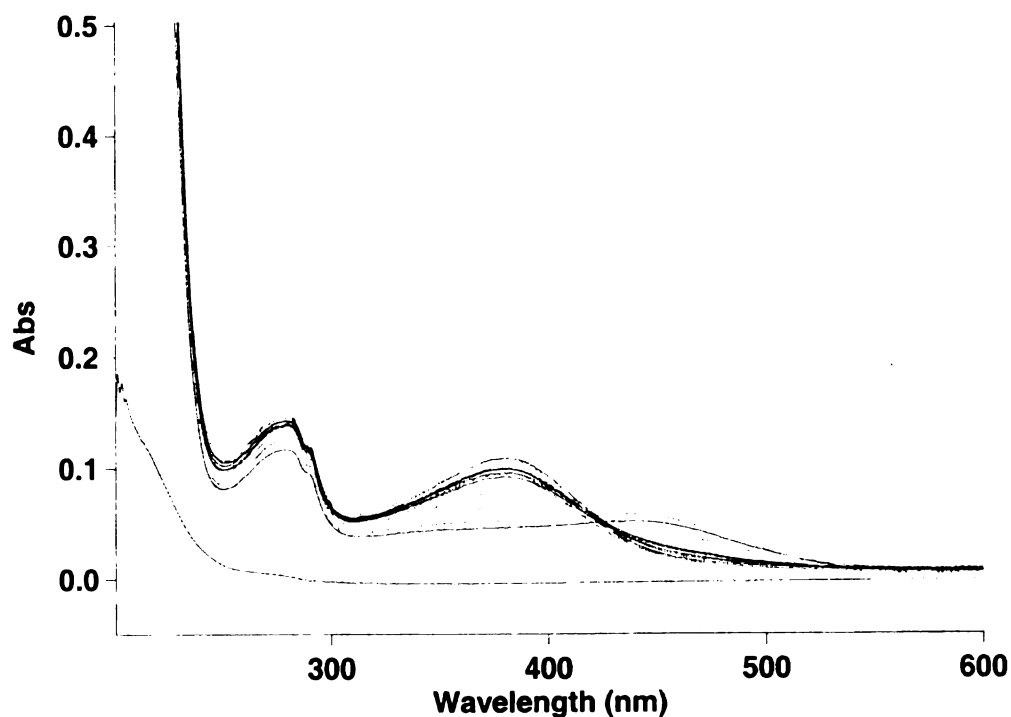


**Figure IV-6. Detergent titration of the protonated Schiff base formed between KLE-CRABP II and retinal.**

By adding the Tween20 containing buffer into the Schiff base complex, it was observed that the absorption went back to 375 nm. A detergent titration experiment was also performed (Figure IV-6). To the Schiff base formed complex was added Tris buffer

containing different concentrations of Tween20. The concentration of Tween20 that starts to destroy the protonated Schiff base was found out to be between 0.001% and 0.005% (v/v).

#### **4.2.5. Purification of RAR $\gamma$ -LBD without detergent.**

Since the detergent was the reason for disrupting the protonated Schiff base, RAR $\gamma$ -LBD was then purified without detergent. After Ni column, the protein solution was dialyzed against 10 mM Tris, 100 mM NaCl, pH 8.0. It was then concentrated, followed by gel filtration purification. However, the spectrum of the gel filtration looked quite different from the previous run when Tween20 was used in the buffer. RAR $\gamma$ -LBD purified this way came off the column quite early and covered a much broader range of fractions. What's more, the UV of RAR $\gamma$ -LBD after purification does not look normal. Absorption at 260 nm is strongly interfering the protein absorption at 280 nm, suggesting possible nucleotide contamination.

The fact that RAR $\gamma$ -LBD came off the gel filtration column earlier as well as the fact that the UV spectrum of RAR $\gamma$ -LBD showed an elevated baseline indicate possible aggregation of the protein. To test this possibility, detection for inclusion bodies was performed and insoluble RAR $\gamma$ -LBD was detected in the cell pellet. To reduce the inclusion bodies and aggregation problems, several things were modified in the RAR $\gamma$ -LBD purification. The optimized purification included the following steps. After OD<sub>600</sub> reached 0.6, IPTG was added and the growth was continued at 16°C for 20 h (previously 5 h at r.t.). The proteins were eluted off the Ni-NTA column by 250 mM imidazole, 100 mM NaCl, 10 mM Tris, pH 8.0 (previously 100 mM EDTA, 500 mM NaCl, 20 mM Tris,

pH 8.0). After the Ni column, each individual fraction was examined by UV and the best fraction(s) were immediately loaded onto the Sephadex G-50 gel filtration column. It was then eluted with 10 mM Tris, 100 mM NaCl, 10% glycerol, pH 8.0. The fractions were again examined under UV and it turned out that most of the fractions obtained this way showed maximum absorption very close to or exactly at 280 nm, suggesting much less or even no contamination from nucleotides.

#### **4.2.6. Circular dichroism of RAR $\gamma$ -LBD and fluorescence titration of RAR $\gamma$ -LBD with retinoic acid.**

The purified RAR $\gamma$ -LBD was then characterized first with CD. Both apo- and holo-RAR $\gamma$ -LBD were measured and the obtained spectra resemble the literature data (21).  $\alpha$ -Helix content was indicated by the negative ellipticity with minima at 222 and 208 nm. There are no major changes before and after tRA binding, which is also consistent with the published data.

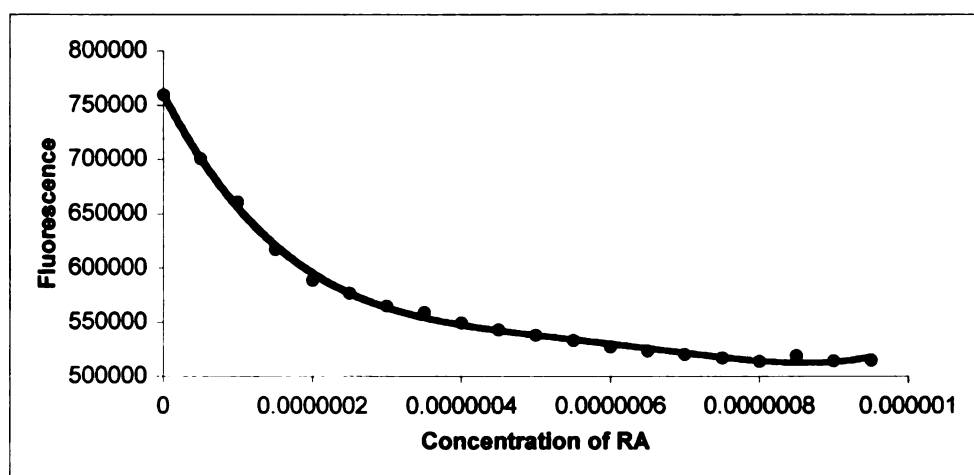


**Figure IV-7. Fluorescence titration of RAR $\gamma$ -LBD with all-*trans*-retinoic acid.**

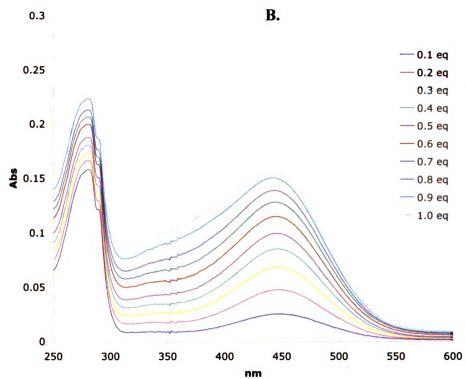
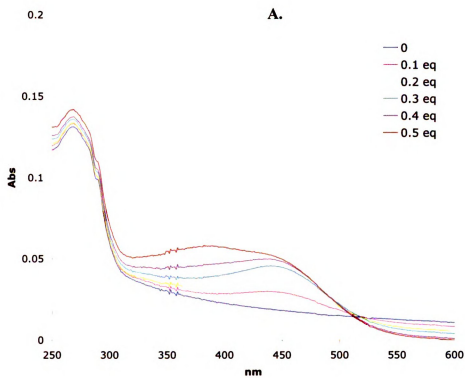


**Figure IV-8. Titration of KLE-CRABPII with retinal.** A. Using KLE-CRABPII purified earlier; B. Using fully active KLE-CRABPII.

Fluorescence titration of RAR $\gamma$ -LBD with all-*trans*-retinoic acid was also performed to verify the ligand binding ability of the purified protein. The extinction coefficient of RAR $\gamma$ -LBD was measured to be 11,972 cm<sup>-1</sup>M<sup>-1</sup>. Titration data is shown in Figure IV-7. The calculated  $K_d$  is 0.5 nM, which is very close to the 0.6 nM binding affinity reported in the literature.

#### **4.2.7. Titration of KLE-CRABP II with retinal followed by UV.**

A perfect KLE-CRABP II (R132K:R111L:L121E) should bind retinal up to 1 equivalent and still maintain the maximum absorption at around 440 nm corresponding to the protonated Schiff base. However, the KLE-CRABP II that was purified in the previous batch failed to give a decent titration (Figure IV-8A). The retinal could only be added up to 0.5 eq and after that the absorption started to blue shift. Later the same titration using KLE-CRABP II purified in a different batch turned out to be fully active (Figure IV-8B). This batch of protein was later used in the *in vitro* binding assays.

#### **4.2.8. *In vitro* binding assay using RAR $\gamma$ -LBD directly from Ni-NTA resin.**

Since we had concerns on loss of activity of RAR $\gamma$ -LBD due to dialysis and other handling of the protein, we decided to try the binding assay one more time using the RAR $\gamma$ -LBD directly from the Ni resin. This way we would save the effort of eluting the protein off the Ni resin and later on binding it again onto the resin and also exert

minimum handling of the protein. Moreover, since the purity of the protein was proved to be fairly good after Ni-NTA purification, this seemed to be a method worth trying.

Besides RAR $\gamma$ -LBD, retinal solution was also freshly prepared. The KLE-CRABP II used here is the one proved to be fully functional based on the titration experiments described earlier. In this assay the interaction between KLE-CRABP II and RAR $\gamma$ -LBD was investigated and that between WT-CRABP II and RAR $\gamma$ -LBD was not. The procedure is the same as described earlier in the first *in vitro* binding assay. The results are shown in Figure IV-9. KLE-CRABP II showed up together with RAR $\gamma$ -LBD on the gel either in the absence (lane 3) or presence of retinal (lane 4), however, in the same intensity as the control (lane 2), indicating again lack of interaction between the two proteins. Lane 5, 6 and 7 showed the protein content of the supernatants corresponding to lane 2, 3 and 4 respectively. As shown, the same amount of KLE-CRABP II appeared on the gel, suggesting the same degree of binding for KLE-CRABP II both in control and in real assays and therefore no interaction between the two proteins.

Lane    1    2    3    4    5    6    7    8    9    10



**Figure IV-9. *In vitro* binding assay using RAR $\gamma$ -LBD directly from Ni-NTA resin.** 1. RAR-LBD on Ni beads; 2. Ni-NTA beads + KLE-CRABP II; 3. Ni-NTA beads + His $_6$ -RAR-LBD + KLE-CRABP II; 4. Ni-NTA beads + His $_6$ -RAR-LBD + KLE-CRABP II + retinal 5. Supernatant of lane 2; 6. Supernatant of lane 3; 7. Supernatant of lane 4; 8. Washed off lane 2; 9. Washed off lane 3; 10. Washed off lane 4.



### **4.3. Conclusions**

Despite several efforts, no *in vitro* protein-protein interaction between CRABPII and RAR-LBD is detected. CD270 should be used to set up a positive control for future binding experiments.

## References

1. Gronemeyer, H., and Laudet, V. (1995) Transcription factors .3. Nuclear receptors, *Protein Profile* 2, 1173-1308.
2. Leid, M., Kastner, P., and Chambon, P. (1992) Multiplicity Generates Diversity in the Retinoic Acid Signaling Pathways, *Trends Biochem Sci* 17, 427-433.
3. Hoffmeier. [http://en.wikipedia.org/wiki/Image:Nuclear\\_Receptor\\_Structure.png](http://en.wikipedia.org/wiki/Image:Nuclear_Receptor_Structure.png).
4. Steinmetz, A. C. U., Renaud, J. P., and Moras, D. (2001) Binding of ligands and activation of transcription by nuclear receptors, *Annu Rev Bioph Biom* 30, 329-359.
5. Renaud, J. P., Rochel, N., Ruff, M., Vivat, V., Chambon, P., Gronemeyer, H., and Moras, D. (1995) Crystal-Structure of the Rar-Gamma Ligand-Binding Domain Bound to All-Trans-Retinoic Acid, *Nature* 378, 681-689.
6. Bourguet, W., Ruff, M., Chambon, P., Gronemeyer, H., and Moras, D. (1995) Crystal-Structure of the Ligand-Binding Domain of the Human Nuclear Receptor Rxr-Alpha, *Nature* 375, 377-382.
7. Mangelsdorf, D. J., and Evans, R. M. (1995) The Rxr Heterodimers and Orphan Receptors, *Cell* 83, 841-850.
8. Aranda, A., and Pascual, A. (2001) Nuclear hormone receptors and gene expression, *Physiol Rev* 81, 1269-1304.
9. Glass, C. K., and Rosenfeld, M. G. (2000) The coregulator exchange in transcriptional functions of nuclear receptors, *Gene Dev* 14, 121-141.
10. Nagy, L., Kao, H. Y., Love, J. D., Li, C., Banayo, E., Gooch, J. T., Krishna, V., Chatterjee, K., Evans, R. M., and Schwabe, J. W. R. (1999) Mechanism of corepressor binding and release from nuclear hormone receptors, *Gene Dev* 13, 3209-3216.
11. Perissi, V., Staszewski, L. M., McInerney, E. M., Kurokawa, R., Krones, A., Rose, D. W., Lambert, M. H., Milburn, M. V., Glass, C. K., and Rosenfeld, M. G. (1999) Molecular determinants of nuclear receptor-corepressor interaction, *Gene Dev* 13, 3198-3208.
12. Boylan, J. F., and Gudas, L. J. (1992) The Level of Crabp-I Expression Influences the Amounts and Types of All-Trans-Retinoic Acid Metabolites in F9 Teratocarcinoma Stem-Cells, *J Biol Chem* 267, 21486-21491.

13. Fiorella, P. D., and Napoli, J. L. (1991) Expression of Cellular Retinoic Acid Binding-Protein (Crabp) in Escherichia-Coli - Characterization and Evidence That Holo-Crabp Is a Substrate in Retinoic Acid Metabolism, *J Biol Chem* 266, 16572-16579.
14. Fiorella, P. D., and Napoli, J. L. (1994) Microsomal Retinoic Acid Metabolism - Effects of Cellular Retinoic Acid-Binding Protein (Type-I) and C18-Hydroxylation as an Initial Step, *J Biol Chem* 269, 10538-10544.
15. Napoli, J. L., Boerman, M. H. E. M., Chai, X., Zhai, Y., and Fiorella, P. D. (1995) Enzymes and Binding-Proteins Affecting Retinoic Acid Concentrations, *J Steroid Biochem* 53, 497-502.
16. Ong, D. E., Newcomer, M. E., & Chytil, F. (1994) Cellular retinoid-binding proteins, in *The Retinoids: Biology, Chemistry, and Medicine* (Sporn, M. B., Roberts, A. B., Goodman, D. S., Ed.) 2nd ed., pp 283-318, Raven Press, New York.
17. Budhu, A., Gillilan, R., and Noy, N. (2001) Localization of the RAR interaction domain of cellular retinoic acid binding protein-II, *Journal of Molecular Biology* 305, 939-949.
18. Budhu, A. S., and Noy, N. (2002) Direct channeling of retinoic acid between cellular retinoic acid-binding protein II and retinoic acid receptor sensitizes mammary carcinoma cells to retinoic acid-induced growth arrest, *Molecular and Cellular Biology* 22, 2632-2641.
19. Dong, D., Ruuska, S. E., Levinthal, D. J., and Noy, N. (1999) Distinct roles for cellular retinoic acid-binding proteins I and II in regulating signaling by retinoic acid, *J Biol Chem* 274, 23695-23698.
20. Delva, L., Bastie, J. N., Rochette-Egly, C., Kraiba, R., Balitrand, N., Despouy, G., Chambon, P., and Chomienne, C. (1999) Physical and functional interactions between cellular retinoic acid binding protein II and the retinoic acid-dependent nuclear complex, *Molecular and Cellular Biology* 19, 7158-7167.
21. Lupisella, J. A., Driscoll, J. E., Metzler, W. J., and Reczek, P. R. (1995) The Ligand-Binding Domain of the Human Retinoic Acid Receptor-Gamma Is Predominantly Alpha-Helical with a Trp Residue in the Ligand-Binding Site, *J Biol Chem* 270, 24884-24890.

## **CHAPTER V. Preliminary X-Ray Crystallographic Studies of Cellular Retinaldehyde Binding Protein**

### **5.1. Background**

As stated earlier, the lack of a three-dimensional structure of the cellular retinaldehyde binding protein (CRALBP) has hindered many research efforts in addressing important biological questions associated with this protein. So we decided to tackle this problem.

### **5.2. Crystallization of the full-length CRALBP**

The CRALBP (rCRALBP) gene was generously provided by professor John W. Crabb. The rCRALBP gene was then cloned into both His-tagged (pET19b) and non-fusion (pET17b) plasmids and each was expressed respectively in BL21(DE3) cells.

#### **5.2.1. His-tagged full-length CRALBP crystallization.**

The His-tagged rCRALBP was purified using Ni-NTA affinity chromatography to homogeneity (Figure V-1). The binding property of this His-tagged rCRALBP was tested by observing UV shifts while titrating the protein with one of its natural ligands, 11-*cis*-retinal.

The purified His-rCRALBP was then tested at room temperature for crystallization. Primary screen of the apo protein at different concentrations (25 mg/mL,

10 mg/mL, and 5 mg/mL) were performed and results obtained were compared. None of these trials gave protein crystals.

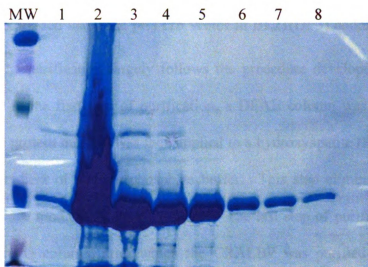


**Figure V-1. Pure fractions of His-rCRALBP eluted after Ni-NTA purification.**

Since room temperature crystallization did not work well. Crystallization in the cold room (4°C) was then pursued. Primary screen of this protein (9 mg/mL) at 4°C gave several hits, which later on were all proven to be salt crystals.

Since the apo protein failed to crystallize, we turned to the holo-protein based on the knowledge that ligand-bound CRALBP was more soluble than the protein itself (1). The protein was concentrated to 10 mg/mL and 11-*cis*-retinal was added up to 2.5 eq. The primary screen was set up in the cold room (4°C) under dim red light. Boxes were wrapped with aluminum foil and kept in the dark. Unfortunately, no crystal was observed in any conditions.

### 5.2.2. Non-fusion full-length CRALBP crystallization.

Since the His-tagged protein failed to give any crystals either in the apo form or bound to 11-*cis*-retinal, we decided to try to crystallize the protein without the His-tag. CRALBP was expressed using the pET17b vector in BL21(DE3) codon<sup>+</sup> cells as a tag-free protein. The purification largely follows the procedure developed by Crabb and colleagues (1). In the first step of purification, a DEAE column was employed. The roughly purified protein mixture was then applied to a hydroxyapatite (HTP) column and eluted with a gradient of sodium phosphate buffer. This step eliminated most of the impurities and gave moderately pure CRALBP. The last step of purification employed the FPLC source Q column, after which the CRALBP was purified to homogeneity (Figure V-2).

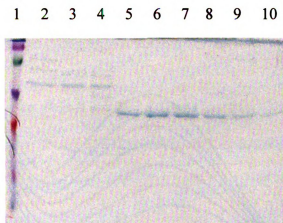


**Figure V-2. Non-fusion CRALBP purified.** This gel displays the fractions after the FPLC Q column purification. Fractions containing CRALBP are 38 through 43. Lane 1. Molecular Weight Standard; 2. fraction 29; 3. fraction 30; 4. fraction 31; 5. fraction 38; 6. fraction 39; 7. fraction 40; 8. fraction 41; 9. fraction 42; 10. fraction 43.

The binding activity of purified CRALBP with its natural ligand 11-*cis*-retinal was tested using the UV titration method. When low equivalents of ligand (up to 0.2 eq) were added, the complex showed a distinct red shift from 380 nm to ~420 nm. However, when more ligand was added, the absorption started to shift back toward 380 nm (Figure V-3). By looking thoroughly in the original paper of Crabb, I found that the protein they purified was also not fully active (1). The only graph that showed the red shift of the bound chromophore in the paper is actually looking very similar to our titration with 0.2 eq of ligand being added.

Primary crystallization trials of the apo form of this protein were performed at 4°C. However, again, no crystals were observed for this non-fusion full-length CRALBP.

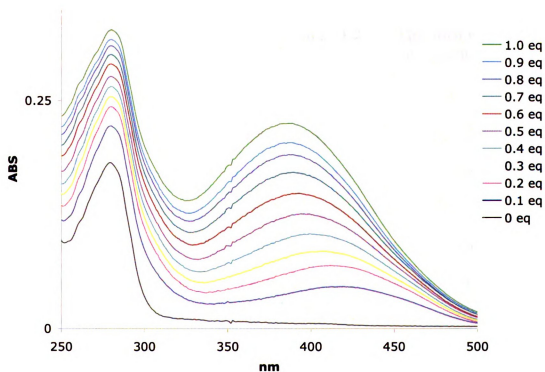


**Figure V-3. UV titration of non-fusion CRALBP with 11-*cis*-retinal.**

### 5.2.3. Full-length CRALBP with a cleavable His-tag.

In previous attempts, the purified non-fusion CRALBP showed reduced activity, probably due to the prolonged purification steps. In order to overcome this possible problem, we decided to introduce a cleavable tag to the protein so that the purification could be done in much shorter time and hopefully with similar or even better purity.

A. Overnight cutting



B. 3 hour cutting

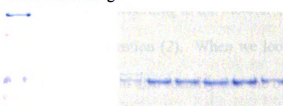


**Figure V-4. Full length CRALBP expressed in pET28a and purified with his-tag cleaved. A.** Overnight cutting followed by FPLC resource Q purification; **B.** 3 hour cutting followed by FPLC resource Q purification.

The full-length gene encoding CRALBP was successfully cloned into the pET28a expression vector. The expressed protein contains a poly-histidine tag at the N-terminal followed by a thrombin-cutting site. The full length CRALBP was first over-expressed and purified by Ni-column. The purified His-tagged protein was then treated with thrombin to cleave the tag. It turned out that this step could be non-specific if the cutting time is too long. The overnight cutting gave two bands, which could not be separated after resource Q FPLC or gel filtration (Figure V-4A). Cutting for 3 hours gave a much better result. The full length protein turned out to be the major component, with very



little over-cut protein present (Figure V-4B). However, crystallization of this construct did not yield any crystals either.

### **5.3. Crystallization of the N-terminal-truncated CRALBP.**

Attempts to crystallize the native, full-length CRALBP all turned out to be not successful. This then lead us to question whether floppy domains exist in native CRALBP, which hinder the crystallization of this protein. According to the literature, the N-terminal of CRALBP is subjected to limited trypsin digestion (2). When we looked back at our trypsin cutting experiment (Figure V-4), we could also identify that the over-digested peptide is only slightly smaller than the full-length protein. This result possibly suggests that a floppy N-terminal exists in CRALBP. What's more, one of the family members of CRALBP,  $\alpha$ -tocopherol transfer protein ( $\alpha$ TTP), was crystallized with a N-terminal truncation (3). These facts all suggest that N-terminal deletion of CRALBP might help the crystallization of the protein.

#### **5.3.1. Truncation at 43/44 on the N-terminal of CRALBP.**

It is vital to make the right decision on where to make the truncation. Certainly, cutting should not disrupt the globular structure of the protein. It is also important that not a lot of unstructured amino acids are left hanging at the N-terminus after the deletion, otherwise they will still hamper the crystal packing of the protein. To make the decision on the cutting position, I first looked at the corresponding position where others have made deletion to help crystallize  $\alpha$ TTP. The first 20 amino acids were actually cleaved off  $\alpha$ TTP, while its first  $\alpha$  helix starts at position 27 based on its crystal structure.

Another family member, Sec14, has its first  $\alpha$  helix start at position 33 (4). Besides, based on the model for CRALBP, the proposed first helix starts at around 66 (5). Two sequence alignment methods, ClustalW and MAP, were used to compare the corresponding position 20 of  $\alpha$ TTP on CRALBP. However, the two disagree with each other to a large extent especially at the N-termini of this family of proteins. By comparing the starting position of the first  $\alpha$ -helix of each protein based on the secondary structure prediction generated with the two methods, MAP seemed to give more accurate estimations (1AA difference) over ClustalW (5AA difference). Therefore, from the comparison of the MAP sequence alignment, position 43 on CRALBP turned out to be the corresponding position 20 on  $\alpha$ TTP. Since 43 is still far enough from position 66, where the first  $\alpha$ -helix starts according to the model built for CRALBP, it should be a safe place to make the deletion. Therefore, it was decided that the truncated protein would start from position 44.

The truncated gene was generated through PCR and cloned into the pET28a vector. However, multiple attempts to express this truncated CRALBP resulted in no expression at all. The inclusion body was later detected in the pellet of cells after sonication, indicating misfolded proteins. To improve the situation, lower temperature growth (16°C) and less IPTG induction were investigated. Fortunately, this time small amounts of the target protein were obtained after Ni column purification (Figure V-5). After cutting with thrombin, the protein was further purified by resource Q FPLC. The protein was mostly pure except for a contaminant with a higher MW.

Lane    1        2        3        4        5        6        7        8

**Figure V-5. N-43/44-truncated CRALBP expressed from pET28a and purified by Ni-column.** 1. MW; 2. Flow through; 3. First wash; 4. Second wash; 5~8. Elution fractions.

However, the 43/44 truncation made at the N-terminus of CRALBP was later proven to be not active for binding to 11-*cis*-retinal. The truncated protein failed to bind to 11-*cis*-retinal based on the fact that no red shift of the absorption maxima was observed when the ligand was introduced to the truncated protein. Although red shift of the absorption maxima does not necessarily equal to ligand binding, it is still safe to say that cleavage of 43 amino acids off the N-terminal is too much, which either results in a completely non-functional protein or removes important protein-ligand interactions that lead to no red shift of the bound chromophore.

### **5.3.2. Discovery of the ideal N-terminal truncation site.**

To look further into truncation options, we decided to make several truncations at the N-terminus ( $\Delta 10$ ,  $\Delta 15$ ,  $\Delta 20$ ,  $\Delta 25$ ,  $\Delta 30$ ,  $\Delta 35$ ). These mutants were successfully cloned, expressed and purified using the same systems that were employed for the 43/44 truncation construct earlier. During expression of these truncation mutants, it turned out

that, as expected, not all the mutants could be expressed. Deletion of up to 25 amino acids was able to maintain good expression of the protein. Deletion of 30 amino acids or more resulted in very poor or no expression (Figure V-6).

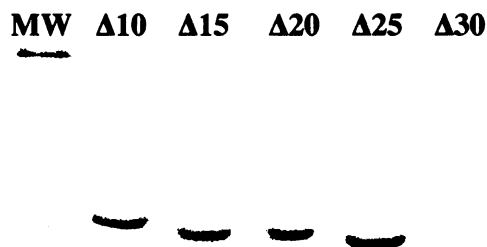


**Figure V-6. Expression of the truncated CRALBPs.**

To further test whether the well expressed proteins are all active, UV titration experiments were carried out for each of the four mutants:  $\Delta 10$ ,  $\Delta 15$ ,  $\Delta 20$  and  $\Delta 25$ . By continuously adding 0.1 equivalent of the ligand 11-*cis*-retinal into the protein solutions, red shifts from 380 nm to 410 nm were observed in all cases. The first three proteins ( $\Delta 10$ ,  $\Delta 15$  and  $\Delta 20$ ) bind to the ligand almost as well as the full length CRALBP. For these three truncations, red shifts continued until up to 0.4~0.5 eq was added for all three truncations (0.5~0.6 eq for the full length protein). Afterwards, the absorption started going back toward 380 nm. However, the last one,  $\Delta 25$ , could only take up to 0.3~0.4 eq

of ligand before the absorption started going back toward 380 nm (Figure V-7). The result suggested that  $\Delta 25$  might not be as active as the other three truncations.

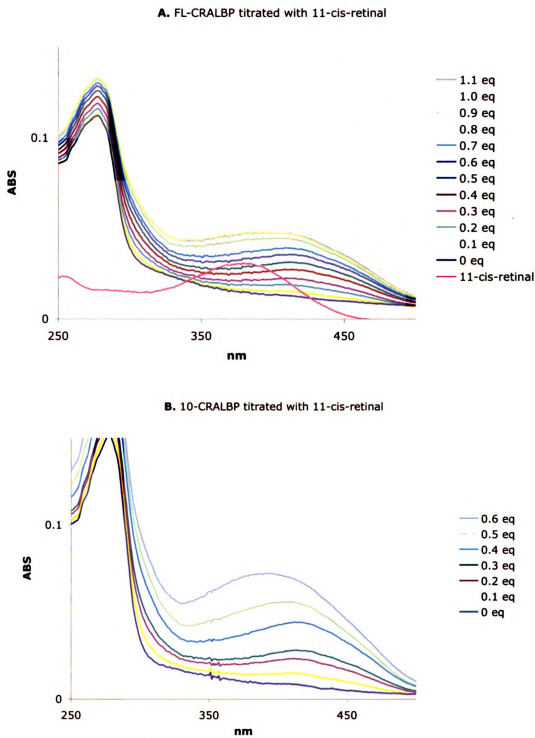
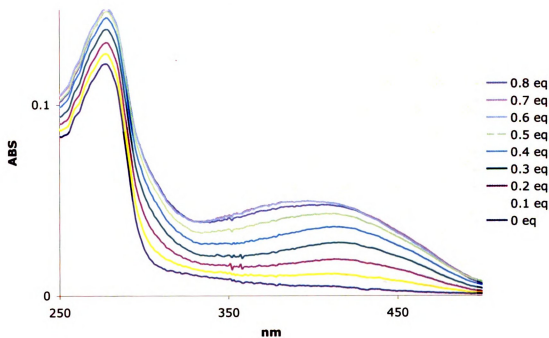


**Figure V-7. UV titration of full-length and truncated CRALBPs with 11-cis-retinal.**

**Figure V-7 (cont'd).**

**C. 15-CRALBP titrated with 11-cis-retinal**



**D. 20-CRALBP titrated with 11-cis-retinal**

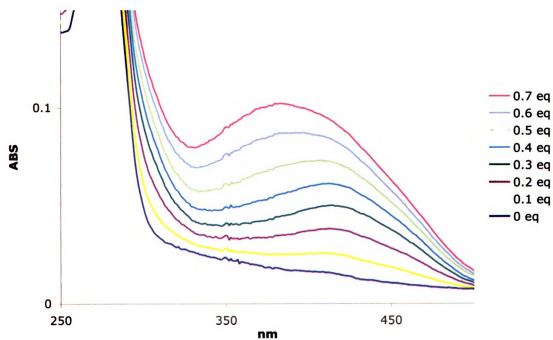
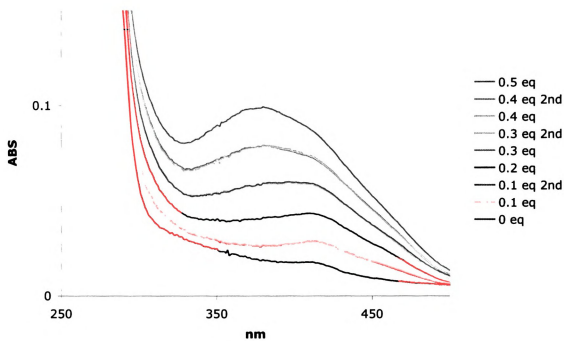
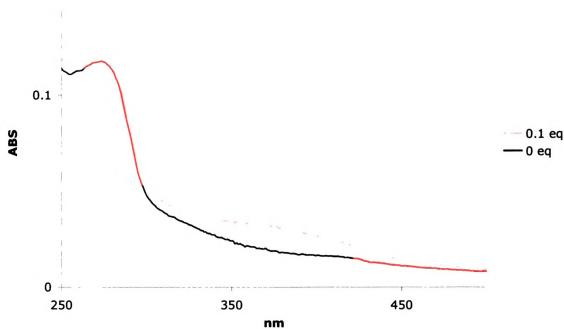


**Figure V-7 (cont'd).**

**E. 25-CRALBP titrated with 11-cis-retinal**



**F. 30-CRALBP titrated with 11-cis-retinal**



Further proof of  $\Delta 25$  being different from other active truncations came from gel filtration experiments. Gel filtration purification for each of the full length CRALBP as well as the four truncations ( $\Delta 10$ ,  $\Delta 15$ ,  $\Delta 20$ ,  $\Delta 25$ ) were carried out, respectively, to further purify the proteins as well as to observe whether they would purify as monomers or dimers or even other association forms.  $\Delta 10$ ,  $\Delta 15$ , and  $\Delta 20$  all gave similar profiles to the wild-type CRALBP for their gel filtration run (a huge peak at the void, a smaller, sharper peak fractions later and a shoulder in between, Figure V-8), while  $\Delta 25$  only gave a peak at the void.

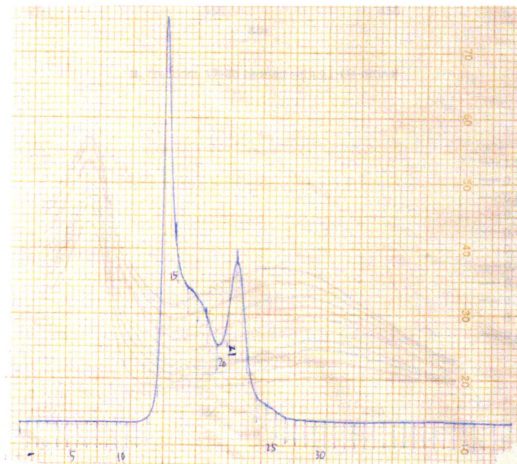
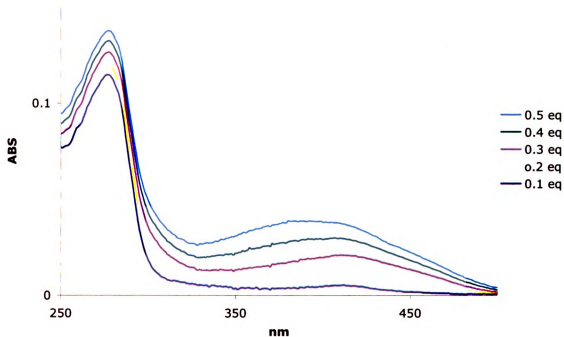


**Figure V-8. Gel filtration separation of full-length-CRALBP.**



**A. Fractions 13-16 titrated with 11-cis-retinal**



**B. Fractions 17-20 titrated with 11-cis-retinal**

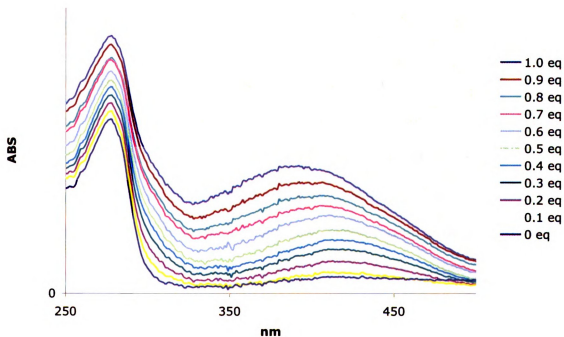
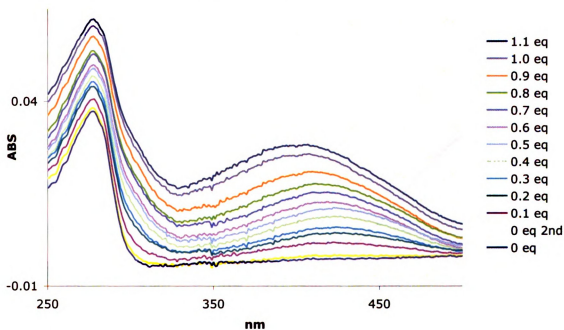


**Figure V-9. UV titration of different fractions from gel filtration separation of  $\Delta 20$ -CRALBP.**

**Figure V-9 (cont'd).**

**C. Fractions 21-23 titrated with 11-cis-retinal**



This observation, together with the previous observation that  $\Delta 25$  was not as active as the other truncations, also led to the suspicion that the more active form of the protein might reside in the fractions that showed up later in the gel filtration runs of  $\Delta 10$ ,  $\Delta 15$ , and  $\Delta 20$ . To test this suspicion, UV titration experiments were carried out for different gel filtration fractions, respectively (Figure V-9). It turned out that the most active protein did come from the later fractions corresponding to the smaller, sharper peak with an approximate molecular weight of 120 KD (0.8 eq, tetramer?). The protein coming out of the void had the worst binding property (0.2~0.3 eq) and the shoulder fractions showed an average binding activity (~0.6 eq).

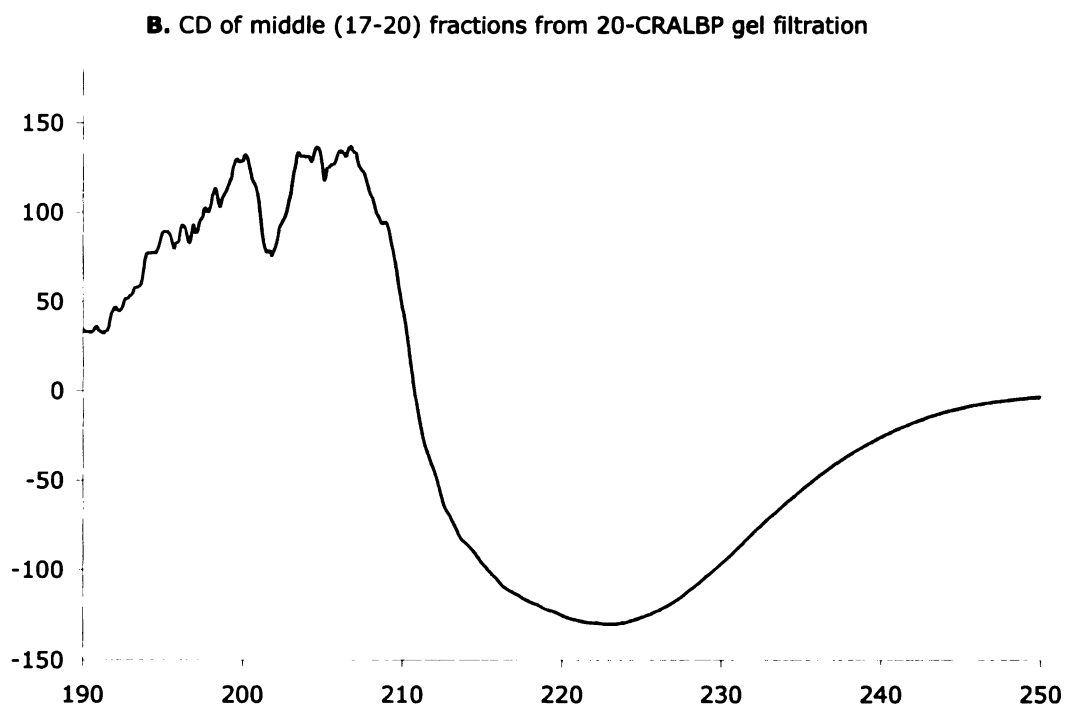
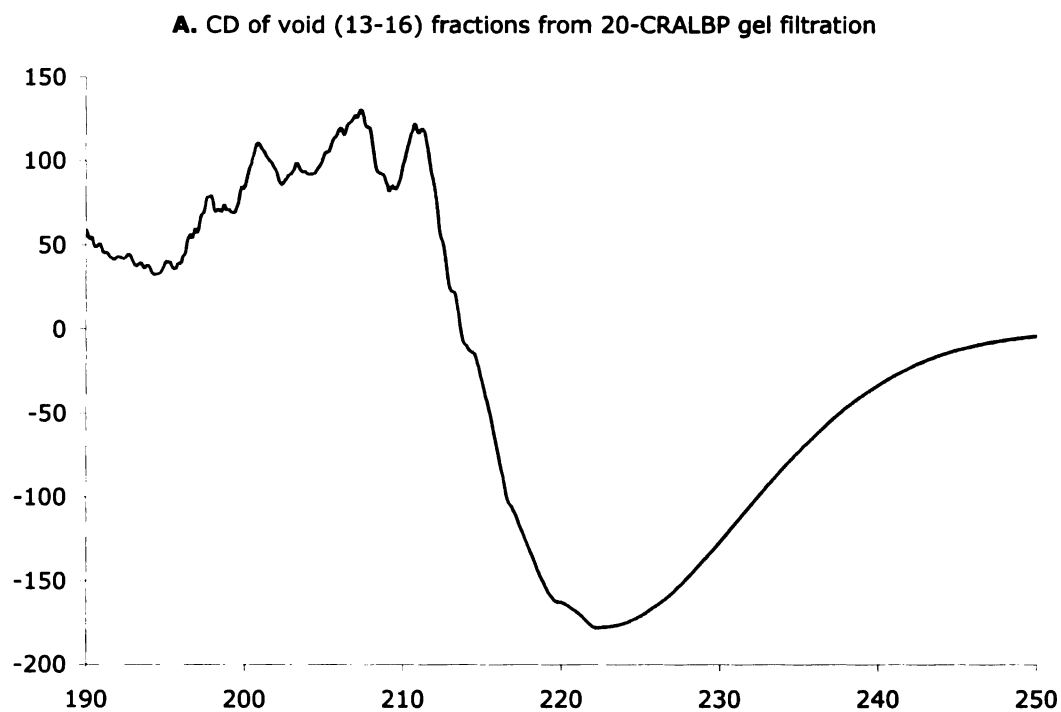
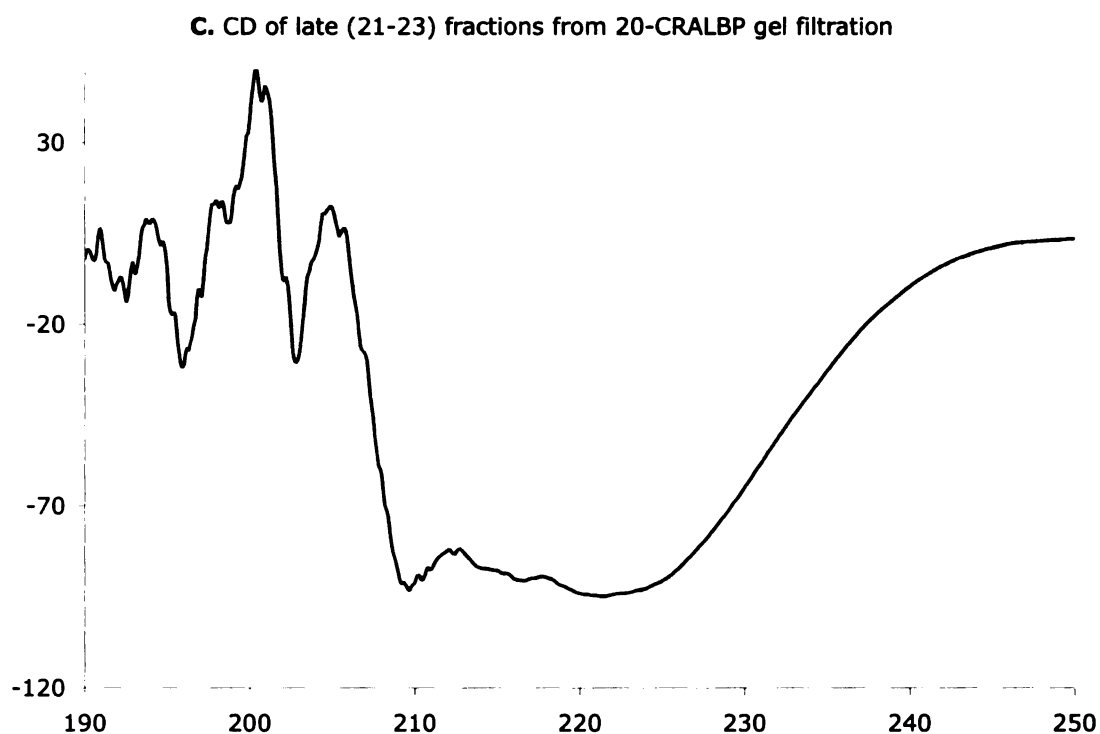


**Figure V-10. CD spectra of different fractions from gel filtration separation of  $\Delta$ 20-CRALBP.**

**Figure V-10 (cont'd).**



The circular dichroism (CD) absorptions of  $\Delta 20$  out of different gel filtration fractions were also measured (Figure V-10). The CD spectrum of the later fractions resembles the reported CD spectrum of active full length CRALBP. The CD of the void fractions only showed a signal at  $\sim 220$  nm and was missing the signal at  $\sim 208$  nm. The middle fractions showed a CD signal as an average of the previous two.

Based on the above results, it turned out that  $\Delta 20$ -CRALBP is the ideal construct, which is hopefully free of floppiness and, at the same time, proven to be able to express well as a functional protein.

A.



B.

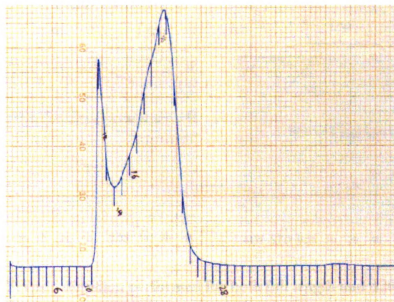


**Figure V-11. Gel filtration purification of the  $\Delta 20$ -CRALBP grown at different temperatures. A. 37°C; B. 16°C.**

### 5.3.3. Enhancing the expression and purification of functional CRALBP.

As shown in Figure V-8, the gel filtration purification of the  $\Delta 20$ -CRALBP results in an elution profile with a majority of the protein being eluted at the void. This suggests possible aggregation of the overexpressed protein. To tackle this problem, different growth temperatures were tried and yielded exciting results. It turned out that lower temperature did greatly favor the functional  $\Delta 20$ -CRALBP over the aggregated form (Figure V-11). The trypsin cutting conditions were also optimized to remove the tag after the Ni-NTA purification (Figure V-12). The complete procedure for optimized growth and purification of CRALBP (both truncated and the full length) is described in Chapter VI.

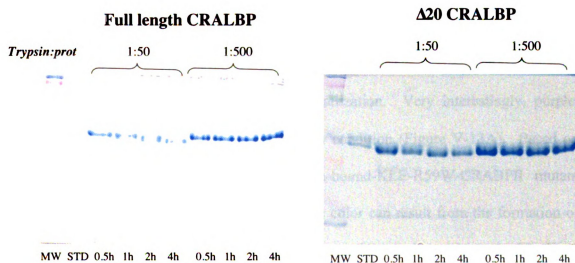


**Figure V-12.** Trypsin digestion performed for both full length and  $\Delta 20$ -CRALBP under 4°C.

#### 5.3.4. Crystallization trials.

The crystallization of the pure, active apo- $\Delta 20$ -CRALBP (10 mg/ml and 20 mg/ml, respectively) at both room temperature and 4°C did not yield any hits.

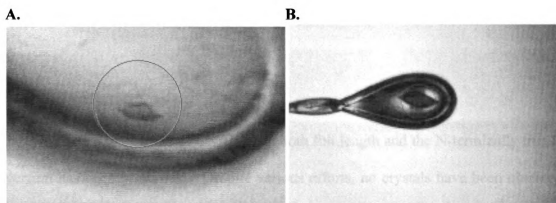


**Figure V-13. Crystals of merocyanin-bound proteins.** A. merocyanin-bound  $\Delta 20$ -CRALBP; B. merocyanin-bound KLE-R59W-CRABPII.

The crystallization efforts then turned to the holo-CRALBP complexes. Merocyanin has been proven to be an excellent substrate for CRALBP. The merocyanin- $\Delta 20$ -CRALBP complex was then used in crystallization. Very interestingly, purple, crystal-like entities were observed in a particular condition (Figure V-13A). Based on our previous experience with the merocyanin-bound-KLE-R59W-CRABPII mutant crystals (Figure V-13B), we know that the purple color can result from the formation of the protonated Schiff base between a protein Lys residue and the aldehyde functional group on the ligand. Therefore, we are hopeful that this entity is formed by proteins instead of salts. Unfortunately, this crystal-like entity failed to diffract X-rays, which probably indicates its lack of a more ordered arrangement of the molecules microscopically. Further efforts toward optimization of the quality of the crystals did not

improve the situation. However, the discovery so far gives us confidence that the  $\Delta 20$ -CRALBP finally showed some tendency toward crystallization and that we might be at the very edge of obtaining the first crystal of the CRALBP protein. The synthesis of 11-*cis*-retinal and ring-locked-11-*cis*-retinal is underway and we hope we will have better luck trying to crystallize CRALBP bound with these new ligands.

#### **5.4. Conclusion.**

The crystallization of CRALBP in both full length and the N-terminally truncated version has been performed. Despite various efforts, no crystals have been obtained so far. However, by introducing retinoid analogs into the protein, we seem to be able to improve the protein's tendency toward crystallization. It seems very promising that future crystallization trials probably with new ligands might lead us to obtaining the first crystal of the CRALBP.



## Reference

1. Crabb, J. W., Chen, Y., Goldflam, S., West, K., Kapron, J. . (1998) Methods for producing recombinant human cellular retinaldehyde-binding protein, *Methods in Molecular Biology* 89, 91-104.
2. Crabb, J. W., Gaur, V. P., Garwin, G. G., Marx, S. V., Chapline, C., Johnson, C. M., and Saari, J. C. (1991) Topological and Epitope Mapping of the Cellular Retinaldehyde-Binding Protein from Retina, *J Biol Chem* 266, 16674-16683.
3. Min, K. C., Kovall, R. A., and Hendrickson, W. A. (2003) Crystal structure, of human alpha-tocopherol transfer protein bound to its ligand: Implications for ataxia with vitamin E deficiency, *P Natl Acad Sci USA* 100, 14713-14718.
4. Sha, B. D., Phillips, S. E., Bankaitis, V. A., and Luo, M. (1998) Crystal structure of the *Saccharomyces cerevisiae* phosphatidylinositol-transfer protein, *Nature* 391, 506-510.
5. Wu, Z. P., Hasan, A., Liu, T. Y., Teller, D. C., and Crabb, J. W. (2004) Identification of CRALBP ligand interactions by photoaffinity labeling, hydrogen/deuterium exchange, and structural modeling, *J Biol Chem* 279, 27357-27364.

## CHAPTER VI. Experimental

### 6.1. Cloning, mutagenesis, expression and purification

#### 6.1.1. Cloning, mutagenesis, expression and purification of CRABP II mutants.

*Mutagenesis.* Site-directed mutagenesis was performed using the CRABP II-pET17b plasmid following Stratagene's Quikchange<sup>®</sup> protocol. The PCR products were transfected into JM109 competent *Escherichia coli* cells for plasmid maintenance.

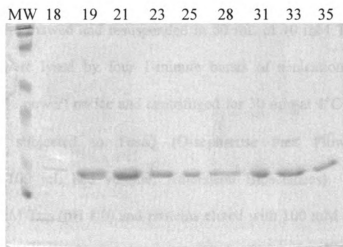


**Figure VI-1. R132K:Y134F:R111L:L121E-CRABP II (KFLE) purified after source-15Q anion exchange column.** The corresponding fraction number is listed on top of each lane.

*Protein Expression and Purification.* Human recombinant CRABP II was expressed and purified as described (1). The target gene (CRABP II/pET17b), as isolated from JM109

using Qiagen's Maxi Prep<sup>®</sup> DNA isolation kit, was transformed into *E. coli* strain BL21(DE3)pLysS cells (Stratagene), according to standard protocols. The transformed cells were grown at 37°C in an LB agar plate containing both ampicillin (100 µg/mL) and chloramphenicol (25 µg/mL). A single colony was inoculated in 50 mL of LB containing the same amount of the two antibiotics and grown overnight with shaking at 250 rpm at 37°C. This culture was then transferred to 1 L of LB with the same antibiotics. The culture was incubated at 37°C until A<sub>600</sub> reached between 0.6 and 0.8. The expression was induced by addition of 0.5 mM isopropyl-1-β-D-galactopyranoside (IPTG). The growth was continued for another 5 h at 30°C. The cells were harvested using centrifugation (5000 rpm, 10 min) and frozen at -80°C. The frozen cells from 2 L of growth culture were thawed and resuspended in 50 mL of 10 mM Tris (pH 8.0). The suspended cells were lysed by four 1-minute bursts of sonication (probe sonicator, Biologics Inc., 60% power) on ice and centrifuged for 30 min at 4°C at 7000 rpm. The supernatant was subjected to FastQ (Q-sepharose Fast Flow Resin) column chromatography (100 mL bed volume; Amersham Biosciences). The column was washed with 10 mM Tris (pH 8.0) and proteins eluted with 100 mM of NaCl in 10 mM Tris (pH 8.0). The fractions were analyzed by SDS 16% polyacrylamide gel electrophoresis and those of the highest purity were combined. The protein solution was desalted by concentration using Centriprep 3 concentrators (Amicon, MWCO 3000), followed by dilution with 10 mM Tris (pH 8.0). The proteins were further purified on a BioRad system (BioLogics Duo Flow, BioRad) using a Source15Q (Amersham Biosciences) anion exchange column. Fractions were analyzed by UV absorption at 280 nm as well as SDS 16% PAGE. All the steps of purification were performed at 4°C. The

most pure fractions were combined and concentrated to ~20 mg/mL, as determined by  $A_{280}$ . The pure and concentrated protein solutions were aliquoted and stored at -80°C.

### 6.1.2. Cloning, expression and purification of RAR $\gamma$ -LBD.

The pDONR vector (gentamycin resistant) containing the RAR $\gamma$ -LBD gene (178-423) with a hexa-His tag at the amino end was obtained from Dr. Marc Ruff in professor Pierre Chambon's lab. The gene was subcloned into the NdeI-BamHI sites of pET15b and the resulting plasmid was amplified in DH5 $\alpha$ . Transformation into *E. coli* BL21(DE3) provided the construct ready for overexpression.

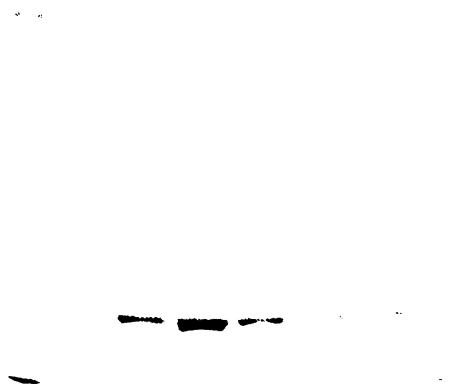


**Figure VI-2. Elution fractions of RAR $\gamma$ -LBD from Ni-NTA purification.**

Cells were grown in LB medium containing ampicillin as described (2, 3). Cell culture from 6 L shake flasks was centrifuged and the cell pellet was resuspended in 50 mL buffer A (5 mM imidazole, 500 mM NaCl, 20 mM Tris, pH 8.0), followed by sonication. The cell lysate, after centrifugation, was mixed with Ni-NTA resin (20 mL)

and shaken at 4°C for about 1 hour. The flow through was collected. The resin was then washed twice with 50 mL of buffer B (50 mM imidazole, 500 mM NaCl, 20 mM Tris, pH 8.0). The proteins were eluted with buffer C (100 mM EDTA, 500 mM NaCl, 20 mM Tris, pH 8.0) as 5 mL fractions, yielding 14 mg of protein (Figure VI-2).

The protein solution was dialyzed against Dialysis buffer (10 mM DTT, 500 mM NaCl, 10 mM Tris, 0.1% Tween20, pH 8.0). It was then concentrated to 2.5 mg/mL, followed by gel-filtration chromatography (Superdex200, Pharmacia) using the same Dialysis buffer. The RAR $\gamma$ -LBD (28 KD) was obtained mainly as a homodimer as expected.

### **6.1.3. Cloning, mutagenesis, expression and purification of CRALBP.**

#### **6.1.3.1. Initial constructs of CRALBP.**

The rCRALBP gene was generously provided by professor John W. Crabb. The rCRALBP gene was then cloned into both His-tagged (pET19b) and non-fusion (pET17b) plasmids and expressed respectively in BL21(DE3) cells. The His-tagged rCRALBP was purified using Ni-NTA affinity chromatography to homogeneity (Figure VI-3). The binding of this His-tagged rCRALBP was tested by observing UV shifts while titrating the protein with its natural ligand 11-*cis*-retinal.

Non-fusion CRALBP was expressed from the pET17b vector in BL21(DE3) codon<sup>⊕</sup> cells as a tag-free protein. The purification largely follows the procedure developed by Crabb and colleagues (4). In the first step of purification, a DEAE column was employed using a gradient of 10 mM to 400 mM of NaOAc in 25 mM Tris buffer with 0.1 mM DTT, pH 7.0. The roughly purified protein mixture was then applied onto a

hydroxyapatite (HTP) chromatography and eluted with a gradient of sodium phosphate (0-80mM) buffer (25 mM Tris, 300 mM NaOAc, 0.1 mM DTT, pH 7.0). This step eliminated most of the impurities and gave moderately pure CRALBP. The last step of purification employed the FPLC Q column (gradient from 50 mM to 500 mM of NaOAc in 20 mM MOPS and 0.1 mM DTT, pH 7.0), after which the CRALBP was purified to homogeneity (Figure VI-4).

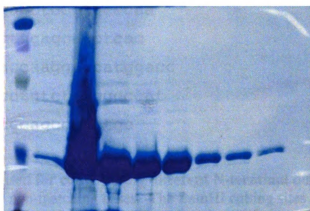


**Figure VI-3.** Pure fractions of the his-tagged rCRALBP eluted off the Ni column.

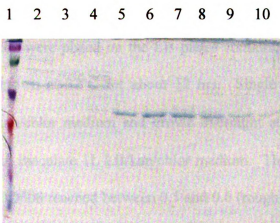


**Figure VI-4.** Non-fusion CRALBP after purification. This gel displays the fractions after the FPLC Q column purification. Fractions containing CRALBP are 38 through 43. Lane 1. Molecular Weight Standard; 2. fraction 29; 3. fraction 30; 4. fraction 31; 5. fraction 38; 6. fraction 39; 7. fraction 40; 8. fraction 41; 9. fraction 42; 10. fraction 43.

### 6.1.3.2. Cloning, mutagenesis, expression and purification of the newer constructs.

*Molecular cloning.* Inserts of full length,  $\Delta 10$ ,  $\Delta 15$ ,  $\Delta 20$ ,  $\Delta 25$ ,  $\Delta 30$ ,  $\Delta 35$ -CRALBP (all N-terminal deletions) were prepared using sequential digestion with BamHI and HindIII. The primers used for generating different deletions are listed in Figure VI-5. The digested genes were then successfully ligated into pET28a vectors, respectively.

```
10 AAGGATCCgtacctgaagaggaacaggag
15 AAGGATCCCaggagctccgtgcccaa
20 AAGGATccccaactggagcagctcac
25 AAGGATCCacaaccaaggaccatggacc
30 AAGGATCCggacctgtcttttgcccgt
35 AAGGATCcccgtgcagccagctgc
```

**Figure VI-5. Primers used for constructing different N-terminal deletion CRALBP.** Capital letters represent non-matching bases. The BamHI cutting sites together with the overhang bases are in purple.

*Expression and purification.* The plasmids were transformed into *E. coli* BL21 codon<sup>+</sup> cells, respectively. Cells were plated on the LB plates containing both kanamycin and chloramphenicol and grown at 37°C for about 12 hrs. Single colonies were used to inoculate 50 mL LB/kan/chlor medium and grown overnight at 37°C. The overnight culture was then used to inoculate 1L LB/kan/chlor medium. The cells were allowed to grow first at 37°C till OD600 reached between 0.5 and 0.6 (roughly 1.5 hrs). The culture was then taken out of the shaker and cooled down in the cold room (4°C) for 2-3 hrs. IPTG was then added to 0.5 mM and the growth was continued at 16°C for ~20 hrs. The

cells were harvested after centrifugation at 4,000 rpm for 10 min at 4°C. If not used immediately, cells were usually frozen using liquid nitrogen and stored at -20°C.

Cells were defrosted and re-suspended in 40 mL of buffer A (same as described in RAR-LBD purification). Protease inhibitor cocktail tablet (complete, EDTA-free, Roche) was then added. The cell suspension was lysed using four 1-minute bursts of sonication (probe sonicator, Biologics Inc., 60% power) on ice and centrifuged for 30 min at 4°C at 7000 rpm. The supernatant was loaded onto Ni-NTA resin (bed volume of ~ 15 mL) and the flow-through was collected. The resin was then washed with 2×50 mL of buffer B (same as used in RAR-LBD purification). The protein of interest was then eluted with 5×10 mL of the elution buffer (250 mM imidazole, 500 mM NaCl, 20 mM Tris, pH 8.0). The pure fractions were combined and thrombin was added to a molar ratio of ~ 1:500 (thrombin : protein). The solution was dialyzed against 20 mM Tris, 50 mM NaCl, pH 8.0 for a total period of 6-9 hours, during which the buffer was changed 3 times. After dialysis, the protein solution was concentrated using Centriprep 3 concentrators (Amicon, MWCO 3000) to a volume of 1-2 mL. The sample was then placed in an eppendorf tube and centrifuged at 14,000 rpm at -4°C for 10 min to remove precipitate. The supernatant was further purified by a size-exclusion column (HiPrep<sup>TM</sup> 16/60, Sephacryl<sup>TM</sup> S-300, Pharmacia Biotech) on FPLC (Pharmacia Biotech) and eluted with the same buffer as used in the dialysis. The elution profile features two peaks, with one at the void and one that immediately follows (Figure VI-6). Although both peaks show very pure CRALBP, only the later peak was verified to contain fully active protein and therefore is collected. The pure, active protein (Figure VI-7) was then concentrated to the desired concentration, frozen in liquid nitrogen and stored at -80°C.



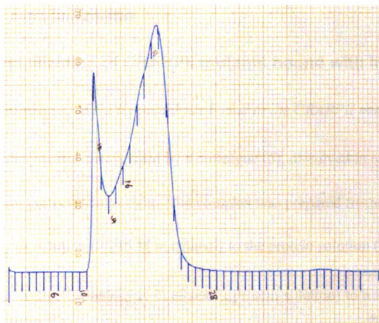


**Figure VI-6. Typical size-exclusion purification profile of CRALBP represented by  $\Delta 20$ -CRALBP grown at 16°C.**

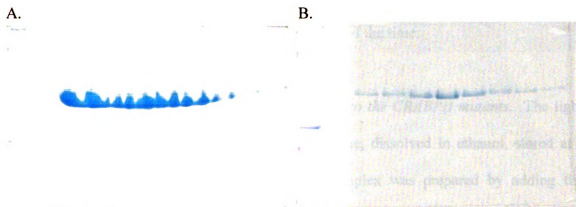


**Figure VI-7. CRALBP after purification. A. Full length CRALBP; B.  $\Delta 20$ -CRALBP.**

## **6.2. Protein crystallization**

### **6.2.1. Co-crystallization of CRABPII mutants bound with ligands.**

*Preparation of complexes of the C<sub>15</sub>-aldehyde bound to the CRABPII mutants.* The light sensitive C<sub>15</sub>-aldehyde was synthesized by a colleague (5), dissolved in ethanol, stored at -20°C, and always protected from light. The complex was prepared freshly by adding the C<sub>15</sub>-aldehyde stock solution (0.245 M in ethanol) to the protein solution (~ 20 mg/mL) in a volume ratio of 1:16 (C<sub>15</sub>-aldehyde in ethanol : protein solution) to a final molar ratio of ~10:1 (C<sub>15</sub>-aldehyde : protein). The complex was first incubated at room temperature for 30 min and then 4°C for 1~2 hrs before being used for crystallization. The complex was only exposed to dim red light when necessary (crystallization, flash freezing or under the microscope) and was kept in the dark for the rest of the time.

*Preparation of complexes of the merocyanin bound to the CRABPII mutants.* The light sensitive merocyanin was synthesized by a colleague, dissolved in ethanol, stored at -20°C, and always protected from light. The complex was prepared by adding the merocyanin stock solution (0.032 M) to the protein solution (~ 20 mg/mL) in a volume ratio of 1:10 (merocyanin in ethanol : protein solution) to a final molar ratio of 2.5:1 (merocyanin : protein). The complex was first incubated at 4°C for over 1 hr and then at room temp for several more hrs before being used for crystallization. The complex was only exposed to dim red light when necessary (crystallization, flash freezing or under the microscope) and was kept in the dark for the rest of the time.

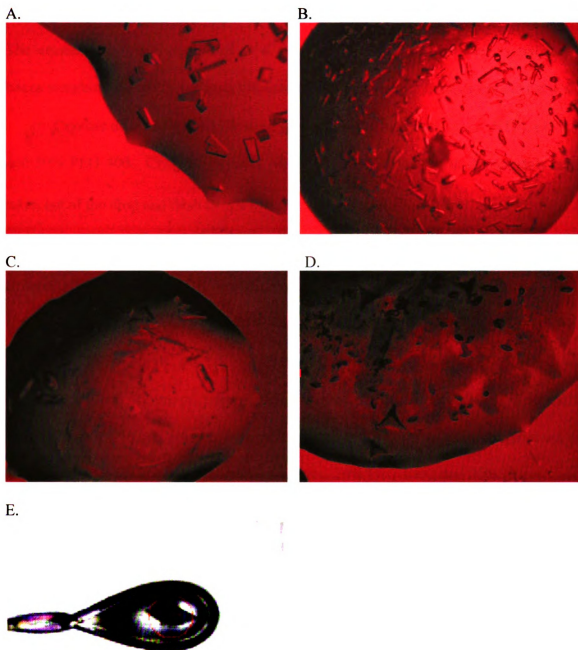


**Figure VI-8. Pictures of crystals of the ligand-bound CRABP II mutants.** A.  $C_{15}$ -aldehyde-bound KL-A32E-CRABP II; B.  $C_{15}$ -aldehyde-bound KL-T54E-CRABP II; C.  $C_{15}$ -aldehyde-bound KFLDV-CRABP II; D. merocyanin-bound KLE-R59W-CRABP II; E. merocyanin-bound KLE-R59W-CRABP II, taken while the crystal was being cryo protected by the nitrogen stream when sitting on the goniometer at the LS-CAT at APS.

*Crystallization and Cryoprotection.* The hanging drop vapor diffusion method was used. The crystallization was performed at 4°C under dim red light and the crystallization boxes were covered with aluminum foil to avoid light exposure. Boxes were kept at 4°C.

Crystals of *holo*-KLE-R59W were grown in 0.1M bis-tris-propane (BTP), pH 7.5, and 30% PEG 400. Crystals appeared within 24 hrs. On the fourth day crystals were taken out of the drop and flash frozen by immersion in liquid N<sub>2</sub>.

Crystals of *holo*-KL-A32E were grown in 0.1M Na citrate, pH 7.5, 0.2M ammonium acetate, and 26% PEG 4000 (Figure VI-8A). Crystals appeared within 24 hrs and were immediately transferred to a soaking drop containing 4 µL of the reservoir solution (0.1M Na citrate, pH 7.5, 0.2M ammonium acetate, and 20% PEG 4000), 1 µL of protein solution (22 mg/mL), and 0.5 µL of ligand stock solution (0.245M in ethanol). After 42 hrs of soaking, crystals were briefly immersed in a cryo solution composed of 0.1M Na citrate, pH 7.5, 0.2M ammonium acetate, 26% PEG 4000, and 20% glycerol and flash frozen in liquid N<sub>2</sub>.

Crystals of *holo*-KL-T54E were grown in 0.1M NaOAc, pH 5.8, and 18% PEG 6000 (Figure VI-8B). Crystals appeared after 1 week. On the same day crystals were soaked briefly in 0.1M NaOAc, pH 5.8, 18% PEG 6000, and 30% glycerol and flash frozen.

Crystals of *holo*-KFLDV were grown and frozen in the same way as *holo*-KL-T54E (Figure VI-8C). Crystals appeared after 40 hrs and were flash frozen right after appearance.

Crystals of merocyanin-bound KLE-R59W were grown in 0.1M MES, pH 6.3, 0.2M ammonium sulfate, and 30% polyethylene glycol mono-methyl-ether (PEGMME)

5000 (Figure VI-8D,E). Crystals displayed a distinctive purple color and grew bigger gradually for two weeks. Crystals were soaked briefly in 0.1M MES, pH 6.3, 0.2M ammonium sulfate, and 30% PEGMME, and 20% glycerol and flash frozen.

### **6.2.2. Crystallization of apo-CRABP II mutants.**

The hanging drop vapor diffusion method was used. The droplet consisted 1  $\mu$ l of concentrated protein (~20 mg/ml) and 1  $\mu$ l of the reservoir. The crystallization was performed at room temperature. All crystals appeared within 24 hours and were frozen within a week after appearance. Cryoprotectants were prepared with either 20% or 30% glycerol in addition to the components of the corresponding growth conditions in the same concentrations. All of these apo CRABP II mutant structures are in the P 1 spacegroup.

Crystals of the apo-R132K:R111L:A32E-CRABP II (KL-A32E) were grown in 0.1M Tris, pH 8.5, 0.2M NaOAc, and 26% PEG 4000 (Figure VI-9A). The crystals were briefly immersed in a cryo solution containing 20% glycerol before they were flash frozen in liquid nitrogen.

Crystals of the apo-R132K:R111L:T54E-CRABP II (KL-T54E) were grown in 0.1M bis-tris-propane (BTP), pH 7.5, and 30% PEG 4000. Two microliters of the cryoprotectant (20% glycerol) was added to the crystal-containing droplet and the crystals were then taken out of the drop after ~30 seconds, followed by flash freezing in liquid nitrogen.

Crystals of the apo-R132K:Y134F:R111L:L121D:T54V-CRABP II (KFLD-T54V or KFLDV) were grown in 0.1M Tris, pH 7.5, 0.2M NaOAc, and 24% PEG 4000 (Figure

VI-9B). Two microliters of the cryoprotectant (20% glycerol) was added to the crystal-containing droplet and the crystals were incubated in the new drop for ~30 sec before being flash frozen in liquid nitrogen.

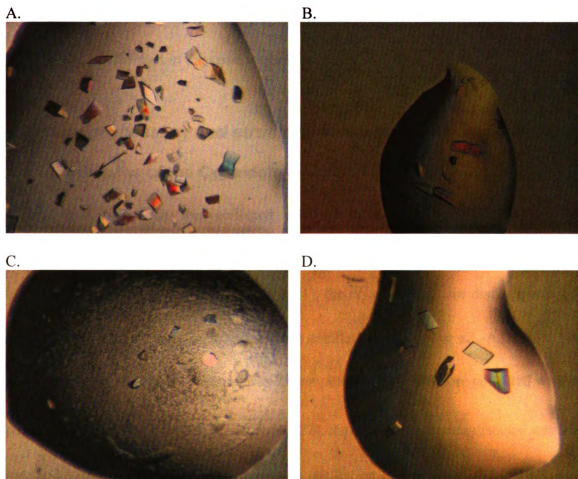


**Figure VI-9. Pictures of crystals of the apo-CRABP II mutants.** A. apo-KL-A32E-CRABP II; B. apo-KFLDV-CRABP II; C. apo-KFLD-CRABP II; D. apo-KFLE-CRABP II.

The apo-R132K:R111L:L121E:R59E-CRABP II (KLE-R59E) was crystallized in 0.1M BTP, pH 7.5, and 22% PEG 8000. Two microliters of the cryoprotectant (30% glycerol) was added to the crystal-containing droplet and the crystals were incubated in the new drop for ~30 sec before flash frozen in liquid nitrogen.

The apo-R132K:Y134F:R111L:L121D-CRABPII (KFLD) was crystallized in 0.1M BTP, pH 8.1, and 22% PEG 4000 (Figure VI-9C). Cryoprotection and flash freezing were performed in the same way as for apo-KLE-R59E.

The apo-R132K:Y134F:R111L:L121E-CRABPII (KFLE) was crystallized in 0.1M BTP, pH 7.0-8.5, and 20-30% PEG 4000 (Figure VI-9D). Cryoprotection and flash freezing were performed in the same way as for apo-KLE-R59E.

### **6.3. Data processing and structure determination**

#### **6.3.1. Structures of the C<sub>15</sub>-aldehyde-bound CRABPII mutants.**

*Data Collection.* Datasets were collected at the Advanced Photon Source LS-CAT 21-ID at Argonne National Laboratory. Processing and scaling was done using HKL2000 (6).

For the dataset of KLE-R59W (1.95 Å, P<sub>3</sub><sub>1</sub>2<sub>1</sub>), the crystal to detector distance was 200 mm and 120° of data were collected with an oscillation of 1°. For KL-A32E (1.22 Å, P<sub>2</sub><sub>1</sub>), the crystal to detector distance was 75 mm and 200° of data were collected with an oscillation of 1°. For KL-T54E (2.00 Å, P<sub>6</sub><sub>1</sub>2<sub>2</sub>), the crystal to detector distance was 200 mm and 150° of data were collected with an oscillation of 0.5°. For KFLDV (1.54 Å, P<sub>2</sub><sub>1</sub>2<sub>1</sub>2<sub>1</sub>), the crystal to detector distance was 150 mm and 360° of data were collected with an oscillation of 1° (only the first 120° were scaled).

All datasets were collected at the Advanced Photon Source at Argonne National Laboratory. Datasets for KL-A32E, KL-T54E, KFLD-T54V and KLE-R59E were collected at LS-CAT 21-ID. The dataset for KFLD was collected at SBC-CAT 19-BM.

The dataset for KFLE was collected at COM-CAT 32-ID. All datasets were processed with HKL2000 (6).

*Structure solution and refinement.* Structures of KLE-R59W and KL-A32E were solved using Molrep (7) in CCP4 (8) with KLE-CRABPII as the search model (PDB ID:2G7B). Structures of KL-T54E and KFLDV were solved using Phaser (9) with the same model.

Model building was accomplished in both TURBO-FRODO (10) and COOT (11) for each of the four structures. REFMAC5 (12-15) within the CCP4 suite of programs was used to refine the structures against 95% of the data, while 5% of data was chosen randomly for cross validation,  $R_{\text{free}}$ . For KL-A32E, SHELXL-97 (16) was used in the later stages of refinement. For KL-T54E, TLSMD analysis (17, 18) was performed and TLS refinement in REFMAC5 with 3 groups for Chain A and 4 groups for Chain B resulted in improved B factors and  $R/R_{\text{free}}$ .

Asp126 was the only residue outside of the allowed region in the Ramachandran plot in all four structures after refinement. In *holo*-KL-A32E it resides in the generously allowed region, while in the other three structures in the disallowed region. The same Asp126 was found to reside in disallowed regions in all previously determined CRABPII structures (19). The good electron density maps at this position greatly enhanced our confidence in the non-favorable geometry of this residue.

### **6.3.2. Structure of the merocyanin-bound KLE-R59W-CRABPII mutant.**

*Data Collection.* The dataset was collected at the Advanced Photon Source LS-CAT 21-ID at Argonne National Laboratory. Processing and scaling was done using HKL2000



(6). The dataset was determined to be in P3<sub>1</sub>21 spacegroup with the highest resolution at 2.60 Å. The crystal to detector distance was 250 mm and 180° of data were collected with an oscillation of 1°.

*Structure solution and refinement.* Structure of the merocyanin-bound KLE-R59W and was solved using Molrep (7) in CCP4 (8) with KLE-CRABPII as the search model (PDB ID:2G7B).

Model building was accomplished in both TURBO-FRODO (10) and COOT (11). REFMAC5 (12-15) within the CCP4 suite of programs was used to refine the structure against 95% of the data, while 5% of data was chosen randomly for cross validation, R<sub>free</sub>. TLSMD analysis (17, 18) was performed and TLS refinement in REFMAC5 with 5 groups resulted in improved overall B-factor and R-factors.

### **6.3.3. Structures of the apo-CRABPII mutants.**

All structures were solved using either Molrep (7) or rigid body refinement in Refmac5 (12-14) in CCP4 with apo-WT-CRABPII MolA as the search model (PDB ID: 2FS6). Model building was accomplished in both COOT (11) and TURBO-FRODO (10) for every structure. Restrained refinement in Refmac5 was used to refine the structures against 90-95% of the date, while 5-10% of data were chosen randomly for cross validation, R<sub>free</sub>. Anisotropic refinement for temperature factors was employed for KL-A32E and KFLD-T54V (13). For KL-T54E, TLSMD analysis was performed and TLS refinement with 9 groups for both chain A and chain B resulted in improved B factors as well as R<sub>work</sub>/R<sub>free</sub> (15, 17, 18).

**Table VI-1. X-ray data collection statistics of the ligand-bound CRABPII mutant crystals.**

	C <sub>15</sub> -aldehyde- KLE-R59W	C <sub>15</sub> -aldehyde- KL-A32E	C <sub>15</sub> -aldehyde- KL-T54E	C <sub>15</sub> -aldehyde- KFLDV	Merocyanin- KLE-R59W
Spacegroup	P 3 <sub>1</sub> 12	P 2 <sub>1</sub>	P 6 <sub>1</sub> 22	P 2 <sub>1</sub> 2 <sub>1</sub> 2 <sub>1</sub>	P 3 <sub>1</sub> 21
Z (mol/asymm. unit)	1	1	2	2	1
Unit cell dimensions					
a (Å)	58.5	34.8	87.5	37.3	55.8
b (Å)	58.5	46.3	87.5	89.6	55.8
c (Å)	104.0	37.3	211.0	90.6	108.2
α (°)	90.0	90.0	90.0	90.0	90.0
β (°)	90.0	92.5	90.0	90.0	90.0
γ (°)	120.0	90.0	120.0	90.0	120.0
Wavelength (Å)	0.97869	0.97869	0.97869	0.97869	0.97850
Resolution range (Å)	28.61-1.95 (2.02-1.95)	23.17-1.22 (1.25-1.22)	43.75-2.00 (2.05-2.00)	32.17-1.54 (1.58-1.54)	48.34-2.60 (2.69-2.60)
Redundancy	6.7 (4.9)	3.8 (3.5)	16.9 (15.0)	4.6 (3.4)	9.2 (4.5)
Average I/σ	48.3 (2.6)	9.5 (4.0)	56.1 (7.0)	31.3 (2.5)	43.3 (1.9)
Total reflections	98767	158823	652041	208473	52112
Unique reflections	14428	42691	33179	45201	5671
Completeness	95.0 (77.5)	95.3 (79.8)	99.97 (100)	98.7 (95.8)	88.4 (41.3)
R <sub>merge</sub> (%)	0.056 (0.372)	0.046 (0.249)	0.074 (0.404)	0.054 (0.366)	0.058 (0.544)

Values in parentheses refer to the last resolution shell.

**Table VI-2. Structure refinement statistics of the ligand-bound CRABPII mutant crystals.**

	C <sub>15</sub> -aldehyde- KLE-R59W	C <sub>15</sub> -aldehyde- KL-A32E	C <sub>15</sub> -aldehyde- KL-T54E	C <sub>15</sub> -aldehyde- KFLDV	Merocyanin- KLE-R59W
Average B-Factor (Å)	28.208	20.928	22.918	25.323	38.856
R <sub>work</sub> (%)	20.5	11.37	19.8	19.3	23.0
R <sub>free</sub> (%)	25.1	18.48	23.8	24.1	29.9
Num. of water	151	313	281	386	78
Total reflections used	13996	32033	31499	42922	5394
RMSD from ideality					
Bond length (Å)	0.010	0.014	0.010	0.014	0.006
Bond angle (°)	1.271	2.3	1.293	1.608	0.887
Ramachandran plot					
Most favored (%)	95.2	92.7	95.2	94.8	83.9
Allowed (%)	4.0	6.5	4.0	4.4	15.3
Generously allowed (%)	0	0.8	0	0	0
Disallowed (%)	0.8	0	0.8	0.8	0.8
PDB code	3F8A	3CR6	3F9D	3FA6	3FEP

**Table VI-3. X-ray data collection statistics of the apo-CRABPII mutant crystals.**

	KLE-R59E		KFLE		KFLD		KFLDV		KL-T54E		KL-A32E	
Spacegroup	P 1		P 1		P 1		P 1		P 1		P 1	
Z (mol/asymm. unit)	2		2		2		2		2		2	
Unit cell dimensions												
a (Å)	34.7		34.6		34.6		34.6		34.8		34.7	
b (Å)	37.2		37.2		37.2		37.2		36.7		37.1	
c (Å)	61.3		60.8		60.5		57.1		56.9		58.5	
$\alpha$ (°)	74.5		106.1		74.2		73.6		75.5		102.6	
$\beta$ (°)	73.4		106.5		73.2		76.7		74.9		106.4	
$\gamma$ (°)	90.5		90.0		90.5		87.7		88.4		92.9	
Wavelength (Å)	0.97869		1.000		1.0332		0.97850		0.97850		1.0000	
Resolution range (Å)	35.7-1.9 (1.95-1.90)		55.8-1.8 (1.83-1.78)		55.6-1.9 (1.99-1.94)		53.5-1.5 (1.55-1.51)		53.2-1.9 (1.90-1.85)		54.6-1.6 (1.60-1.56)	
Redundancy	4.0 (3.8)		4.4 (4.3)		2.0 (1.9)		4.2 (3.4)		2.4 (1.7)		3.5 (2.8)	
Average I/ $\sigma$	20.7 (4.8)		18.2 (6.7)		12.4 (2.2)		46.2 (4.5)		26.6 (2.4)		37.2 (5.7)	
Total reflections	85924		172871		38605		165351		42840		123511	
Unique reflections	21661		25808		18587		39062		18943		35378	
Completeness	97.7 (93.9)		96.7 (95.1)		90.5 (87.7)		94.2 (77.0)		84.6 (40.7)		92.3 (69.3)	
R <sub>merge</sub> (%)	7.3 (36.8)		5.6 (18.1)		5.5 (29.9)		4.1 (23.2)		5.1 (29.7)		6.4 (22.1)	

Values in parentheses refer to the last resolution shell.

**Table VI-4. Structure refinement statistics of the apo-CRABPII mutant crystals.**

	KLE-R59E	KFLE	KFLD	KFLDV	KL-T54E	KL-A32E
Average B-Factor (Å)	28.9	23.1	30.1	29.3	24.0	26.3
R <sub>work</sub> (%)	18.6	18.0	21.0	17.1	18.8	15.3
R <sub>free</sub> (%)	24.8	23.8	27.7	21.2	24.4	19.9
Num. of water	254	300	169	349	217	372
Total reflections used	19452	23232	16634	37100	17972	33597
RMSD from ideality						
Bond length (Å)	0.009	0.010	0.007	0.012	0.008	0.013
Bond angle (°)	1.20	1.37	1.10	1.42	1.25	1.54
Ramachandran plot						
Most favored (%)	93.5	94.0	94.0	92.7	93.5	94.4
Allowed (%)	5.6	5.2	5.2	6.5	5.6	4.7
Generously allowed (%)	0	0	0	0.4	0.4	0.4
Disallowed (%)	0.8	0.8	0.8	0.4	0.4	0.4
PDB code	3FA7	3FA8	3FA9	3FEK	3FEL	3FEN

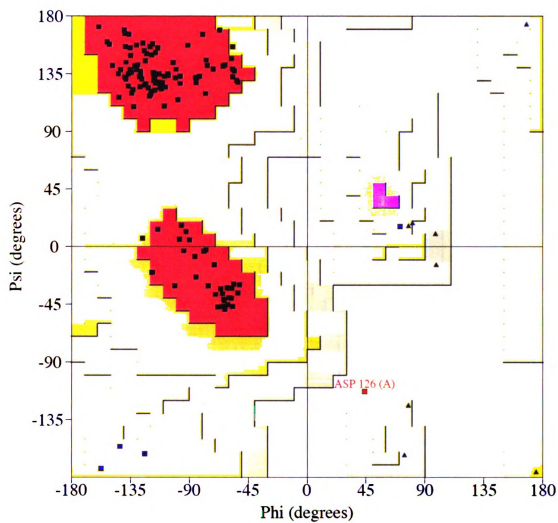


**Figure VI-10.** Ramachandran plot of the C<sub>15</sub>-aldehyde-bound-KLE-R59W-CRABPII.

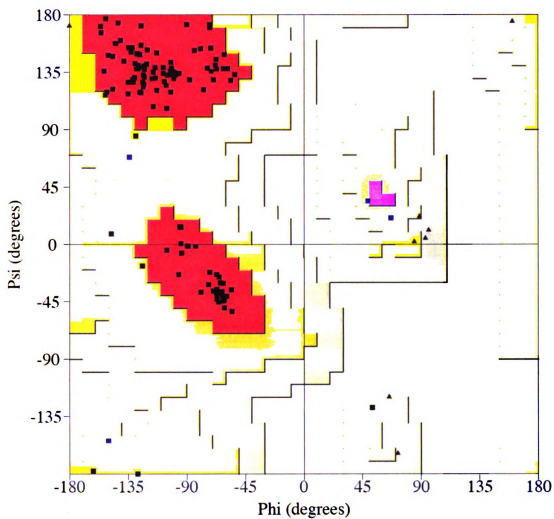


**Figure VI-11. Ramachandran plot of the C<sub>15</sub>-aldehyde-bound-KL-A32E-CRABPIL.**

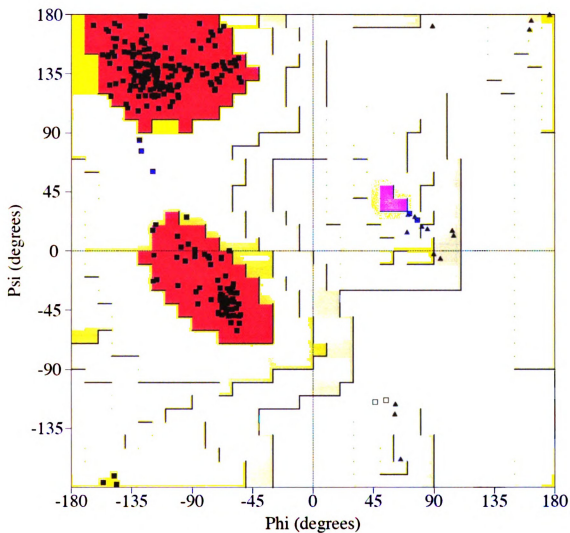


**Figure VI-12. Ramachandran plot of the C<sub>15</sub>-aldehyde-bound-KL-T54E-CRABPII.**





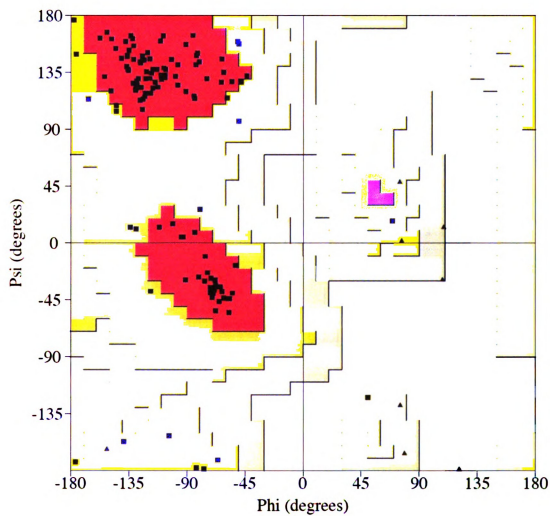


**Figure VI-14. Ramachandran plot of the merocyanin-bound-KLE-R59W-CRABP II.**

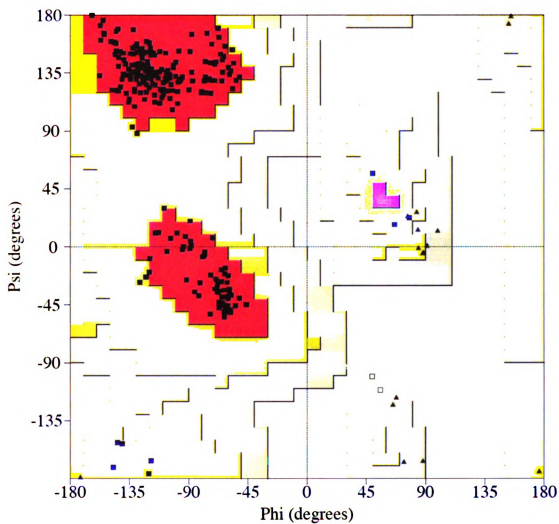


**Figure VI-15. Ramachandran plot of the apo-KLE-R59E-CRABPII.**

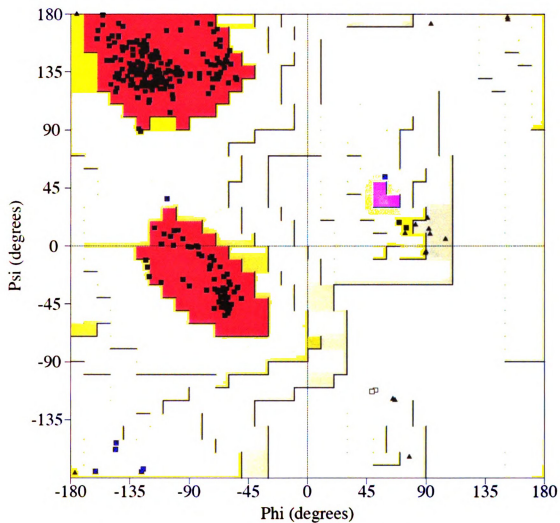


**Figure VI-16. Ramachandran plot of the apo-KFLE-CRABPII.**

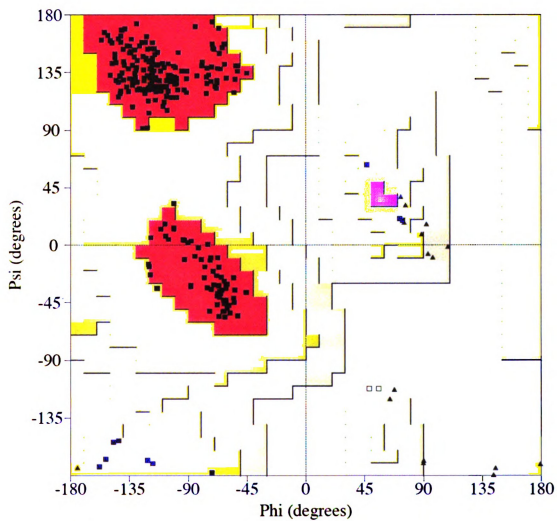


**Figure VI-17. Ramachandran plot of the apo-KFLD-CRABPII.**

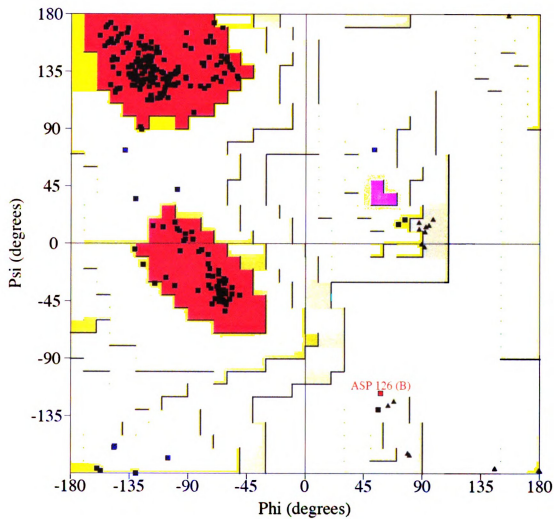


**Figure VI-18. Ramachandran plot of the apo-KFLDV-CRABPII.**

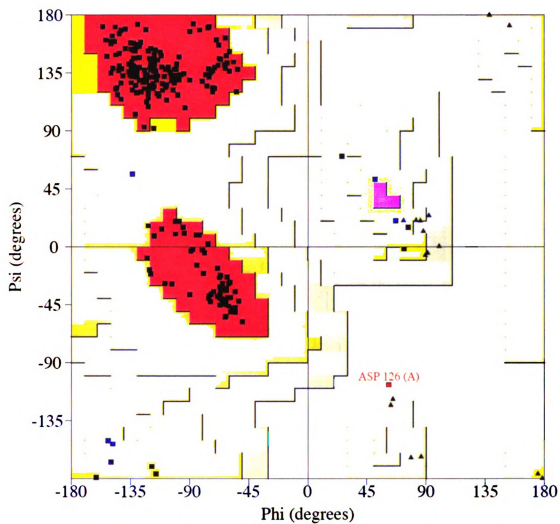


**Figure VI-19. Ramachandran plot of the apo-KL-T54E-CRABPIL.**





## **6.4. Protein characterization**

### **6.4.1. General procedure for UV-vis titrations of CRABPII/CRALBP with retinoids.**

A stock solution of the specific retinoid (retinoic acid, all-*trans*-retinal, 11-*cis*-retinal or C<sub>15</sub>-aldehyde) was prepared in 95% spectroscopy grade EtOH. To a protein solution, 0.1 equivalent of the retinoid was added as increments and spectra was recorded at room temperature from 200 nm to 600 nm (Lambda 40, Perkin Elmer and Cary WinUv, Varian). The secondary derivative of the spectra was calculated by using the corresponding software provided with the UV instrument. The determination of the  $\lambda_{\max}$  of a UV peak using mathematical equations has been established as a valid method and has been used in a variety of applications (20-24).

### **6.4.2. Determination of the extinction coefficients of proteins.**

The absorption extinction coefficients ( $\epsilon$ ) for the various proteins were determined according to the method first described by Gill and von Hippel.(25) The  $\epsilon_{\text{den}}$  ( $\epsilon$  of denatured proteins in 6 M Guanidine HCl) is dependant primarily on the number of Tyr, Trp and Cys residues present and can be calculated according to equation:

$$\epsilon_{\text{den}} = a\epsilon_{\text{tyr}} + b\epsilon_{\text{trp}} + c\epsilon_{\text{cys}}$$

where a, b, and c represent the number of respective amino acids per molecule of protein, and their  $\epsilon$  values have been determined experimentally ( $\epsilon_{\text{trp}} = 5690 \text{ M}^{-1} \text{ cm}^{-1}$ ,  $\epsilon_{\text{tyr}} =$

$1280 \text{ M}^{-1} \text{ cm}^{-1}$ ,  $\epsilon_{\text{cys}} = 120 \text{ M}^{-1} \text{ cm}^{-1}$ , wild type CRABPII protein contains 3 Trp, 2 Tyr, and 3 Cys residues).

Two protein solutions are prepared, at identical concentrations, one in the native buffer (4 mM  $\text{NaH}_2\text{PO}_4$ , 16 mM  $\text{Na}_2\text{HPO}_4$ , 150 mM NaCl, pH = 7.3) and the other in a denaturing buffer (6 M guanidine HCl, 4 mM  $\text{NaH}_2\text{PO}_4$ , 16 mM  $\text{Na}_2\text{HPO}_4$ , 150 mM NaCl), and the  $\text{Abs}_{280}$  for each sample is measured.

The  $\epsilon_{\text{nat}}$ , the extinction coefficient for the native protein, can be determined according to Beer's law:

$$\text{Abs}_{\text{den}} + \epsilon_{\text{den}} = c_{\text{den}}$$

$$\text{Abs}_{\text{nat}} + \epsilon_{\text{nat}} = c_{\text{nat}}$$

where Abs is the UV absorbance at 280 nm, under both native and denatured conditions. Since the concentration of both samples is the same, we can equate the two equations and solve for the extinction coefficient. The measurement must be repeated until a consistent number is obtained.

*Molar absorbance determined :*

$$\text{RAR}\gamma\text{-LBD} : 11,972 \text{ cm}^{-1} \text{ M}^{-1}$$

$$\text{Full length CRALBP} : 24,514 \text{ cm}^{-1} \text{ M}^{-1}$$

$$\Delta 20\text{-CRALBP} : 24,267 \text{ cm}^{-1} \text{ M}^{-1}$$

#### **6.4.3. Reductive amination procedure.**

CRABPII (0.3 mg) in PBS buffer (1 mL) was mixed with 1.2 equivalents of retinal from an ethanol stock (final ethanol volume less than 35  $\mu$ L). The mixture was incubated at 25°C in darkness for 10 min after which 15  $\mu$ L of 5 M NaCNBH<sub>3</sub> in H<sub>2</sub>O were added. The reaction was left for 4 hours. Absorption at 330 nm was observed of the reaction mixture, indicating a successful reduction.

#### **6.6.4. Circular Dichroism of protein samples.**

Circular dichroism (CD) spectra of protein samples were obtained in order to verify the correct folding of each protein. The use of CD spectroscopy for protein characterization depends mostly on empirical rules applied by comparing the obtained spectrum with characteristic spectra of peptides with specific folding patterns.(26)

Instrument settings and sample concentrations were very important in acquiring reproducible CD spectra. The protein concentrations used had to be in the range of 1 – 5  $\mu$ M. Lower concentrations gave noisy spectra, while higher concentrations produced spectra where the amino acid absorbance overshadowed the structural features. A similar problem was also observed when the bandwidth of the instrument, which defines how much light is allowed to enter the sample chamber, was set higher than 1 unit.

In a typical protocol, a 5  $\mu$ M solution of protein in buffer was used for CD measurement (JASCO 710). The spectra were scanned from 500 nm to 200 nm at 100 nm/min, with a bandwidth of 1 nm. Extended degassing of the sample chamber with nitrogen must be performed to ensure quality spectra near the 200 nm region.

#### 6.4.5. Fluorescence.

Fluorescence quenching is used for the determination of dissociation constants for binding of both retinal and retinoic acid to CRABP II proteins.(1, 27) It is known that proteins containing Trp residues absorb light at 280 nm and fluoresce at ~340 nm. This fluorescence can be quenched in the presence of a chromophore that is close to Trp residues in space. As the chromophore is titrated into the protein solution, some amount of the Trp fluorescence will be quenched, until the pocket is fully saturated and a change is no longer detected in the Trp fluorescence. Therefore, by monitoring the fluorescence of Trp residues in the protein as a function of the concentration of added chromophore an apparent dissociation constant for the ligand-protein complex can be calculated (detailed description follows).

Due to the sensitive nature of the experiment, the optimization of the fluorescence titration experiments has been particularly tedious. Air bubbles and small particles cause noisy spectra, therefore buffers should be degassed and samples filtered before used (28). In addition, it has been found that the oily residue from fingerprints can demonstrate fluorescence, so care has to be taken not to touch the quartz cuvettes (29). When handling the cuvettes lint free gloves should always be worn, as lint on the outside of a cuvette interferes with the reading as well. All samples should be stored in glass containers (29). In the case of protein samples, silanized glassware should be used, as many plastic containers will leach fluorescent materials into the sample.

Sample concentrations are also very important. Literature reports suggest the use of a sample concentration as close as possible to the expected  $K_d$ , maintaining an accurate measurement. Considering that the  $K_d$  values would be in the nM range, protein

concentration of 500 nM was found to be the optimal for our experiments. Anything lower would compromise the accuracy of our experiment.

At the same time, the low solubility of retinal in water can cause problems, since precipitation when high numbers of equivalents are added can produce cloudy samples, resulting in erroneous results. In addition, since the ligand is titrated into the protein from a stock in EtOH one must make sure that the final EtOH concentration is kept below 2%, to prevent possible protein denaturation. It has also been shown that EtOH concentrations between 2-8% can red shift the maximum wavelength up to 40 nm (30).

Additionally, an optimum salt concentration must be used for protein analysis in buffer. Polar solvents, including water have been shown to quench some amount of Trp fluorescence (31). A high salt concentration (150 mM) potentially helps to shield the protein and reduce the amount of unwanted quenching. All salts used in the buffer must be of the highest grade available to ensure minimal background fluorescence.

Maintenance of temperature and pH of the measurement samples is also critical. If the temperature rises above ambient, the wavelength of the Trp emission red-shifts and the intensity of the peak decreases. At higher temperatures, the excited state can return to the ground state via other means such as phosphorescence.(28, 32) Likewise, an optimal pH is required for the protein sample, if it is either too acidic or too basic, the protein sample may denature (33). Typical protein samples have a Trp emission in the range of 330 – 350 nm, but this varies with the protein, the number of Trp residues, and whether or not they are solvent-exposed (34-36). Free Trp emits at 365 nm. A denatured protein will red shift towards 365 nm and provide a false saturation point for the titration.

Another point of concern is the fact that proteins tend to stick to the surface of glass. When storing the samples, silanized glassware should be used to avoid loss of protein and a change in protein concentration. When performing the actual fluorescence titration with low concentration of protein, a dummy protein, such as gelatin, should be used to stabilize the protein and avoid loss due to binding with the surface of the cuvette. Gelatin does not contain Trp residues, therefore it will not interfere with the fluorescence measurements.

A final note to mention is the fact that retinal alone actually interferes to some extent with the Trp fluorescence detection. The free chromophore can quench some of the Trp emission. To correct for this, one must perform a blank titration with *N*-acetyltryptophanamide and add back this lost fluorescence (37). Details of this process are described below. Interestingly, retinoic acid, which has a closer  $\lambda_{\text{max}}$  value to the Trp emission wavelength, does not have the same effect.

#### **6.4.6. General protocol followed for Fluorescence Quenching and $K_d$ determination experiments.**

The cuvette is allowed to sit with 3 mL of a 0.01% gelatin containing PBS (4 mM  $\text{NaH}_2\text{PO}_4$ , 16 mM  $\text{Na}_2\text{HPO}_4$ , 150 mM  $\text{NaCl}$ , pH=7.3) for 30-60 min. This buffer is discarded and the cell is rinsed once with distilled water. The cuvettes are all handled while wearing gloves so as to avoid both fingerprints and lint. Then 3 mL of a room temperature 500 nM protein is added to the cell. The sample is excited at 283 nm with a slit width about 1.5 nm (this varies in order to ensure that the intensity of each sample remains below one million counts). The fluorescence is measured at the peak maximum,

about 345 nm (varies with different proteins). The chromophore is added at varying equivalents from a ~1.5 mM stock (in 95% spectroscopy grade EtOH) sample maintained in the dark. A measurement is taken after each addition at the same wavelength. The results are plotted as concentration of chromophore versus relative fluorescence intensity. When the curve levels off, the titration is complete.

If the chromophore is all-*trans*-retinoic acid (Sigma,  $\epsilon = 45,000 \text{ M}^{-1} \text{ cm}^{-1}$ ,  $\lambda_{\text{max}} = 350 \text{ nm}$ ), the data can be plotted as it is. There is minimal effect of retinoic acid on the Trp emission as seen in a blank titration run with N-acetyltryptophanamide.

If the chromophore is all-*trans*-retinal (Toronto Research Company,  $\epsilon = 48,000 \text{ M}^{-1} \text{ cm}^{-1}$ ,  $\lambda_{\text{max}} = 380 \text{ nm}$ ), a blank titration must be run with 3 mL of 1.5  $\mu\text{M}$  N-acetyltryptophanamide. The peak maximum for the blank is at 365 nm. This curve is plotted as concentration of retinal versus change in intensity. The retinal absorbs some of the emission observed through the Trp residues. This will be added back into each of the protein / chromophore titrations.

The correction for the retinal titrations involves a four step calculation after completion of both the protein titration and the blank titration (37).

$$\alpha = \frac{F_{\text{max}} - F}{F_{\text{max}} - F_o}$$

$F_{\text{max}}$  = fluorescence upon saturation

$F_o$  = initial fluorescence

$F$  = observed fluorescence

$\alpha$  = fraction of free binding sites

1. Determine the free ligand concentration,  $R$ .

$$R = R_o - nP_o(1-\alpha)$$

$R_o$  = ligand concentration

$n$  = number of binding sites / protein, assume  $n=1$

$P_o$  = protein concentration

2. Find fluorescence contribution of free ligand,  $F_R$ , to be deduced from blank (see solved example below).
3. Subtract fluorescence contribution of free ligand from actual readings, plot vs. ligand concentration.

$(F-F_R)$  vs.  $R_o$

The dissociation constant is calculated with the program SigmaPlot through non-linear least square regression analysis.(27, 38) Within SigmaPlot, the corrected relative fluorescence intensities are plotted against the concentration of retinal. The protein concentration and the final fluorescence intensity upon saturation are the other two values needed to solve the equation for the dissociation constant:



$$\frac{F}{F_f} = 1 + \left( \frac{F_b}{F_f} - 1 \right) \cdot \left( \frac{P_t + R_t + K_d - \sqrt{(P_t + R_t + K_d)^2 - 4P_t R_t}}{2P_t} \right)$$

$F$  = observed fluorescence

$F_f$  = fluorescence of free protein

$F_b$  = fluorescence of bound protein

$P_t$  = total protein concentration

$R_t$  = total chromophore concentration

As input into SigmaPlot (for our specific example):

$$y = p1 + p1 * ((p2/p1 - 1) * (p3 + x + k - ((p3 + x + K_d)^2 - 4 * p3 * x)^{0.5})) / (2 * p3)$$

$y$  = fluorescence value

$x$  = chromophore concentration

$p1$  = initial fluorescence intensity = 1

$p2$  = fluorescence intensity upon saturation = 0.66

$p3$  = protein concentration =  $5 \cdot 10^{-7}$

#### • *Cleaning of Fluorescence Cuvettes:*

As both fingerprints and protein residue on the surface of the fluorescence cells may cause interference in the measurements, they should be thoroughly cleaned regularly, depending on volume of use. A proper cleaning procedure entails:



1. Soak 24 h in chromic acid, then rinse with water.
2. Soak 8 h in a KOH / MeOH solution (20 pellets / 100 mL), then rinse with water.
3. Soak 4 h in HNO<sub>3</sub>, then rinse with water

## References

1. Wang, L. C., Li, Y., and Yan, H. G. (1997) Structure-function relationships of cellular retinoic acid-binding proteins - Quantitative analysis of the ligand binding properties of the wild-type proteins and site-directed mutants, *Journal of Biological Chemistry* 272, 1541-1547.
2. Renaud, J. P., Rochel, N., Ruff, M., Vivat, V., Chambon, P., Gronemeyer, H., and Moras, D. (1995) Crystal-Structure of the Rar-Gamma Ligand-Binding Domain Bound to All-Trans-Retinoic Acid, *Nature* 378, 681-689.
3. Rochel, N., Renaud, J. P., Ruff, M., Vivat, V., Granger, F., Bonnier, D., Lerouge, T., Chambon, P., Gronemeyer, H., and Moras, D. (1997) Purification of the human RAR gamma ligand-binding domain and crystallization of its complex with all-trans retinoic acid, *Biochem Bioph Res Co* 230, 293-296.
4. Crabb, J. W., Chen, Y., Goldflam, S., West, K., Kapron, J. . (1998) Methods for producing recombinant human cellular retinaldehyde-binding protein, *Methods in Molecular Biology* 89, 91-104.
5. Lee, K. S., Jia, X., Vasileiou, C., Geiger, J. H., and Borhan, B., To be published.
6. Otwinowski, Z., and Minor, W. (1997) Processing of X-ray diffraction data collected in oscillation mode, *Macromolecular Crystallography, Pt A* 276, 307-326.
7. Vagin, A., and Teplyakov, A. (1997) MOLREP: an automated program for molecular replacement, *J. Appl. Cryst.* 30, 1022-1025.
8. Bailey, S. (1994) The Ccp4 Suite - Programs for Protein Crystallography, *Acta Crystallographica Section D-Biological Crystallography* 50, 760-763.
9. McCoy, A. J., Grosse-Kunstleve, R. W., Adams, P. D., Winn, M. D., Storoni, L. C., and Read, R. J. (2007) Phaser crystallographic software, *Journal of Applied Crystallography* 40, 658-674.
10. Roussel, A., and Cambillau, C. (1989) Turbo-Frodo, in *Silicon Graphics Geometry Partners Directory*, Silicon Graphics, Mountain View.
11. Emsley, P., and Cowtan, K. (2004) Coot: model-building tools for molecular graphics, *Acta Crystallographica Section D-Biological Crystallography* 60, 2126-2132.
12. Murshudov, G. N., Vagin, A. A., and Dodson, E. J. (1997) Refinement of macromolecular structures by the maximum-likelihood method, *Acta Crystallographica Section D-Biological Crystallography* 53, 240-255.

13. Murshudov, G. N., Vagin, A. A., Lebedev, A., Wilson, K. S., and Dodson, E. J. (1999) Efficient anisotropic refinement of macromolecular structures using FFT, *Acta Crystallographica Section D-Biological Crystallography* 55, 247-255.
14. Pannu, N. S., Murshudov, G. N., Dodson, E. J., and Read, R. J. (1998) Incorporation of prior phase information strengthens maximum-likelihood structure refinement, *Acta Crystallographica Section D-Biological Crystallography* 54, 1285-1294.
15. Winn, M. D., Isupov, M. N., and Murshudov, G. N. (2001) Use of TLS parameters to model anisotropic displacements in macromolecular refinement, *Acta Crystallographica Section D-Biological Crystallography* 57, 122-133.
16. Sheldrick, G. M., and Schneider, T. R. (1997) Shelxl: High-Resolution Refinement, *Macromolecular Crystallography, Pt B* 277, 319-343.
17. Painter, J., and Merritt, E. A. (2006) Optimal description of a protein structure in terms of multiple groups undergoing TLS motion, *Acta Crystallographica Section D-Biological Crystallography* 62, 439-450.
18. Painter, J., and Merritt, E. A. (2006) TLSMD web server for the generation of multi-group TLS models, *Journal of Applied Crystallography* 39, 109-111.
19. Vaezeslami, S., Mathes, E., Vasilelou, C., Borhan, B., and Geiger, J. H. (2006) The structure of apo-wild-type cellular retinoic acid binding protein II at 1.4 Å and its relationship to ligand binding and nuclear translocation, *Journal of Molecular Biology* 363, 687-701.
20. Cahill, J. E. (1979) Derivative Spectroscopy - Understanding Its Application, *Am Lab* 11, 79-&.
21. Cahill, J. E., and Padera, F. G. (1980) Derivative Analysis of Uv-Visible Spectra, *Am Lab* 12, 101-&.
22. Horvath, M. P., Copeland, R. A., and Makinen, M. W. (1999) The second derivative electronic absorption spectrum of cytochrome c oxidase in the Soret region, *Biophys J* 77, 1694-1711.
23. LEE, D. C., Hayward, J. A., Restall, C. J., and Chapman, D. (1985) 2nd-Derivative Infrared Spectroscopic Studies of the Secondary Structures of Bacteriorhodopsin and Ca-2+-Atpase, *Biochemistry-Us* 24, 4364-4373.
24. Sehgal, A. C., Tompson, R., Cavanagh, J., and Kelly, R. M. (2002) Structural and catalytic response to temperature and cosolvents of carboxylesterase EST1 from the extremely thermoacidophilic archaeon *Sulfolobus solfataricus* P1, *Biotechnol Bioeng* 80, 784-793.

25. Gill, S. C., and Vonhippel, P. H. (1989) Calculation of Protein Extinction Coefficients from Amino-Acid Sequence Data, *Analytical Biochemistry* 182, 319-326.
26. Venyaminov, S. Y., and Yang, J. T. (1996) Determination of protein secondary structure., in *Circular dichroism and the conformational analysis of biomolecules*. (Fasman, G. D., Ed.), pp 69-107, Plenum Press, New York, NY.
27. Norris, A. W., Cheng, L., Giguere, V., Rosenberger, M., and Li, E. (1994) Measurement of Subnanomolar Retinoic Acid-Binding Affinities for Cellular Retinoic Acid-Binding Proteins by Fluorometric Titration., *Biochim. Biophys. Acta-Protein Struct. Molec. Enzym.* 1209, 10-18.
28. Gally, J. A., and Edelman, G. M. (1962) The effect of temperature of the fluorescence of some aromatic amino acids and proteins., *Biochim. Biophys. Acta* 60, 499-509.
29. Miller, J. N. (1981) Standards in fluorescence spectrometry., in *Techniques in visible and ultra-violet spectroscopy*. (Miller, J. N., Ed.), pp 1-7, Chapman and Hall, New York.
30. Kronman, M. J. (1967) Fluorescence studies of the molecular conformation of  $\alpha$ -lactalbumin., *Biochim. Biophys. Acta* 133, 19-32.
31. Steiner, R. F., and Edelhoch, H. (1962) Effect of thermally induced structural transitions on the ultra-violet fluorescence of proteins., *Nature* 193, 375-376.
32. Valeur, B. (2002) Characteristics of fluorescence emission., in *Molecular Fluorescence*, pp 34-71, Wiley-VCH, Weinham, Germany.
33. White, A. (1959) Effect of pH on fluorescence of tyrosine, tryptophan and related compounds., *Biochem. J.* 71, 217-220.
34. Chen, R. F. (1967) Extrinsic and intrinsic fluorescence in the study of protein structure., in *Fluorescence: Theory, Instrumentation, and Practice* (Guilbault, G. G., Ed.), pp 443-509, Marcel Dekker, Inc., New York.
35. Eftink, M. R. (2000) Intrinsic fluorescence of proteins., in *Topics in Fluorescence Spectroscopy* (Lakowicz, J. R., Ed.), pp 1-15, Kulwer Academic / Plenum Publishers, New York.
36. Konev, S. V. (1967) *Fluorescence and phosphorescence of proteins and nucleic acids*., Plenum Press, New York.
37. Cogan, U., Kopelman, M., Mokady, S., and Shinitzky, M. (1976) Binding affinities of retinol and related compounds to retinal binding proteins., *Eur. J. Biochem.* 65, 71-78.

38. Wang, L., Li, Y., and Yan, H. (1997) Structure-function relationships of Cellular Retinoic Acid-binding proteins., *J. Biol. Chem.* 272, 1541-1547.